8-30-2017

Design, Synthesis and Characterization of Hydrophobic Polydivinylbenzene Adsorbent for Environmental Applications

Tahereh Jafari
University of Connecticut - Storrs, tahereh.jafari@uconn.edu

Design, Synthesis and Characterization of Hydrophobic Polydivinylbenzene Adsorbent for Environmental Applications

Tahereh Jafari, Ph.D.

University of Connecticut, 2017

In this thesis, my focus will be on the synthesis of mesoporous functionalized polydivinylbenzene (PDVB) for diverse environmental applications including siloxane adsorption, CO_2 capture and heavy metal (Arsenic) removal. Controlled synthesis of the porous polymeric adsorbent will be carried out to obtain an improved adsorptive activity. The effect of textural properties and functional moieties on adsorption efficiency will be studied. Finally, the adsorptive characteristics of obtained adsorbents will be evaluated for various environmental applications.

In the first section, I will demonstrate the synthesis of a new class of siloxane (D4) adsorbent at ambient temperature and atmospheric pressure. Vinyl imidazole (VI) group polymerized with divinylbenzene (DVB) in the hydrothermal reaction with variable ration of VI/DVB in order to obtain optimal adsorption efficiency. The adsorbent was evaluated under humid conditions of 50% moisture. The effect of presence of CO_2 in the gas mixture up to 35% was also studied. The adsorbent regeneration was conducted for five cycles.

In the second section, amine-functionalized PDVB with vinyltriazole (VT) was synthesized through a hydrothermal approach and optimized to remove arsenate ions from aqueous solution. The adsorption isotherms described by the Sips model indicates information about homogenous adsorption sites and monolayer adsorption. DFT calculations indicate that the co-monomer of

Tahereh Jafari, Ph.D.

University of Connecticut, 2017

VT improved the stability of anionic-pi interactions thermodynamically. Computational studies also show the adsorption mechanism was dominant with anion-induced interactions for non-functionalized PDVB. However, electrostatic interactions become dominant by introducing amine-moieties (VT) to the polymeric materials.

The third section exhibits the synthesis of amine-functionalized PDVB with a microwave-assisted approach. There is a correlation between the amounts of incorporated VT with CO_2 adsorptive activity of resulted adsorbents. The initiator amounts have an effect on adsorbent activity toward CO_2. The addition of amine functionality of VT led to enhance CO_2 adsorption efficiency while an optimum surface area and pore volume were maintained. Optimal amounts of initiator also help improve the incorporation of VT into PDVB while textural properties remain intact. Recycling of adsorbent was conducted up to seven cycles. Theoretical modeling indicates that nitrogen sites on the triazole ring are the active site toward CO_2 molecules.

Design, Synthesis and Characterization of Hydrophobic Polydivinylbenzene Adsorbent for Environmental Applications

Tahereh Jafari

B.Sc., Sharif University of Technology, [2006]

M.Sc., Sharif University of Technology, [2009]

A Dissertation

Submitted in Partial Fulfillment of the

Requirements for the Degree of

Doctor of Philosophy

at the

University of Connecticut

2017

APPROVAL PAGE

Doctor of Philosophy Dissertation

Design, Synthesis and Characterization of Hydrophobic Polydivinylbenzene Adsorbent for Environmental Applications

Presented by

Tahereh Jafari

Major Advisor _____

Steven L. Suib

Associate Advisor _____

S. Pamir Alpay

Associate Advisor _____

Rajeswari Kasi

University of Connecticut
2017

Dedicated to my family and all my friends

Acknowledgement

I would like to express my sincere gratitude to my advisor Dr. Steven L. Suib for all his support, inspiration, and supervision throughout my graduate studies who is the best any students can ask. I am also grateful to my associate advisors, Dr. S. Pamir Alpay, Dr. Rajeswara Kasi, for their generous help and advice. I also highly appreciate Dr. Frank Galasso for his motivation and discussions throughout my Ph.D. time and Mrs. Bonnie Suib for her generous support and help.

My sincere thanks also go to my colleagues for helpful discussions and contributions to my research and Ph.D. life, Dr. Sanjubala Sahoo, Dr. Curtis Guild, Dr. Ran Miao, Dr. Ting Jiang, Dr. Abdelhamid El-Sawy, Ehsan Moharreri, Panteha Toloueenia, Alireza Shirazi, Junkai He, Wei Zhong, Biswanath Dutta, and everyone else in Dr. Suib's group.

Finally, I especially thank my parents and my husband, Nasser Khakpash. Their love and support keep me moving forward. I could not imagine myself getting this far without them.

Table of Contents

List of Figures

List of Tables

Chapter 1. Introduction

1.1 Overview

Biogas has been considered as an alternative source of energy for fossil fuel in which the biggest challenge is to remove volatile organic silicon compounds (siloxanes) for energy generation. Biogas is produced from anaerobic digestion[1] of micro-organism in the absence of air which contains adverse compounds of siloxanes due to extensive use of siloxane containing compounds including pharmaceuticals, personal care products, lubricants, cosmetics, and elastomeric usage.[2,3] Combustion of biogas containing siloxanes leads to deposition of abrasive silicon oxide, which damage energy recovery systems considerably.[4,5] Therefore, biogas purification has been an essential process to avoid high cost of maintenance of combustion engines, fuel cells, and turbines which could be conducted through siloxane capture by a proper adsorbent. Current challenge in the biogas clean-up is mainly considered as moisture sensitivity of adsorbent material which leads to a decrease in performance in the presence of water vapor.

Heavy metal pollution has been considered as a challenging environmental concern especially for arsenic contamination which occurred naturally and anthropogenically in wastewater and drinking water.[6–9] Different techniques and materials have been applied to remove arsenate ions among which adsorption with various porous materials has drawn lots of attention.[10–14] Recently, functionalization of readily available adsorbents opens new outlooks for the design of more efficient adsorbents with extensive possible industrial applications.[15–17]

On the other hand, global warming issues are other environmental concerns which result from extensive use of fossil fuel leading to greenhouse gas emissions, especially CO_2 emission to the

atmosphere. Mitigation of CO_2 emission could be conducted through carbon capture and storage (CCS) technology.[18,19] Currently aqueous amine absorbent applies to capture of CO_2 from flue gas that is associated with several drawbacks due to high corrosiveness and volatility of amine solution and high-energy requirements of the absorption process.[20] Therefore an alternative technique has been required to overcome current challenges for CO_2 capture which lead to an extensive study on using porous solid adsorbent. To develop an effective porous adsorbent with high selectivity and capacity, well-organized porosity and pore volume with CO_2-philic moieties is required.

For each of the applications of biogas purification, arsenic removal and CO_2 capture from flue gas, design and development of an efficient adsorbent with high surface area and suitable functionality would be beneficial. Herein, we propose to design and advance materials that are moisture resistant, and produce stable porous adsorbents to be modified and optimized for each application in order to effectively capture pollutant molecules of siloxane and CO_2 from biogas and flue gas respectively.

1.2 Background and Significance

1.2.1 Siloxane Removal from Biogas

Biogas from landfill gases (LFG), anaerobic digester gases (ADG), and wastewater has been considered as an alternative source of energy to use in energy generation systems as a substitution for fossil fuels.[21,22] However, the presence of impurities in the biogas adversely influence energy generation especially where siloxane impurities during combustion in engines lead to formation of an abrasive layer of silicon oxide resulting in huge annual costs for repair and maintenance.[4,5,23] Linear (L2-L4) and cyclic (D2-D5) siloxanes are environmentally friendly compounds, which are widely used in cosmetics, lubricants, shampoos, and detergents. Volatile

siloxanes such as hexamethyldisiloxane (D2) are eliminated from wastewater easily by dispersion in air. Less volatile siloxanes such as octamethylcyclotetrasiloxane (D4) or decamethylcyclopentasiloxane (D5) remain due to less water solubility. Depending on the location of biogas reservoirs and biogas sources (LFG or ADG or wastewater), the concentration of siloxane compositions varies.[24] Among siloxanes components in biogas, D4 is one of the most abundant components in biogas. Several methodologies including absorption,[25] peroxidation,[26] membrane,[27] and adsorption[21] have been employed to remove siloxanes from biogas, among which adsorption has been the most promising technique.[28,29] Therefore, developing a highly efficient porous adsorbent with high capacity and good regenerability has attracted lots of attention. Various adsorbents have been investigated to capture siloxanes including activated carbons (ACs),[30] zeolite, silica,[31] and polymeric adsorbents (Tenax and Amberlite).[32] Porous polymers have several advantages over other materials including high surface area, tunable pore size and pore volume, weight advantages, and ability to be decorated with different functional groups. The main drawback of most current adsorbents is the deactivation in the presence of moisture as biogas always contains some humidity. Therefore, hydrophobic materials, which are not poisoned by water molecules, would enhance the adsorptive efficiency of adsorbents.

1.2.2 Arsenic Adsorption from Aqueous Solution

Industrial activities lead to ground water contamination with heavy metals [6] that are not able to break down into less harmful species[7]. This emphasises the importance of their removal from water. According to the released studies from WHO (world health organization) on human health, the maximum acceptable level of arsenic in drinking water is 10 $\mu g l^{-1}$ which is critical because of arsenic abundance in water.[8,33] Low cost, regenerability of adsorbents, flexibility in design and setup, high metal binding capacity, and no pH adjustment requirement of adsorption

techniques[14,34–36] provide several advantages over other methods (oxidation,[11,37] filtration,[10] co-precipitation,[12] ion-exchange,[38,39] and electrodialysis[40,41]). Numerous adsorbent materials have been designed for arsenic adsorption including activated carbons (AC), activated alumina (AA), natural zeolites, metal oxide nanoparticles.[44–46] In order to elevate adsorptive efficiency of current materials, surface modification with active functional groups (oxygen, sulfur, and nitrogen) has been performed.[15–17,45] High productivity of nitrogen containing functional groups (amino, imidazole) makes them more useful in heavy metal adsorption techniques due to their complexation with metal ions[16,17]. As conventional surface functionalization is a complex and time consuming approach with several steps, developing a facile approach with less steps would be favorable to enhance the adsorption efficiency of adsorbents.[46]

1.2.3 Post-Combustion CO_2 Adsorption

Greenhouse gases (GHG) emission especially CO_2 emissions contribute directly to elevating earth surface temperatures[47,48] which could be mitigated by CO_2 capture and storage techniques (CCS) to the current fossil-fueled power plants[49] based on post-combustion approaches with advantages over other approaches.[50] Conventionally, post-combustion CO_2 capture has been conducted by amine-solutions which suffer from several drawbacks of corrosion, energy loss, and inefficient regeneration. [20] However, porous adsorbents provide some benefits of high CO_2 uptake capacity, low energy for regeneration, fast kinetics, easy handling, and less moisture sensitivity.[51,52] Physical and chemical adsorption of CO_2 could be affected by the quadrupole moment of the adsorbent,[53,54] and surface functionalities respectively.[55] Various porous materials have been employed as an adsorbent to capture CO_2 including alkaline earth metal oxides,[56] porous carbons,[57] silicas,[58,59] zeolites,[60] metal organic frameworks (MOFs),[61] porous organic frameworks (POFs),[62] and mesoporous organic polymers (NOPs).[63] High energy requirement for

regeneration of alkaline earth metal oxides and metal salts results from strong chemical interaction with CO_2 molecules as a result of chemisorptive adsorption.[64–66] However, physical adsorption with ACs offers some advantages of abundant precursor materials, moisture sensitivity, and low heat of adsorption. To overcome low selectivity and capacity of ACs[18], other materials such as silicas and zeolites have been widely studied as CO_2 adsorbents,[60,67] which offer rapid CO_2 uptake with high chemical and thermal stability.[68] However, the moisture sensitivity, the low selectivity and high energy of regeneration have limited their application[69–71]. Functionalization of ACs and zeolites with carboxylic, sulfonic, and amine groups have been conducted in order to address their low selectivity.[72,73] Amine functionality provides Lewis base sites with lone pair electrons which coordinate favorably with CO_2 molecules.[74] So amine functionalities have been widely applied through different approaches of impregnation and grafting.[75–78] Although amine impregnated adsorbents have been synthesized easily with high CO_2 capacity, few challenges still remained including pore blockage, decomposition of loaded amines upon heating, and high diffusion resistivity.[79] On the other hand, amine grafting by chemical reaction provides higher thermal stability for the adsorbent.[77,80] Although the newly emerged porous materials called MOFs have shown very high CO_2 selectivity and capacity, their high sensitivity toward moisture has been reported.[81] Recently, several porous polymers (mesoporous or microporous) have been developed for CO_2 capture[82,83] Porous polymers can be readily designed with high surface area and well-defined porosity with easy processing, and light elemental composition (weight advantages).[84] Amine functionalization of porous polymers with triazine groups have been reported for more efficient adsorption of CO_2.[62,85–88]

1.3 References

(1) Ryckebosch, E.; Drouillon, M.; Vervaeren, H. Techniques for transformation of biogas to biomethane. *Biomass and Bioenergy* **2011**, *35* (5), 1633–1645.

(2) Cabrera-Codony, A.; Gonzalez-Olmos, R.; Mart??n, M. J. Regeneration of siloxane-exhausted activated carbon by advanced oxidation processes. *J. Hazard. Mater.* **2015**, *285*, 501–508.

(3) Dewil, R.; Appels, L.; Baeyens, J. Energy use of biogas hampered by the presence of siloxanes. *Energy Convers. Manag.* **2006**, *47* (13-14), 1711–1722.

(4) Nair, N.; Zhang, X.; Gutierrez, J.; Chen, J.; Egolfopoulos, F.; Tsotsis, T. Impact of siloxane impurities on the performance of an engine operating on renewable natural gas. *Ind. Eng. Chem. Res.* **2012**, *51* (48), 15786–15795.

(5) Nair, N.; Vas, A.; Zhu, T.; Sun, W.; Gutierrez, J.; Chen, J.; Egolfopoulos, F.; Tsotsis, T. T. Effect of siloxanes contained in natural gas on the operation of a residential furnace. *Ind. Eng. Chem. Res.* **2013**, *52* (18), 6253–6261.

(6) Fu, F.; Wang, Q. Removal of heavy metal ions from wastewaters: A review. *J. Environ. Manage.* **2011**, *92* (3), 407–418.

(7) Shawabkeh, R.; Al-Harahsheh, A.; Al-Otoom, A. Copper and zinc sorption by treated oil shale ash. *Sep. Purif. Technol.* **2004**, *40* (3), 251–257.

(8) Järup, L. Hazards of heavy metal contamination. *Br. Med. Bull.* **2003**, *68*, 167–182.

(9) Roy, P.; Mondal, N. K.; Bhattacharya, S.; Das, B.; Das, K. Removal of arsenic(III) and

arsenic(V) on chemically modified low-cost adsorbent: batch and column operations. *Appl. Water Sci.* **2013**, *3* (1), 293–309.

(10) Zhu, W. P.; Gao, J.; Sun, S. P.; Zhang, S.; Chung, T. S. Poly(amidoamine) dendrimer (PAMAM) grafted on thin film composite (TFC) nanofiltration (NF) hollow fiber membranes for heavy metal removal. *J. Memb. Sci.* **2015**, *487*, 117–126.

(11) Kobya, M.; Gebologlu, U.; Ulu, F.; Oncel, S.; Demirbas, E. Removal of arsenic from drinking water by the electrocoagulation using Fe and Al electrodes. *Electrochim. Acta* **2011**, *56* (14), 5060–5070.

(12) Santhosh, P.; Sridevi, A. a Lab-Scale Study on Reduction of Heavy Met- Als From Electroplating Effluent Using Conventional Chemical Precipitation. **2013**, *8* (1), 102–108.

(13) Sudilovskiy, P. S.; Kagramanov, G. G.; Kolesnikov, V. A. Use of RO and NF for treatment of copper containing wastewaters in combination with flotation. *Desalination* **2008**, *221* (1-3), 192–201.

(14) Hua, M.; Zhang, S.; Pan, B.; Zhang, W.; Lv, L.; Zhang, Q. Heavy metal removal from water/wastewater by nanosized metal oxides: A review. *J. Hazard. Mater.* **2012**, *211-212*, 317–331.

(15) Ajmal, M.; Demirci, S.; Uzun, Y.; Siddiq, M.; Aktas, N.; Sahiner, N. Introduction of double amidoxime group by double post surface modification on poly(vinylbenzyl chloride) beads for higher amounts of organic dyes, As (V) and Cr (VI) removal. *J. Colloid Interface Sci.* **2016**, *470* (February), 39–46.

(16) Xing, H. T.; Chen, J. H.; Sun, X.; Huang, Y. H.; Su, Z. B.; Hu, S. R.; Weng, W.; Li, S. X.; Guo, H. X.; Wu, W. B.; et al. NH2-rich polymer/graphene oxide use as a novel adsorbent for removal of Cu(II) from aqueous solution. *Chem. Eng. J.* **2015**, *263*, 280–289.

(17) Hong, G.; Li, X.; Shen, L.; Wang, M.; Wang, C.; Yu, X.; Wang, X. High recovery of lead ions from aminated polyacrylonitrile nanofibrous affinity membranes with micro/nano structure. *J. Hazard. Mater.* **2015**, *295*, 161–169.

(18) Rashidi, N. A.; Yusup, S. An overview of activated carbons utilization for the post-combustion carbon dioxide capture. *J. CO2 Util.* **2016**, *13*, 1–16.

(19) Samanta, A.; Zhao, A.; Shimizu, G. K. H.; Sarkar, P.; Gupta, R. Post-combustion CO 2 capture using solid sorbents: A review. *Ind. Eng. Chem. Res.* **2012**, *51* (4), 1438–1463.

(20) Hwang, C.-C.; Tour, J. J.; Kittrell, C.; Espinal, L.; Alemany, L. B.; Tour, J. M. Capturing carbon dioxide as a polymer from natural gas. *Nat. Commun.* **2014**, *5*, 3961.

(21) Yu, M.; Gong, H.; Chen, Z.; Zhang, M. Adsorption characteristics of activated carbon for siloxanes. *J. Environ. Chem. Eng.* **2013**, *1* (4), 1182–1187.

(22) Cabrera-Codony, A.; Montes-Moran, M. A.; S??nchez-Polo, M.; Martin, M. J.; Gonzalez-Olmos, R. Biogas upgrading: Optimal activated carbon properties for siloxane removal. *Environ. Sci. Technol.* **2014**, *48* (12), 7187–7195.

(23) Turkin, A. A.; Dutka, M.; Vainchtein, D.; Gersen, S.; van Essen, V. M.; Visser, P.; Mokhov, A. V.; Levinsky, H. B.; De Hosson, J. T. M. Deposition of SiO2 nanoparticles in heat exchanger during combustion of biogas. *Appl. Energy* **2014**, *113*, 1141–1148.

(24) Papadias, D.; Ahmed, S. *Biogas Impurities and Cleanup for Fuel Cells*; 2012.

(25) Ghorbel, L.; Tatin, R.; Couvert, A. Relevance of an organic solvent for absorption of siloxanes. *Environ. Technol.* **2014**, *35* (1-4), 372–382.

(26) Appels, L.; Baeyens, J.; Dewil, R. Siloxane removal from biosolids by peroxidation. *Energy Convers. Manag.* **2008**, *49* (10), 2859–2864.

(27) Ajhar, M.; Melin, T. Siloxane removal with gas permeation membranes. *Desalination* **2006**, *200* (1-3), 234–235.

(28) Mito-oka, Y.; Horike, S.; Nishitani, Y.; Masumori, T.; Inukai, M.; Hijikata, Y.; Kitagawa, S. Siloxane D4 capture by hydrophobic microporous materials. *J. Mater. Chem. A* **2013**, *1* (27), 7885.

(29) Montanari, T.; Finocchio, E.; Bozzano, I.; Garuti, G.; Giordano, A.; Pistarino, C.; Busca, G. Purification of landfill biogases from siloxanes by adsorption: A study of silica and 13X zeolite adsorbents on hexamethylcyclotrisiloxane separation. *Chem. Eng. J.* **2010**, *165* (3), 859–863.

(30) Boulinguiez, B.; Le Cloirec, P. Adsorption on activated carbons of five selected volatile organic compounds present in biogas: Comparison of granular and fiber cloth materials. *Energy and Fuels* **2010**, *24* (9), 4756–4765.

(31) Sigot, L.; Ducom, G.; Benadda, B.; Labouré, C. Adsorption of octamethylcyclotetrasiloxane on silica gel for biogas purification. *Fuel* **2014**, *135*, 205–209.

(32) Schweigkofler, M.; Niessner, R. Removal of siloxanes in biogases. *J. Hazard. Mater.* **2001**, *83* (3), 183–196.

(33) Ungureanu, G.; Santos, S.; Boaventura, R.; Botelho, C. Arsenic and antimony in water and wastewater: Overview of removal techniques with special reference to latest advances in adsorption. *J. Environ. Manage.* **2015**, *151*, 326–342.

(34) Barakat, M. A. New trends in removing heavy metals from industrial wastewater. *Arab. J. Chem.* **2011**, *4* (4), 361–377.

(35) Baccar, R.; Bouzid, J.; Feki, M.; Montiel, A. Preparation of activated carbon from Tunisian olive-waste cakes and its application for adsorption of heavy metal ions. *J. Hazard. Mater.* **2009**, *162* (2-3), 1522–1529.

(36) Ihsanullah; Abbas, A.; Al-Amer, A. M.; Laoui, T.; Al-Marri, M. J.; Nasser, M. S.; Khraisheh, M.; Atieh, M. A. Heavy metal removal from aqueous solution by advanced carbon nanotubes: Critical review of adsorption applications. *Sep. Purif. Technol.* **2016**, *157*, 141–161.

(37) Litter, M. I.; Morgada, M. E.; Bundschuh, J. Possible treatments for arsenic removal in Latin American waters for human consumption. *Environ. Pollut.* **2010**, *158* (5), 1105–1118.

(38) Lin, L. C.; Li, J. K.; Juang, R. S. Removal of Cu(II) and Ni(II) from aqueous solutions using batch and fixed-bed ion exchange processes. *Desalination* **2008**, *225* (1-3), 249–259.

(39) Dabrowski, A.; Hubicki, Z.; Podkocielny, P.; Robens, E. Selective removal of the heavy

metal ions from waters and industrial wastewaters by ion-exchange method. *Chemosphere* **2004**, *56* (2), 91–106.

(40) Hunsom, M.; Pruksathorn, K.; Damronglerd, S.; Vergnes, H.; Duverneuil, P. Electrochemical treatment of heavy metals (Cu2+, Cr 6+, Ni2+) from industrial effluent and modeling of copper reduction. *Water Res.* **2005**, *39* (4), 610–616.

(41) Gumpu, M. B.; Sethuraman, S.; Krishnan, U. M.; Rayappan, J. B. B. A review on detection of heavy metal ions in water - An electrochemical approach. *Sensors Actuators, B Chem.* **2015**, *213*, 515–533.

(42) Lata, S.; Samadder, S. R. Removal of arsenic from water using nano adsorbents and challenges: A review. *J. Environ. Manage.* **2016**, *166*, 387–406.

(43) Mohan, D.; Pittman, C. U. Arsenic removal from water/wastewater using adsorbents-A critical review. *J. Hazard. Mater.* **2007**, *142* (1-2), 1–53.

(44) Montero-campos, V.; Puente-urbina, A.; Rica, T. D. C.; Rica, C. Continuous-Flow Removal of Arsenic in Drinking Water by Filtering down through Fe 3 O 4 @ SiO 2 Magnetic Composite. **2016**, No. May, 619–630.

(45) Kampalanonwat, P.; Supaphol, P. Preparation and adsorption behavior of aminated electrospun polyacrylonitrile nanofiber mats for heavy metal ion removal. *ACS Appl. Mater. Interfaces* **2010**, *2* (12), 3619–3627.

(46) Akhavan, B.; Jarvis, K.; Majewski, P. Plasma polymer-functionalized silica particles for heavy metals removal. *ACS Appl. Mater. Interfaces* **2015**, *7* (7), 4265–4274.

(47) Ipcc. *Contribution of Working Group I to the Third Assessment Report of the Intergovernmental Panel on Climate Change*; 2001; Vol. 446.

(48) IPCC WGI AR5. Climate Change 2013: The Physical Science Basis. *Ipcc* **2013**, 31.

(49) Espinal, L.; Poster, D. L.; Wong-Ng, W.; Allen, A. J.; Green, M. L. Measurement, standards, and data needs for CO2 capture materials: A critical review. *Environ. Sci. Technol.* **2013**, *47* (21), 11960–11975.

(50) Yang, H.; Xu, Z.; Fan, M.; Slimane, R. B.; Bland, A. E.; Wright, I. Progress in carbon dioxide seperation and capture: A review. *J. Environ. Sci.* **2008**, *20*, 14–27.

(51) Kapdi, S. S.; Vijay, V. K.; Rajesh, S. K.; Prasad, R. Biogas scrubbing, compression and storage: Perspective and prospectus in Indian context. *Renew. Energy* **2005**, *30* (8), 1195–1202.

(52) Satyapal, S.; Filburn, T.; Trela, J.; Strange, J. Performance and properties of a solid amine sorbent for carbon dioxide removal in space life support applications. *Energy and Fuels* **2001**, *15* (2), 250–255.

(53) Builes, S.; López-Aranguren, P.; Fraile, J.; Vega, L. F.; Domingo, C. Analysis of CO 2 Adsorption in Amine-Functionalized Porous Silicas by Molecular Simulations. *Energy & Fuels* **2015**, *29* (6), 3855–3862.

(54) Chang, G.; Yang, L.; Yang, J.; Huang, Y.; Cao, K.; Ma, J.; Wang, D. A nitrogen-rich, azaindole-based microporous organic network: synergistic effect of local dipole–π and dipole–quadrupole interactions on carbon dioxide uptake. *Polym. Chem.* **2016**, *7* (37),

5768–5772.

(55) Auta, M.; Umaru, M.; Yahya, M. D.; Adeniyi, O. D.; Aris, I. M.; Suleiman, B. Diethanolamine Functionalized Waste Tea Activated Carbon for CO 2 Adsorption. **2015**.

(56) Kim, K.; Han, J. W.; Lee, K. S.; Lee, W. B. Promoting alkali and alkaline-earth metals on MgO for enhancing CO2 capture by first-principles calculations. *Phys. Chem. Chem. Phys.* **2014**, *16* (45), 24818–24823.

(57) Mahurin, S. M.; Górka, J.; Nelson, K. M.; Mayes, R. T.; Dai, S. Enhanced CO2/N2 selectivity in amidoxime-modified porous carbon. *Carbon N. Y.* **2014**, *67*, 457–464.

(58) Li, K.; Jiang, J.; Tian, S.; Yan, F.; Chen, X. Polyethyleneimine–nano silica composites: a low-cost and promising adsorbent for CO\n 2\n capture. *J. Mater. Chem. A* **2015**, *3* (5), 2166–2175.

(59) Gargiulo, N.; Peluso, A.; Aprea, P.; Pepe, F.; Caputo, D.; Ingegneria, D.; Sannio, U.; Roma, P. CO 2 Adsorption on Polyethylenimine-Functionalized SBA-15 Mesoporous Silica : Isotherms and Modeling. *J. Chem. Eng. Data* **2014**, *59*, 896−902.

(60) Hudson, M. R.; Queen, W. L.; Mason, J. A.; Fickel, D. W.; Lobo, R. F.; Brown, C. M. Unconventional, highly selective CO 2 adsorption in zeolite SSZ-13. *J. Am. Chem. Soc.* **2012**, *134* (4), 1970–1973.

(61) Zhang, Z.; Yao, Z.-Z.; Xiang, S.; Chen, B. Perspective of microporous metal–organic frameworks for CO 2 capture and separation. *Energy Environ. Sci.* **2014**, *7* (9), 2868.

(62) Wang, K.; Huang, H.; Liu, D.; Wang, C.; Li, J.; Zhong, C. Covalent Triazine-Based

Frameworks with Ultramicropores and High Nitrogen Contents for Highly Selective CO2 Capture. *Environ. Sci. Technol.* **2016**, *50* (9), 4869–4876.

(63) Xiong, S.; Fu, X.; Xiang, L.; Yu, G.; Guan, J.; Wang, Z.; Du, Y.; Xiong, X.; Pan, C. Liquid acid-catalysed fabrication of nanoporous 1,3,5-triazine frameworks with efficient and selective CO2 uptake. *Polym. Chem.* **2014**, *5* (10), 3424.

(64) Martunus; Helwani, Z.; Wiheeb, A. D.; Kim, J.; Othman, M. R. Improved carbon dioxide capture using metal reinforced hydrotalcite under wet conditions. *Int. J. Greenh. Gas Control* **2012**, *7*, 127–136.

(65) Lee, Z. H.; Lee, K. T.; Bhatia, S.; Mohamed, A. R. Post-combustion carbon dioxide capture: Evolution towards utilization of nanomaterials. *Renew. Sustain. Energy Rev.* **2012**, *16* (5), 2599–2609.

(66) Besson, R.; Rocha Vargas, M.; Favergeon, L. CO 2 adsorption on calcium oxide: An atomic-scale simulation study. *Surf. Sci.* **2012**, *606* (3-4), 490–495.

(67) Chen, C.; Park, D. W.; Ahn, W. S. CO2 capture using zeolite 13X prepared from bentonite. *Appl. Surf. Sci.* **2014**, *292*, 63–67.

(68) Cheung, O.; Bacsik, Z.; Liu, Q.; Mace, A.; Hedin, N. Adsorption kinetics for CO2 on highly selective zeolites NaKA and nano-NaKA. *Appl. Energy* **2013**, *112*, 1326–1336.

(69) Li, G.; Xiao, P.; Webley, P. A.; Zhang, J.; Singh, R. Competition of CO2/H2O in adsorption based CO2 capture. *Energy Procedia* **2009**, *1* (1), 1123–1130.

(70) Ferreira, L. S.; Trierweiler, J. O. Modeling and simulation of the polymeric nanocapsule

formation process. *IFAC Proc. Vol.* **2009**, *7* (PART 1), 405–410.

(71) Himeno, S.; Tomita, T.; Suzuki, K.; Yoshida, S. Characterization and selectivity for methane and carbon dioxide adsorption on the all-silica DD3R zeolite. *Microporous Mesoporous Mater.* **2007**, *98* (1-3), 62–69.

(72) Lu, W.; Yuan, D.; Sculley, J.; Zhao, D.; Krishna, R.; Zhou, H. C. Sulfonate-grafted porous polymer networks for preferential Co 2 adsorption at low pressure. *J. Am. Chem. Soc.* **2011**, *133* (45), 18126–18129.

(73) Ragon, F.; Campo, B.; Yang, Q.; Martineau, C.; Wiersum, A. D.; Lago, A.; Guillerm, V.; Hemsley, C.; Eubank, J. F.; Vishnuvarthan, M.; et al. Acid-functionalized UiO-66(Zr) MOFs and their evolution after intra-framework cross-linking: structural features and sorption properties. *J. Mater. Chem. A* **2015**, *3* (7), 3294–3309.

(74) Yang, F.-M.; Liu, Y.; Chen, L.; Au, C.-T.; Yin, S.-F. Synthesis of amine-modified solid Fe-Zr adsorbents for CO_2 adsorption. *J. Chem. Technol. Biotechnol.* **2015**, No. August, n/a – n/a.

(75) Lee, M. S.; Park, S. J. Silica-coated multi-walled carbon nanotubes impregnated with polyethyleneimine for carbon dioxide capture under the flue gas condition. *J. Solid State Chem.* **2015**, *226*, 17–23.

(76) Guo, L.; Hu, X.; Hu, G.; Chen, J.; Li, Z.; Dai, W.; Dacosta, H. F. M.; Fan, M. Tetraethylenepentamine modified protonated titanate nanotubes for CO2 capture. *Fuel Process. Technol.* **2015**, *138*, 663–669.

(77) Yao, M.; Dong, Y.; Feng, X.; Hu, X.; Jia, A.; Xie, G.; Hu, G.; Lu, J.; Luo, M.; Fan, M. The effect of post-processing conditions on aminosilane functionalizaiton of mesocellular silica foam for post-combustion CO2 capture. *Fuel* **2014**, *123*, 66–72.

(78) Wang, D.; Sentorun-Shalaby, C.; Ma, X.; Song, C. High-capacity and low-cost carbon-based "molecular basket" sorbent for CO2 capture from flue gas. *Energy and Fuels* **2011**, *25* (1), 456–458.

(79) Yu, C. H.; Huang, C. H.; Tan, C. S. A review of CO2 capture by absorption and adsorption. *Aerosol Air Qual. Res.* **2012**, *12* (5), 745–769.

(80) Bollini, P.; Brunelli, N. A.; Didas, S. A.; Jones, C. W. Dynamics of CO2 adsorption on amine adsorbents. 1. impact of heat effects. *Ind. Eng. Chem. Res.* **2012**, *51* (46), 15145–15152.

(81) Kizzie, A. C.; Wong-Foy, A. G.; Matzger, A. J. Effect of humidity on the performance of microporous coordination polymers as adsorbents for CO2 capture. *Langmuir* **2011**, *27* (10), 6368–6373.

(82) Neti, V. S. P. K.; Wang, J.; Deng, S.; Echegoyen, L. High and selective CO 2 adsorption by a phthalocyanine nanoporous polymer. *J. Mater. Chem. A* **2015**, *3* (19), 10284–10288.

(83) Tan, M. X.; Zhang, Y.; Ying, J. Y. Mesoporous poly(melamine-formaldehyde) solid sorbent for carbon dioxide capture. *ChemSusChem* **2013**, *6* (7), 1186–1190.

(84) Wu, D.; Xu, F.; Sun, B.; Fu, R.; He, H.; Matyjaszewski, K. Design and preparation of porous polymers. *Chem. Rev.* **2012**, *112* (7), 3959–4015.

(85) Puthiaraj, P.; Kim, S. S.; Ahn, W. S. Covalent triazine polymers using a cyanuric chloride precursor via Friedel-Crafts reaction for CO<inf>2</inf> adsorption/separation. *Chem. Eng. J.* **2016**, *283*, 184–192.

(86) Das, S. K.; Wang, X.; Ostwal, M. M.; Zhao, Y.; Han, Y.; Lai, Z. Highly stable porous covalent triazine-piperazine linked nanoflower as a feasible adsorbent for flue gas CO2 capture. *Chem. Eng. Sci.* **2016**, *145*, 21–30.

(87) Gu, C.; Liu, D.; Huang, W.; Liu, J.; Yang, R. Synthesis of covalent triazine-based frameworks with high CO 2 adsorption and selectivity. *Polym. Chem.* **2015**, *6*, 7410–7417.

(88) Liebl, M. R.; Senker, J. Microporous functionalized triazine-based polyimides with high CO 2 capture capacity. *Chem. Mater.* **2013**, *25* (6), 970–980.

Chapter 2. Hydrophobic Mesoporous Polymeric Adsorbent for Siloxane Removal

2.1 Introduction

One of the main challenges in the consumption of biogas is volatile organic silicon compounds impurities including siloxanes. Biogas was produced by micro-organisms in the absence of air produce through anaerobic metabolism[1] which may contain traces of various adverse compounds[2]. During biogas combustion in engines which has siloxanes impurities, an abrasive microcrystalline silica gets deposited[3, 4] that results in considerable damage to the energy recovery systems. D6 as a large molecule of siloxane may decompose to smaller molecules such as D4 or D5, which evaporate easily[5]. In order to meet the limitation of manufacturers of energy recovery systems (0.03-28 mg/m^3), the siloxane level should be kept under one part per million (ppm)[6]. Therefore, biogas cleaning becomes a crucial process to prevent high annual costs of maintenance and renovation.

The extensive applications of siloxane-contained compounds such as personal care products, pharmaceuticals, lubricants, adhesives, elastomeric usage and heat-transfer fluids lead to a considerable amount of siloxane in sewage gases [5, 7] which is due to the favourable properties of siloxanes such as low surface tension, high compressibility, low allergy generation, and low toxicity.

To remove siloxanes from biogas, several techniques have been applied including absorption[8], bio-filtration[9], adsorption[10], peroxidation[11], cryogenic separation[12], membrane filtering[13] and catalytic processing[14]. Adsorption methods are the most widely

used techniques for several solid adsorbents[15-19] including inorganic adsorbents of silica[16], alumina[20], activated carbons or activated charcoal (ACs)[21] and organic adsorbents such as amorphous organic polymers[15], Tenax, and Amberlite[22]. Most of them indicated relatively low capacity (100-400 mg/g) and poor regenerability. However, ACs have shown interesting adsorption capacities (800-1700 mg/g), so they have been extensively used to remove siloxane contaminants with the advantages of their high surface areas and large pore volumes[5, 10, 17, 23]. Although several ACs are commercially used as adsorbents, their complete regeneration remains a challenge. Strong binding between adsorbate and adsorbent[19] or polymerization of siloxanes on the surfaces of AC[5] could be an explanation for difficult recovery. Also, partial hydrophilicity of ACs negatively effect siloxane adsorption from humid gas streams.

Some porous polymers have shown enormous potential in the area of adsorption of different organic molecules such as dyes and oils[24]. Polymers can be modified readily by a functional group to develop adsorptive properties. Another interesting feature of polymeric structures is the potential of becoming hydrophobic[25] by varying the copolymer type or becoming hydrophilic[26] with loaded heteroatoms (such as LiCl) which makes such materials applicable as a humidity sensor. The synthesis of a hydrophobic material with high adsorption properties for organic molecule removal is necessary to solve current problems in biogas purification technology. PDVB has been synthesized in many structures such as microspheres[27], macroporous monoliths[28], and mesoporous[24-26, 29] structures for diverse applications including water treatment[24], humidity sensing[26], benzoin condensation[25] and adsorption[29].

In this study, we examined the selective capture of siloxane by several PDVB adsorbents, with the focus on the removal of octamethylcyclotetrasiloxane (D4) which is highly abundant in biogas. The synthesis of mesoporous polymer was done by copolymerization of monomers of DVB and 1-vinylimidazole (PDVB-VI-x, where x stands for the molar ratio of DVB over VI) under solvothermal conditions. An investigation on improvement of porous PDVB was conducted with the objective of copolymer incorporation into the polymer structure for siloxane capture.

The superhydrophobic adsorbents perform as novel sorbents and possess abundant mesopores, good air-stability and super wettability for siloxane removal, which results in their very high adsorption capacities. High surface area and large pore volume of PDVB-VI-x lead to effective routes to efficient and stable adsorbents, which is important for the wide applications of solid bases in the adsorption industry.

2.2 Experimental Section

2.2.1 Chemicals

Divinylbenzene (technical grade, 80%) 1-Vinylimidazole (VI) (99%), 2,2 ´ -Azobis(2-methylpropionitrile) (AIBN), Ethyl acetate (EtoAC) and Tetrahydrofuran (THF) were purchased from Sigma-Aldrich. All chemicals were used as received and used without further purification.

2.2.2 Preparation of Imidazole Functionalized-Polydivinylbenzene (PDVB-VI-x)

Imidazole functionalized mesoporous polymers of PDVB-VI-x were solvothermally synthesized from the copolymerization of DVB with VI (as shown in **Figure 2.1**), which was achieved with DVB/VI at molar ratios in the range of 1/0.5 to 1/0.12. In a typical experiment, 2.0 g of divinylbenzene (DVB) and 0.74 g of VI were added into a solution containing 0.0625 g of

azobisisobutyronitrile (AIBN) and 30 mL of ethyl acetate. After stirring at room temperature for 3 h, the mixture was transferred into an autoclave and heated at 100°C for 24 h. After slowly evaporating the solvent at room temperature for 2 days, the solid with monolith morphology designated as PDVB-VI was obtained. For comparison, PDVB was synthesized according to the literature[24, 26]. In a typical synthesis, 2 g DVB was dissolved in 20 mL tetrahydrofuran (THF) with 0–2 mL deionized water, and then 0.05 g AIBN was added. After stirring for 4 h at room temperature, the solution was placed in an autoclave and then treated at 60–100°C for 24 h. The system was cooled to room temperature and a dry solid monolith was obtained after the slow evaporation of the solvent.

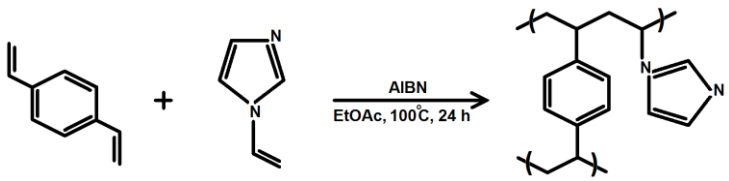

Figure 2.1 Synthesis procedure for PDVB-VI-x.

2.2.3 Characterization of PDVB-VI-x

Nitrogen adsorption desorption isotherms were obtained using a Micromeritics ASAP 2020M system. The samples were outgassed for 10 h at 150°C before the measurements. The pore size distribution of the samples was calculated using the Barrett–Joyner–Halenda (BJH) model. Fourier transform infrared spectroscopy (FTIR) spectra were recorded by using a Bruker 66V FTIR spectrometer. Thermo-gravimetric analyses (TGA) were achieved on a Perkin-Elmer TGA7 with a heating rate of 10°C/min. Scanning electron microscopy (SEM) images were performed on JSM-6700F electron microscopes. Contact angles were obtained with a DSA10MK2G140 instrument, Kruss Company, Germany.

2.2.4 Siloxane Adsorption by PDVB-VI-x

A nitrogen stream passes through two separate bubblers containing D4 and water (in the case of having relative humidity). ALICAT mass flow controllers control the flow rate. Then the gas passes through the adsorbent bed, which is fixed with glass wool at the two ends of a tube with dimensions of 0.25 inch diameter and 7.0 inch length. The gas stream was finally trapped by a hexane solution, which is placed in an ice-bath. A blank run was conducted with only glass wool in the tube (no adsorbent). The amount of siloxane in the trap was determined using gas chromatography mass spectroscopy (GC/MS), GCMSD-5975 from Agilent (Single quad spectrometer with a Quadrex 007-5-15-0.33F column) for a limited length of time (3 h). Then for each adsorbent GC, which is calibrated based on standard solutions of siloxane, evaluated the amount of D4 in hexane. The difference between siloxanes in the trap for the blank run and adsorbent loaded one would be the adsorbed D4 on the adsorbent bed. GC (with split ratio of 20:1) detects D4 by auto-sampler injection. In the adsorption process, our material was compared with the widely used commercial activated charcoal (AC) purchased from Sigma-Aldrich.

2.3 Results

2.3.1 Characterization of Fresh Adsorbent

Scanning Electron Microscopy (SEM). Figure 2.2 showed the electron microscopic images of PDVB and PDVB-VI. SEM images (**Figure 2.2A** and **B**) showed that PDVB and PDVB-VI have a rough surface with abundant mesopores. Given the pore size, ranged 5-100 nm, this is in agreement with N_2 isotherms results (**Figure 3**). The scanning electron microscopy images indicated that PDVB and PDVB-VI exhibit a mesoporous

structure, ideal for facilitating fast diffusion, which further results in their high exposure on adsorption.

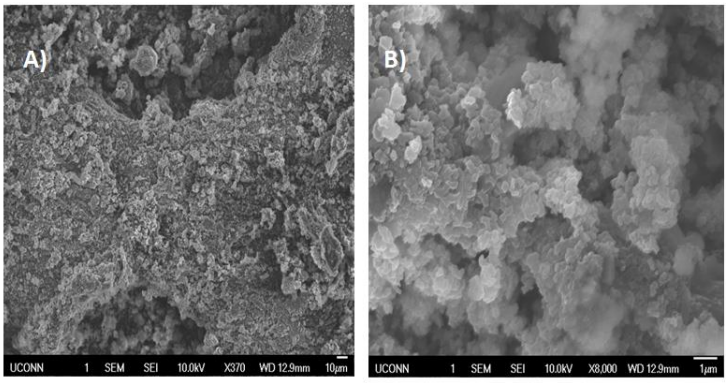

Figure 2.2 SEM image of PDVB-VI-0.5 A)X370, B)X8000.

Brunauer–Emmett–Teller (BET) Isotherm. Figure 2.3A shows the N_2 adsorption-desorption isotherms of PDVB and PDVB-VI-x. For all PDVB samples, Type IV curves were observed with a sharp capillary condensation step at a relative pressure of P/P_0 = 0.7–1.0, indicating the presence of abundant mesopores in these samples[30]. Additionally, all porous PDVB have large BET surface areas in the range of 594 to 830 m^2/g and uniform pore diameters centred at 25.3 to 15.97 nm were observed. Additionally, the changes in total pore volume are relatively linear because of VI addition. At a very low amount of copolymer (x=0.12), total pore volume increased from 1.66 to 1.75 cc/g by incorporation of VI to PDVB structure. Further copolymerization reduces the total pore to 1.16 cc/g. The large surface area, uniform large pore sizes, and high pore volume were the factors behind their superior adsorption performances.

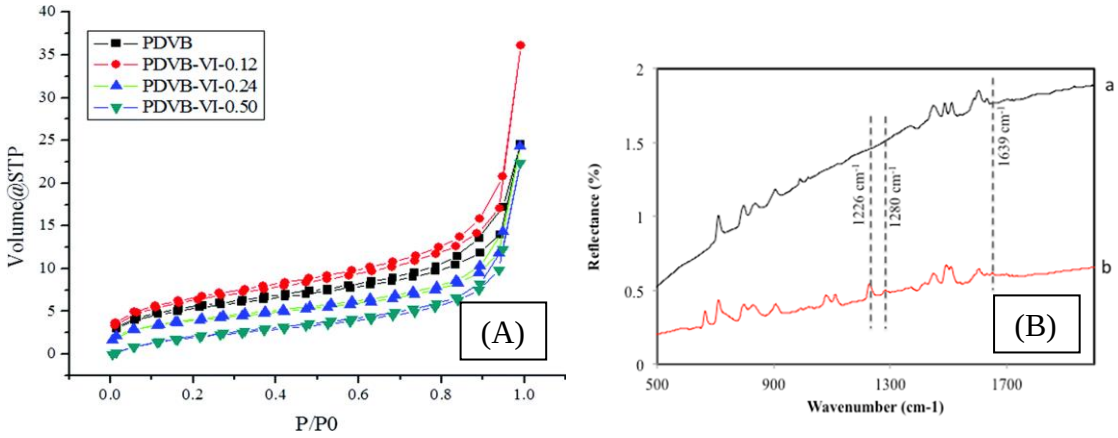

Figure 2.3 (A) Nitrogen isotherms of PDVB (black), PDVB-VI-0.12 (red), PDVB-VI-0.24 (blue) and PDVB-VI-0.5 (green), (B) FT-IR of (a) PDVB and (b) PDVB-VI-0.5.

Fourier Transform Infrared Spectroscopy (FTIR). Figure 2.3B showed PDVB, PDVB-VI infrared peaks. In the FTIR characterization, the reflectance mode was used. Comparing PDVB-VI to PDVB, peaks around 1679, 1280 and 1226 cm^{-1} associated with C-N and C=N species indicate successful incorporation of the imidazole group into the network of the porous polymer to make PDVB-VI[31]. Vinylimidazole underwent radical polymerization along with the DVB to form a copolymerized and cross-linked network comprising the two co-monomers in PDVB-VI.

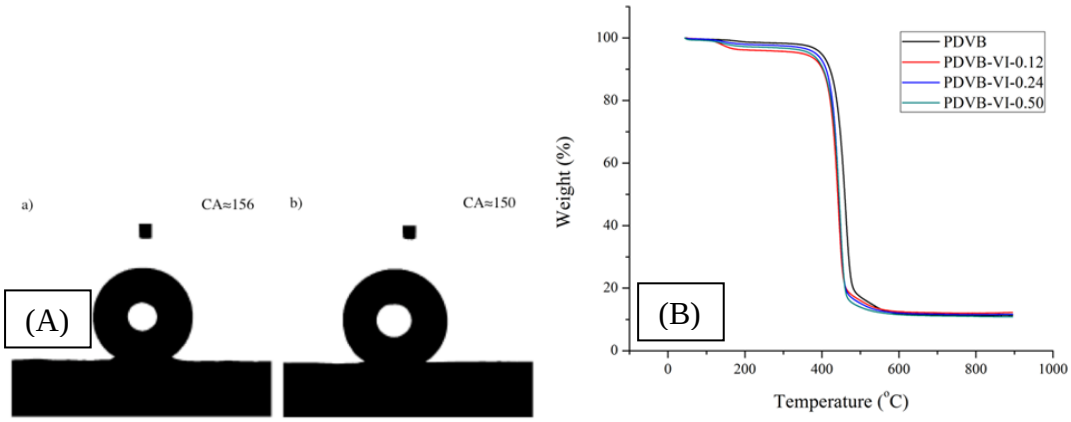

Figure 2.4 (A) The water contact angle results of a) PDVB and b) PDVB-VI-0.5, (B) Thermo gravimetric analysis of PDVB and PDVB-VI-x (x=0.12, 0.24, and 0.5)

Contact Angle Measurement. Figure 2.4A shows the water contact angle of PDVB and PDVB-VI, which indicate their hydrophobicity. A water droplet, in contact with PDVB yielded a contact angle up to 156° (Figure 5a), indicating its super-hydrophobic character. In the sample of PDVB-VI-0.5, the water contact angle was 148° (Figure 5b). While there was a small drop in the water contact angle with PDVB-VI-0.5, this value is still high enough for the sample to exhibit excellent hydrophobicity.

Thermo Gravimetric Analysis (TGA). Figure 2.4B shows the thermal stability of PDVB-VI-x mesoporous polymers. Both types of PDVB (with and without imidazole group incorporation) have good thermal stability in which less than 3% weight loss was observed up to 400°C, which may relate to remaining solvent in the polymer.

2.3.2 Characterization of Spent Adsorbent

In **Figure 2.5A**, the FTIR spectrums of the PDVB-VI before and after adsorption are shown. The qualitative analysis of siloxane D4 in the PDVB-VI can be performed by following the intensity of the bands at 1074 and/or 810 cm^{-1}, which may be ascribed to

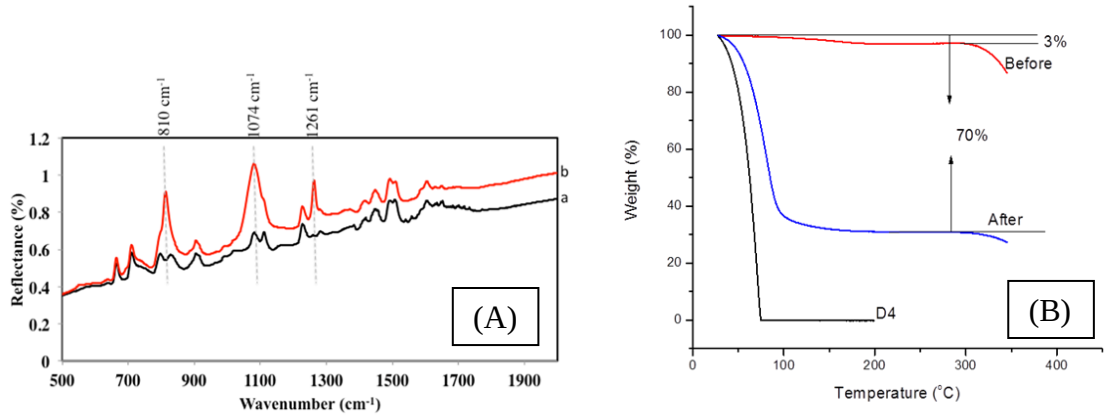

Figure 2.5 (A) FTIR of PDVB-VI-x before and after adsorption (x=0.5), (B) Thermo gravimetric analysis of D4, PDVB-VI-x before and after adsorption process (x=0.5).

the asymmetric and symmetric stretching of the Si-O-Si siloxane bridge bonds of siloxane D4. The Si-CH_3 bond can be seen clearly at 1261 cm^{-1}. Furthermore, the TGA result (**Figure 2.5B**) confirms the huge adsorption of D4 by our material, which shows rapid weight loss (67%) of PDVB-VI-0.5 after exhaustion in the temperature range of 25 to 100^{o}C, which is in the range of D4 decomposition.

To investigate the exhausted PDVB-VI textural changes, solid-state ^{29}Si NMR measurements were carried out (**Figure 2.6A**). While there is no Si peak in the porous adsorbent prior to adsorption, a bulk siloxane-D4 peak appears at -19.2 ppm after adsorption showing the adsorption and possible entrapment of the siloxane inside the porous adsorbent structure.

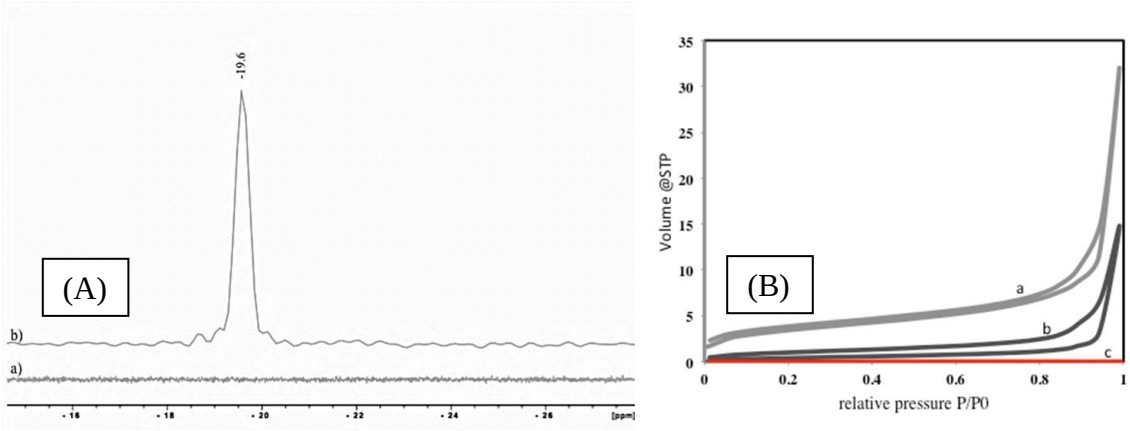

Figure 2.6 (A) ^{29}Si NMR on PDVB-VI-0.5 a) before and b) after adsorption, (B) Effect of adsorption on BET surface area of PDVB-VI-0.5, a) before and b,c) after adsorption.

Figure 2.6B shows the BET isotherms for the adsorbent before and after D4 capture. The surface area of the adsorbent, shown as (a), is computed to be 594 m^2/g, which reduced to 72 m^2/g after several hours of exposure to the adsorbent, shown as (b) and then to 0 m^2/g after complete saturation, shown as (c). This demonstrated that the siloxane keeps filling up the pores of the porous adsorbent until a saturation point is reached wherein no more adsorption can take place.

The average pore volume, after adsorption is reduced to 0.76 cc/g after three hours of exposure to the high concentration of siloxane. After the saturation, pore volume is reduced to a level that was below the computation capability of the instrument. This indicates there are probably multiple adsorption and entrapment sites inside each pore, which fill up gradually as indicated by the gradual decrease in the average pore size. This continues until the pores can accommodate no more siloxane moieties and becomes unavailable for further adsorption.

Adsorption Curves under Dry Condition. In order to obtain the adsorptive activity of PDVB-VI-x in comparison with available commercial AC, 10 sccm of nitrogen flow was

bubbled in D4, which passes through the adsorbent bed. A flow rate of 10 sccm provides an even higher amount of D4 than real concentration of siloxane in the biogas. **Figure 2.7A** shows the adsorptive activity of PDVB-VI samples in comparison with commercial AC. None of PDVB-VI-x was exhausted during the adsorption process. Similarly, commercial AC does not show failure of adsorption under the same conditions.

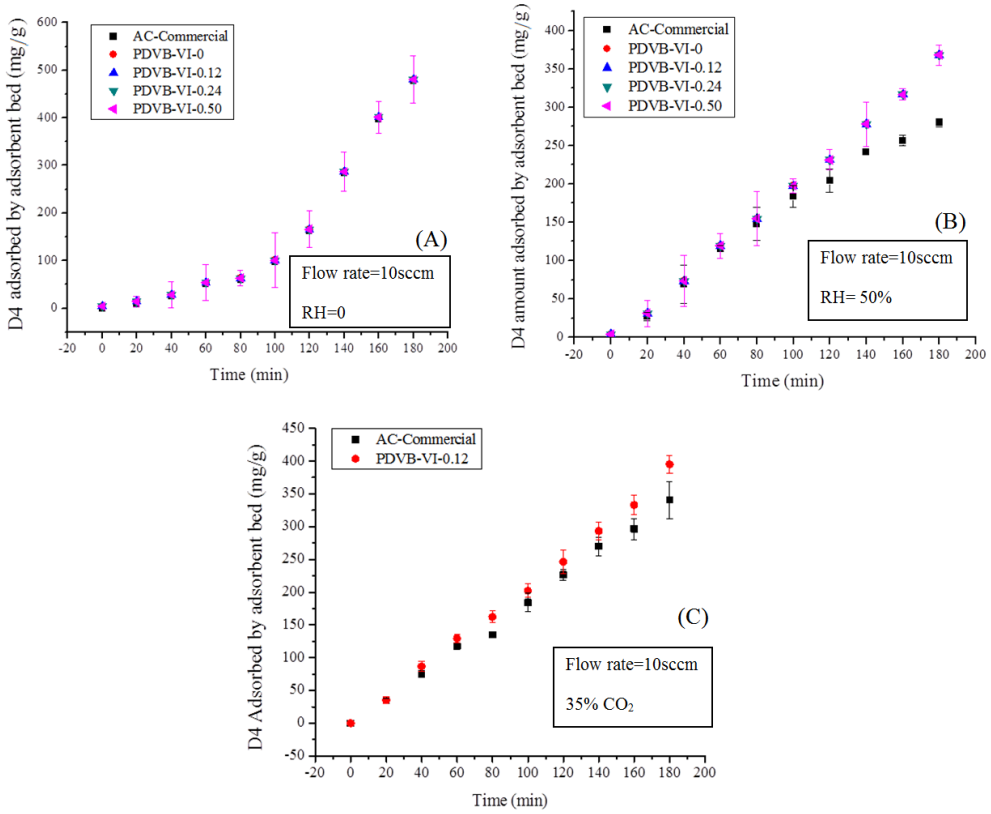

Figure 2.7 (A) Adsorption activity of AC and PDVB-VI-x under dry conditions with flow rates of 10 sccm (x=0, 0.12, 0.24 and 0.5), (B) Breakthrough curve (adsorption activity) of AC and PDVB-VI-x at 50% relative humidity and 10 sccm flow rates (x=0, 0.12, 0.24 and 0.5), (C) Breakthrough curve (adsorption activity) of AC and PDVB-VI-x under 10 sccm flow of 35%CO2 (x= 0.12).

Adsorption Curves under Humid Condition. As biogas usually contains moisture, it is important to consider this kind of harsh condition during the adsorption process. The

mesoporous PDVB-VI-x materials were assessed under moisture conditions with a relative humidity (RH) of 50%. **Figure 2.7B** illustrates that commercial AC starts to breakthrough after 100 min, which indicates its earlier failure in compare with PDVB-VI. When RH was increased, PDVB-VI samples still adsorbed all D4 in the gas stream (similar to dry conditions, no exhaustion was observed). This activity might be attributed to the superhydrophobicity of PDVB materials that leads to its high activity even under wet conditions. While commercial AC adsorption performance reduces under humid environments, PDVB-VI-x not only has a high ability to capture D4, but also overcomes the limitation of deactivation of ACs by water vapor.

Adsorption Curves under Mixed Gas. The presence of CO_2 may change the adsorption performance of siloxane because of its high concentration (up to 35% (vol-%)). The mesoporous PDVB-VI-x materials were evaluated under a mixture of CO_2 and siloxane (35% CO_2). **Figure 2.7C** displays no exhaustion of PDVB-VI-x and commercial AC under a gas mixture of CO_2. However, the commercial AC shows less activity toward siloxane capture than PDVB-VI-x.

2.3.3 Capacity Determination

To calculate the capacity (mg-D4/g-adsorbent), the solid adsorbent was saturated by siloxane with continuous gas flow for 17 h (100 sccm). The exhausted adsorbent was washed off by hexane and then the solvent was tested by GC/MS to evaluate the amount of captured D4. As mentioned before, synthesized PDVB contains about 3% solvent residue (THF), which may have an effect on adsorption performance of the material.

Table 2.1 Adsorption capacity of PDVB-VI-x and AC under dry and moisture conditions.

Materials	Surface area (m^2/g)	Pore volume (cc/g)	Capacity (GC) (mg/g) RH=0	Capacity (GC) (mg/g) RH=50%
Commercial AC	695	0.52	856±54	547±83
PDVB	831	1.66	1951±74	1940±32
PDVB-VI-0.12	780	1.75	2370±92	2360±50
PDVB-VI-0.24	670	1.3	1586±71	1582±38
PDVB-VI-0.50	594	1.15	1384±62	1381±40

Table 2.1 shows textural and adsorptive comparison of commercial AC and PDVB-VI-x (x=0-0.5). PDVB-VI-x actively remove D4 as a non-precedent "super-adsorbent" which may markedly help the problematic issue related to the utilization of biogas. Such a huge capacity for siloxane removal has not been reported to date.

Table 1, also explains the effect of the copolymer (VI) addition to the PDVB structure simultaneously, revealing the moisture resistance of PDVB-VI-x. Addition of the copolymer in the synthesis of PDVB-VI enhanced the adsorption performance of the material at an optimum level of VI. As the amount of VI increased in the x ratio to 0.12,

the adsorption behavior improved. However, further enhancement of x to 0.24 and 0.50 decreased the adsorption activity in comparison with PDVB.

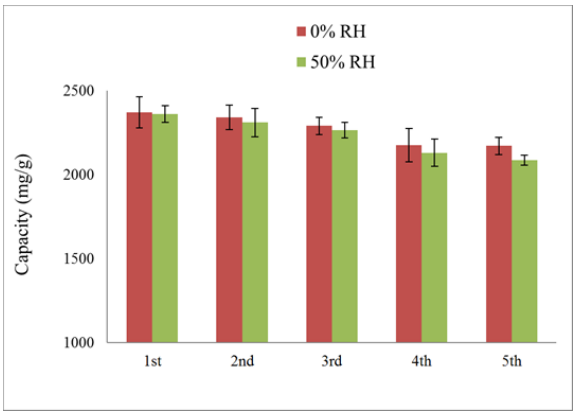

Figure 2.8 Regeneration of PDVB-VI-x under both dry and moisture conditions (x= 0.12).

2.3.4 Adsorbent Regeneration

Not only does the adsorbent need to have high capacity of adsorption under dry and humid mixture conditions, but its capacity also needs to remain the same after being exhausted repeatedly. For the developed super-adsorbent PDVB-VI-0.12, the reusability was tested under dry and moist conditions (**Figure 2.8**). For regeneration, the adsorbent was heated to 100^{o}C in air overnight. This showed that PDVB-VI is able to adsorb almost the same amount of siloxane with less than 5% loss in capacity. This indicates that siloxane molecules are not tightly bonded to PDVB-VI because of its ease-recovery at low temperatures. However, ACs were hardly recovered at higher temperatures (250-300^{o}C) for a longer period of time[19] which might be related to the polymerization of D4 on the surface of ACs suggested by Cabrera-Codony due to the phenolic and carboxylic on its surface[5]. Readily regenerated PDVB-VI might be an

indication that such a phenomenon could not occur for this mesoporous polymer since D4-polymerization hinders the thermal regeneration process.

2.4 Discussion

Figure 2.9 shows the correlation of the adsorptive capacity with BET surface area and total pore volume data. **Figure 2.9a** indicated that for the imidazole incorporated to PDVB, surface area controls the adsorption performance at both low and high amounts of the copolymer. Overall, there is a relatively good relationship between D4 capture and the surface area of PDVB-VI-x. Additionally, there is a good correlation between adsorptive capacity and total pore volume (**Figure 2.9b**). The addition of the copolymer at a specific level reduces the surface area in comparison with PDVB. However, copolymerization still leads to a high total pore volume, which controls the adsorption procedure. As the cross sectional size of D4 molecule is reported to be 1.08×1.03 nm[32], larger pore volumes are expected to capture more D4 molecules. Consequently, a higher pore volume is more relevant to D4 adsorption. These results are in agreement with literature reports on textural behavior of various ACs[5].

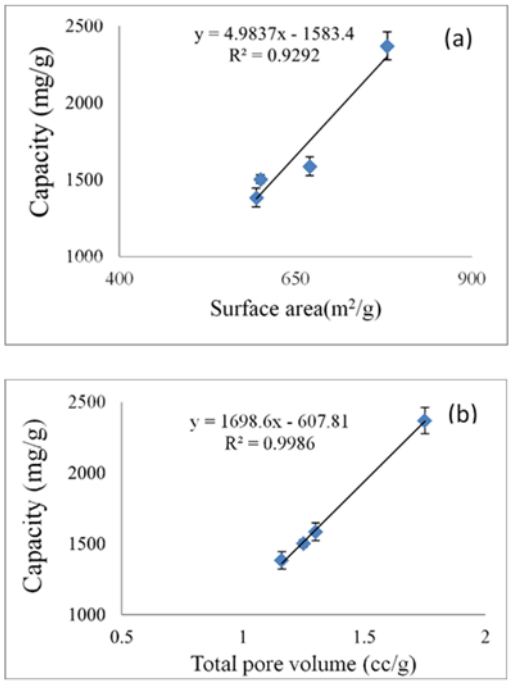

Figure 2.9 (a) Capacity of PDVB-VI-x in correlation with N2 adsorption/desorption isotherm data, a) surface area, b) total pore volume.

2.5 Conclusions

This study suggests a new type of organic D4 adsorbent, which has not been reported up to now. PDVB with a very simple and inexpensive synthesis procedure, showed great adsorption performance, even better than the best ACs reported to date[5]. High surface area and large total pore volume make this mesoporous polymer an efficient siloxane adsorbent. PDVB with Imidazole group incorporation (PDVB-VI-x) opens a new path in the utilization of biogases for energy generation. This work indicates that an optimum amount of copolymer ratio to primary monomer (x=0.12) enhanced the adsorptive capacity of PDVB which also shows a good regenerability at low temperatures. Investigation of textural properties of PDVB-VI reveals that total pore volume is the key parameter in siloxane capture. The PDVB-VI-x activity toward siloxane has not been significantly influenced by the presence of moisture. However, the presence of CO_2 has

interestingly enhanced the adsorption performance of PDVB-VI, which will be explored in the future. In conclusion, development of mesoporous PDVB-VI may open new vistas for the manufacture of more efficient and stable adsorbents with wide potential industrial applications.

2.6 References

(1) E. Ryckebosch, M. Drouillon and H. Vervaeren, *Biomass. Bioenerg.*, 2011, **35**, 1633.

(2) N. de Arespacochaga, C. Valderrama, C. Mesa, L. Bouchy and J.L. Cortina, *Chem. Eng. J.*, 2014, **255**, 593.

(3) N. Nair, A. Vas, T. Zhu, W. Sun, J. Gutierrez, J. Chen, F. Egolfopoulos and T. Tsotsis, *Ind. Eng. Chem. Res.*, 2013, **52**, 6253.

(4) N. Nair , X. Zhang, J. Gutierrez, J. Chen, F. Egolfopoulos and T. Tsotsis, *Ind. Eng. Chem. Res.*, 2012, **51**, 15786.

(5) Cabrera-Codony, M.A. Montes-Moran, M. Sanchez-Polo, M.J. Martin and R. Gonzalez-Olmos, *Environ. Sci. Technol.*, 2014, **48**, 7187.

(6) P. Gilson, S. Galli and G. Monteleon, *Wast. Manage.*, 2013, **33**, 2687.

(7) R. Dewil, L. Appels and J. Baeyens, *Energ. Convers. Manage.*, 2006, **47**, 1711.

(8) L. Ghorbel, R. Tatin and A. Couvert, *Environ. Technol.*, 2014, **35**, 372.

(9) F. Accettola, G.M. Guebitz and R.Schoeftner, *Clean. Technol. Envir.* , 2008, **10**, 211.

(10) M. Yu, H. Gong, Z. Chen and M. Zhang, *J. Environ. Chem. Eng.*, 2013, **1**, 1182.

(11) L. Appelsa, J. Baeyens and R. Dewil, *Energ. Convers. Manage.*, 2008, **49**, 2859.

(12) M. Hagmann, E. Hesse, P. Hentschel and T. Bauer, in *The eighth international waste management and landfill symposium*, eds. T. H. Christensen, R. Cossu and R. Stegmann, Litotipografia Kalb, Cagliari, Italy, 2001, vol. II, pp. 641.

(13) M. Ajhar and T. Melin, *Desalination*, 2006, **200**, 234.

(14) L. Lamaa, C. Ferronatoa, S. Prakasha, L. Finea, F. Jaberb and J.M. Chovelon, *Appl. Catal. B-Environ.*, 2014, **156-157**, 438.

(15) Y. Mito-oka, S. Horike, Y. Nishitani, T. Masumori, M. Inukai, Y. Hijikata and S. Kitagawa, *J. Mater. Chem. A*, 2013, **1**, 7885.

(16) L. Sigot, G. Ducom, B. Benadda and C. Labouré, *Fuel*, 2014, **135**, 205.

(17) E. Finocchio, T. Montanari, G. Garuti, C. Pistarino, F. Federici, M. Cugino and G. Busca, *Energ. Fuel.*, 2009, **23**, 4156.

(18) T. Montanaria, E. Finocchio, I. Bozzano, G. Garuti, A. Giordano, C. Pistarino and G. Busca, *Chem. Eng. J.*, 2010, **165**, 859.

(19) M. Ajhar, M. Travesset, S. Yücea and T. Melina, *Bioresource Technol.*, 2010, **101**, 2913.

(20) E. Finocchio, G. Garuti, M. Baldi and G. Busca, *Chemosphere*, 2008, **72**, 1659.

(21) B. Boulinguiez and P.L. Cloirec, *Energ. Fuel.*, 2010, **24**, 4756.

(22) M. Schweigkofler and R. Niessner, *J. Hazrd. Mater. B*, 2001, **83**, 183.

(23) S. Giraudet, B. Boulinguiez and P. Le Cloirec, *Energ. Fuel.*, 2014, **28**, 3924.

(24) Y. Zhang, S. Wei, Y. He, F. Nawaz, S. Liu, H. Zhang and F. Xiao, *J. Mater. Chem.*, 2010, **20**, 4609.

(25) D. Kuzmicz, P. Coupillaud, Y. Men, J. Vignolle, G. Vendraminetto, M. Ambrogi, D. Taton and J. Yuan, *Polymer*, 2014, **55**, 3423.

(26) T. Fei, K. Jiang, S. Liu and T. Zhang, *Sensor. Actuat. B-Chem.*, 2014, **190**, 523.

(27) F. Bai, X. Yang and W. Huang, *Macromolecules*, 2004, **37**, 9746.

(28) K. Kanamori, K. Nakanishi and T. Hanada, *Adv. Mater.*, 2006, **18**, 2407.

(29) X. Feng, C. Gao, Z. Gua, Y. Zhou and J. Wang, *R. Soc. Chem. Adv.*, 2014, **4**, 23389.

(30) Y. Zhang, S. Wei, F. Liu, Y. Du, S. Liu, Y. Ji, T. Yokoi, T. Tatsumi and F.S. Xiao, *Nano Today*, 2009, **4**, 135.

(31) F. Liu, R.K. Kamat, I. Noshadi, D. Peck, R.S. Parnas, A. Zheng, C. Qi and Y. Lin, *Chem. Commun.*, 2013, **49**, 8456.

(32) J.L. Hamelink, P.B. Simon and E.M. Silberhorn, *Environ. Sci. Technol.*, 1996, **30**, 1946.

Chapter 3. Functionalized PDVB for Arsenate Adsorption

3.1 Introduction

The presence of heavy metals in surface water and ultimately drinking water is one of the most challenging environmental and health threats due to clean water shortages. This condition may get worse because of industrial activities such as battery manufacturing, painting, mining and the use of fertilizers which are the main sources of heavy metal release into water.[1] Over time, heavy metals do not break down to less detrimental species[2] which further necessitates the need for heavy metal elimination from water. International organizations such as WHO (world health organization) regularly study and review the existence of heavy metals and metalloids (chromium, mercury, cadmium, lead and arsenic) and their influence on human health.[3]

Arsenic is a metalloid which is released in water from both natural (weathering and volcanic emissions) and anthropogenic sources (mining wastes, petroleum refining, and ceramic manufacturing). Arsenic is a reported carcinogenic whose exposure is both through breathing and ingestion. High contamination of drinking water by arsenic has been recognized internationally as a serious problem associated with several countries.[4] WHO has recommended the maximum acceptable level of arsenic in drinking water as 10 $\mu g l^{-1}$. Reaching this limit in drinking water would be critical due to the overall abundance of arsenic in different parts of the world.[5] There are different methods to remove heavy metals from drinking water which include oxidation,[6,7] filtration and membrane separation,[8] co-precipitation,[9] flotation,[10] ion-exchange,[11,12] electrodialysis,[13,14] biosorption[15] and adsorption.[16,17] Low cost, and regenerability of adsorbents, flexibility in design and setup, high metal binding capacity, and no pH adjustment requirement,

make adsorption the most promising method.[16,18–20] Various adsorbents have been developed to remove arsenic from aqueous solutions such as activated alumina (AA), natural zeolites, nanoparticles of iron oxides/ hydroxides, alumina, copper oxide, titanium dioxide, zinc oxide, mixed metal oxides, carbon nanotubes, and activated carbons (AC).[4,21–23]

To enhance the efficiency of synthetic adsorbents, different functional groups containing nitrogen, oxygen, or sulfur have been introduced to the surface of adsorbents.[24–27] Functionalization provides an opportunity to make materials with desired surface properties on the already known morphologies.[24] Nitrogen containing functional groups such as amino, imidazole, and amidoxime have been found to be highly effective in heavy metal adsorption due to their complexing nature of metal ions[25,27]. Conventionally, surface functionalization has been achieved through solution based chemistry which is time-consuming, complex and needs several steps. Therefore, development of a facile, fast and single-step approach would be beneficial to make functional adsorbents.[28] Although, nanomaterials offer better diffusibility of heavy metals and consequently better removal, their expensive synthesis approach and high toxicity of the precursors limit their application.[21]

It is imperative to also study the mechanism of interaction between the arsenic anion and the adsorbent. Arsenate anion and aromatic system interactions had previously been deemed unfavorable due to the negative charge associated with both systems. Schneider et al. investigated these interactions and revealed weak but distinct attractive interactions between negative charges and polarizable aryl parts of host–guest systems.[29] Deyà et al. designed the term ‘anionic-π interactions’ to describe these systems.[30] They are defined as non-covalent contacts between electron deficient (π-acidic) aromatic systems and an anion.[31] We propose incorporating

nitrogen functional groups in the polymer backbone of synthetic adsorbents to improve these interactions. The arsenic species that contribute to pollution of drinking water are arsenate (H_3AsO_4, $H_2AsO_4^-$, $HAsO_4^{2-}$ or AsO_4^{3-}) and arsenite (H_3AsO_3, $H_2AsO_3^-$ or $HAsO_3^{2-}$).[23] Arsenate is the most common species found in drinking water so we focus on its removal in our work. We have previously introduced a functionalized high surface area mesoporous polymer of PDVB with an amine group (triazole) in a single-step hydrothermal synthesis to apply for arsenic adsorption from water.[32] Nitrogen sorption (BET), Thermogravimetric analysis (TGA), Fourier transform infrared spectroscopy (FTIR) and X-ray spectroscopy (XPS) has been done to characterize the physical and chemical nature of the adsorbent material. This material proves to be fit for aqueous adsorption application such as arsenate adsorption due to its porous structure, and selective anionic capture. We also correlated theoretical DFT calculations with experimental data which confirmed improved kinetics with the incorporation of triazole.

3.2 Experimental Section

3.2.1 Chemicals

Divinylbenzene (DVB), 1-vinyl-1,2,4-triazole (VT), 2,2 ´ -Azobis(2-methylpropionitrile) (AIBN), dimethylformamide (DMF), disodium hydrogen arsenate (Na2HAsO4.7H2O), Hydrochloric acid and Sodium hydroxide were purchased from Sigma-Aldrich. All chemicals were used without further purification.

3.2.2 Synthesis of mesoporous PDVB and amine functionalized one

Highly hydrophobic poly divinylbenzene was obtained based on reported literature[3334] with small changes. Briefly, divinylbenzene (2 g) in 20 mL of DMF was mixed with the initiator,

AIBN (0.06 g), followed by stirring at room temperature. Then the solution transferred to Teflon-lined autoclave and hydrothermally treated at 100^{o}C for 16 h.

Amine rich PDVB was prepared by radical polymerization of the main monomer of divinyl benzene (2 g) with amine rich co-monomer of VT in 20 mL of DMF. After addition of initiator, AIBN (0.06 g), the solution was stirred at room temperature followed by hydrothermal treatment. PDVB-VT with varied amount of amine rich co-monomer (VT) (0.2-0.9 g) to monomer (DVB) were synthesized in order to obtain the best amine-functionalized adsorbent for the arsenic removal.

3.2.3 Characterization of Functionalized PDVB

A Quantachrome Autosorb-1-1C automated sorption system was used to collect nitrogen sorption isotherms. The adsorbents were degassed at 150°C for 6 h prior to the measurements. The surface areas were calculated by the Brunauer–Emmett–Teller (BET) method and the pore size distributions were calculated by the Barrett–Joyner–Halenda (BJH) method from the desorption isotherm. Thermo-gravimetric analyses (TGA) were achieved on a Perkin-Elmer TGA7 with a heating rate of 10°C/min. Fourier transform infrared spectroscopy (FTIR) spectra were recorded by using a Bruker 66V FTIR spectrometer. To study the surface of synthesized polymer and to further prove the presence of amine moieties, functionalized PDVB was investigated with a PHI 595 multi-probe system using the monochromatic Al Kα source (20 mA, 14 kV).

3.2.4 Arsenate Adsorption

Polymeric adsorbent (20 mg) was mixed with 20 mL of arsenate solution in Nalgene high-speed polycarbonate centrifuge tubes and placed on a Fisher hematology roller mixer to equilibrate at

25°C for 18 h. After equilibration, the solutions were filtered using 0.45μm-PVDF filters. All adsorption experiments were conducted in duplicate and the data reported show the average values. The initial and final solutions were separated and diluted with 1% HNO3 and analysed using an inductively coupled mass spectrometer (ICP-MS) to determine the As (V) concentration. The equilibrium sorption capacity (qe) was calculated based on Equation (1) as follows:

$$qe=((Co-Ce))/m\ V \qquad (1)$$

where Co and Ce represent the concentration of Arsenic before and after adsorption respectively. The mass of the adsorbent is m and *V* is the solution volume.[35]

The effect of pH was investigated in the pH range of 3-13 at a concentration of 200 mg/L. Adjustments of pH were undertaken using 0.1 M NaOH and 0.1 M HCl. For the equilibrium study, the initial As (V) concentrations were varied between 50-250 mg/L at 25 · C. For the kinetics study, the As (V) concentration was kept at 200 mg/L, the adsorbent amount at 100 mg/l and the volume at 300 mL. The pH was kept at the value that corresponded to the highest adsorption. The experiments were carried out in a 500 mL round bottomed flask with a magnetic stirrer. The adsorbent was introduced into the As(V) solution with continuous stirring at 60 rpm and 5 mL aliquots drawn every 20 minutes for 3 h.

The adsorbent being hydrophobic was carefully decanted and then mixed with 10 mL of 0.1 M solution of sodium hydroxide for 2 h allowing the As (V) species to be desorbed from the adsorbent. Then, the adsorbent was washed thoroughly with de-ionized water and left to dry. Five consecutive adsorption-desorption cycles were done. Initially, 100 mg of adsorbent was contacted with 100 mL of As (V) solution at 25°C for 18 h and then separated

3.2.5 Computational Study

Our first-principles calculations were carried out using density functional theory (DFT)[36,37] as implemented by Gaussian 09[38] package for ground state geometrical optimization. Density functional theory with B3LYP functional was incorporated with 6-311+g(d) basis set. At the experimental pH conditions of this study $H_2AsO_4^-$ and $H_2AsO_4^{2-}$ are considered the dominant species. The binding energy (E_{ads}) of $H_2AsO_4^-$ and $H_2AsO_4^{2-}$on the polymer is defined as:

$$E_{ads}(X) = E(X) + E(Polymer) - E(X - Polymer) \qquad (2)$$

where *X* is either $H_2AsO_4^-$ or $H_2AsO_4^{2-}$, *E(X), E(Polymer),* and *E(X-Polymer)* are minimized energies of the free anion, the polymer, and the combined anion with polymer, respectively. First, the minimized energy of isolated monomer and the anion ($H_2AsO_4^-$ or $H_2AsO_4^{2}$) were calculated in isolation and combined. Then the optimized combined structure was placed in a model polymer structure of three monomers and then was optimized again.

3.3 Results

3.3.1 Characterization of Fresh Adsorbent

Nitrogen sorption (BET). Textural properties of mesoporous PDVB before and after insertion of amine-rich co-monomer VT is displayed in **Figure 3.1** and **Table 3.1**.

Table 3.1 Textural properties of hydrothermally synthesized PDVB and amine-functionalized one (PDVB-VT).

Material	Surface area ($m^2.g^{-1}$)	Pore volume ($cc.g^{-1}$)	Pore size (Å)
PDVB	878	1.98	90
PDVB VT0.2	865	2.01	93
PDVB-VT0.7	763	2.04	107
PDVB-VT0.9	745	2.04	110

The surface area was decreased by amine modification of PDVB while both pore volume and pore sizes were increased. The average pore size of both materials is much larger than a single molecule of arsenate ion which is about 4.6 Å.

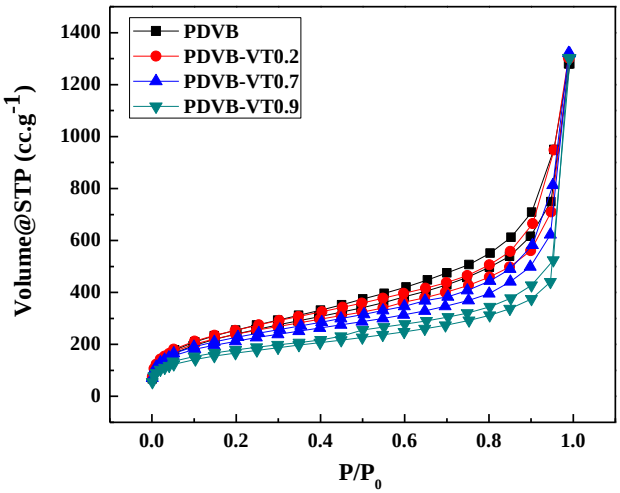

Figure 3.1 Nitrogen sorption isotherms of PDVB and different amount of incorporated amine in the polymer (PDVB-VT).

Thermo-gravimetric analyses (TGA). By introducing amine-functionality to the PDVB, its thermal stability slightly changed (about 40°C) as shown in **Figure 3.2A**. Therefore, amine functionalized PDVB is stable at high temperatures (up to 300°C).

Fourier transforms infrared spectroscopy (FTIR). The comparison between IR bands of PDVB and amine-modified one indicated the presence of amine functionalities in PDVB-VT. The characteristic bands of PDVB were observed at 1500 cm^{-1}, 1600 cm^{-1}, 2920 cm^{-1} and 3030 cm^{-1} for C=C stretching vibration, C-H stretching vibration and aromatic C-H stretching vibration, respectively (**Figure 3.2B**). For PDVB-VT, C-N bands were detected in the range of 1020-1360 cm^{-1} confirming the integration of VT to the polymer.

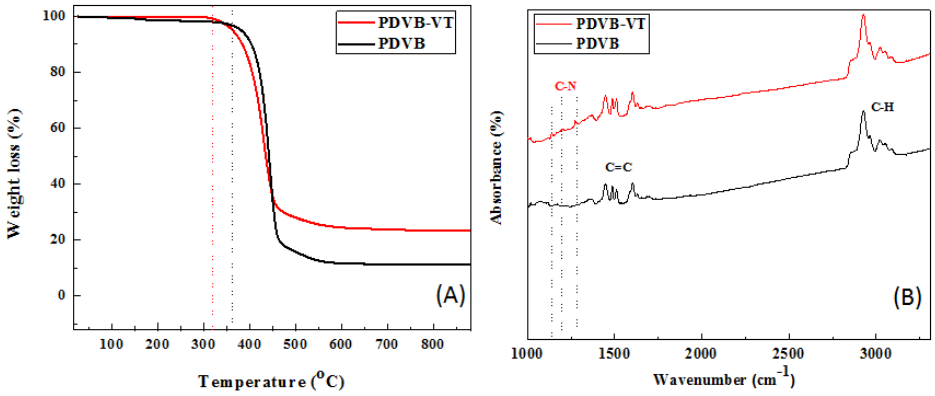

Figure 3.2 (A) Thermal stability of PDVB and PDVB-VT in the nitrogen atmosphere; (B) IR bands of PDVB and PDVB-VT.

X-ray photoelectron spectroscopy (XPS). The 50 eV pass energy was applied to obtain high-resolution spectra of C 1s and N 1s (**Figure 3.3**). Deconvolution of the C 1s and N 1s spectra were conducted using CasaXPS software (version 2.3.12). In C 1s spectrum of PDVB-VT (**Figure 3.3a**), five types of carbon atoms were detected in PDVB-VT. Adventitious carbons were detected at 284.8 eV and other carbon peaks were referenced to that one. The peak at 291.6 eV is a characteristic shake-up line in aromatic compounds (-* transition) which highlighted the aromatic rings that exist in the final polymer. The C=N and C-N bonds were located at 285.8 and 287.0, respectively. The deconvoluted N

1s (**Figure 3.3b**) showed three synthetic peaks which indicated the presence of various types of nitrogen related to the triazole ring. Binding energies of C=N-N, C=N-N, and C-N-N were located at 398.72 eV, 399.75 eV, and 401.10 eV, respectively. The peak at 400.91 eV was assigned to sp^3 nitrogen. Therefore, XPS confirmed the amine incorporation (from VT co-monomer) into PDVB

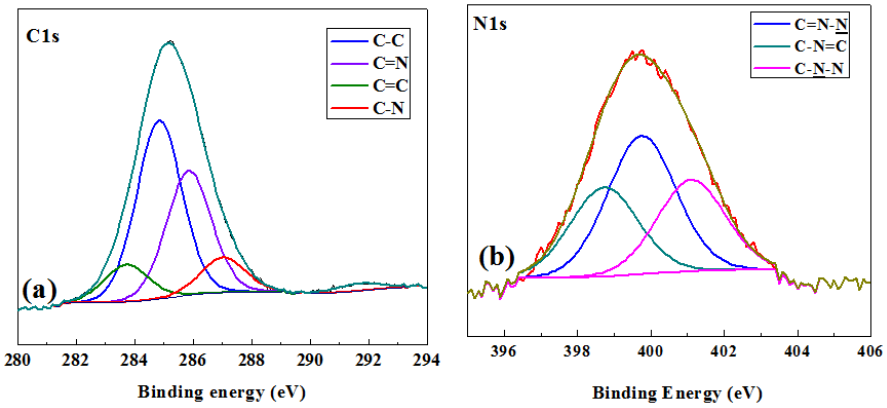

Figure 3.3 XPS of PDVB-VT a) deconvoluted C 1s and b) deconvoluted N 1s

3.3.2 Adsorption Study

Effect of co-monomer loading. The effect of vinyl triazole (VT) loading amount was first investigated without optimization to determine the most efficient amount of VT for adsorption. **Figure 3.4** displays the adsorption efficiency of all PDVB adsorbents for arsenate ions. Integration of VT enhanced the adsorption efficiency significantly in comparison with non-functionalized PDVB. The monomer of VT is known to be hydrophilic and acts as a metal chelator,[39,40] therefore monomer incorporation increased the amount of As (V) ions uptake which could be through both traits. Adsorption of As (V) ions was found to be highest when the amount of VT is 0.2 g. Further increase in the VT loading up to 0.9 g hinders adsorption efficiency which might be an indication that both surface functionalization and the physical characteristics of the adsorbent control the As (V) adsorption. According to BET data, the textural properties of

adsorbents (surface area and pore size) varied by various amount of amine-rich co-monomer incorporation (0.2 to 0.9 g) where surface area decreases from 868 to 750 m^2g^{-1} and pore size of the adsorbent increased from 90 to 110 Å while the pore volume (1.98- 2.04) remained relatively stable. Therefore, the surface area of the amine incorporated PDVB is critical in facilitating adsorption since adsorption decreases with decreasing surface area. However, pure PDVB with the highest surface area showed the lowest adsorption. Therefore, both functionalization and surface area are key elements aiding As (V) adsorption. Amine incorporation increases the rigidity of the polymer backbone [41] which reduces the surface area and increases the pore size.

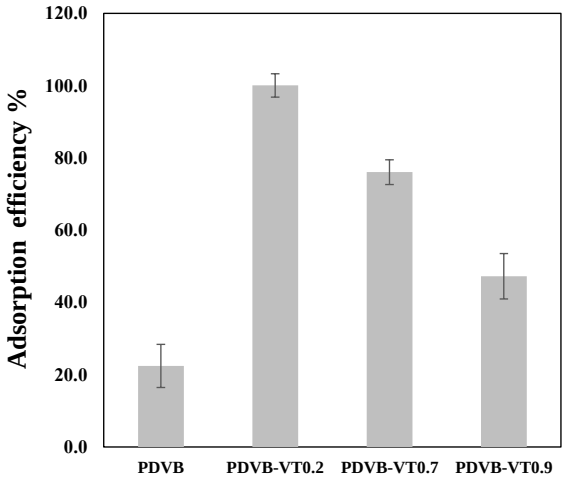

Figure 3.4 Adsorption efficiency of As(V) with different VT ratios. (Conditions: Adsorbent 20mg/L, Volume 20ml, Time 18 h, pH 8.5)

Effect of pH. The pH affects both the speciation of the arsenic species and the surface properties of adsorbent materials.[42] **Figure 3.5a** represents the influence of pH on the adsorption of As (V) on PDVB and PDVB-VT0.2 in the pH range of 3 to 13. The interaction of different arsenic species at different pH can be well understood by **Figure 3.5b**[42] which shows the arsenate ion

speciation at different pH values. Arsenic exists in the 3-, 0, 3+ and 5+ oxidation states which are limited by pH and redox potential. These species include arsenic acids ($HAsO_4^{2-}$, H_2AsO_4, H_3ASO_4), arsenous acids ($HAsO_3^{2-}$, H_2ASO^{3-}, H_3ASO_3), arsine, arsenites, arsenates, etc. [43] The As(V) ions varied as the solution pH increases in which H_3AsO_4 is stable at pH<2.2, $H_2AsO_4^-$ at pH 2.2-6.98, $HAsO_4^{2-}$ at pH 6.98-11.5 and AsO_4^{3-} at pH >11.5.[42–44]

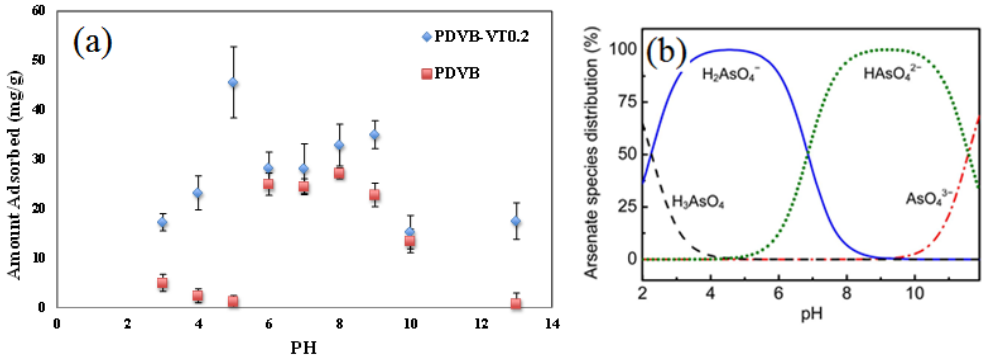

Figure 3.5. Effect of PH on PDVB and PDVB-VT 0.2. b) As(V) ions speciation.

Arsenate adsorption by PDVB-VT0.2 increased from pH 3 to 5 adsorption increased with the maximum absorbance (46 mgg^{-1}) occurring at pH 5. The absorbance decreases by 40% between pH 6-7 and rises by 11-16% between pH 8-9. The absorbance finally decreases by 63-68% between pH 10-13 which indicated great sensitivity to pH. The dominant species around pH of 5 is $H_2AsO_4^-$ in which maximum adsorption efficiency was obtained. $HAsO_4^{2-}$ was also adsorbed efficiently at pH 9 (35 mgg^{-1}). However, non-functionalized PDVB adsorbed arsenate ion ($HAsO_4^{2-}$) efficiently at a pH of 8 (27 mgg^{-1}). There is a 96% drop in the adsorption between pH 9-13. The rest of the experiments were conducted at the pH corresponding to the highest absorbance.

Heavy metal screening. Other than As (V), PDVB-VT0.2 adsorptive properties were evaluated for Cu (II), Cr (III), and Pb (II). **Figure 3.6** shows that As (V) adsorption by PDVB-VT0.2 was the highest at 46 mgg^{-1} and the least was Cu (II) at 4.5 mgg^{-1}. Amine incorporation seems to favor adsorption of the anionic species compared to cationic species.

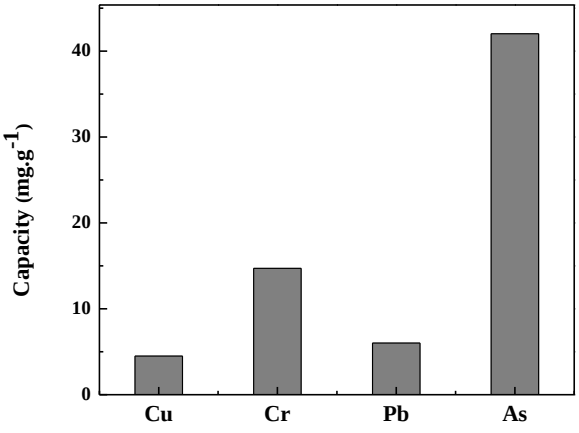

Figure 3.6. Sorption of Cu(II), Cr(III), Pb(II) and As(V) by PDVB-VT0.2. (Conditions - Adsorbent 30 mg/L , Volume 30 mL, Time 18 h) The error bars are in the range of 10^{-2} mgg^{-1}.

Since nitrogen is an electron withdrawing group, introducing the amine groups induces positive charges within the polymer backbone which could have aided the adsorption of the anionic species through electrostatic interactions. Therefore, our amine functionalized polymer (PDVB-VT 0.2) adsorbed As (V) selectively over other cationic species.

Adsorption isotherms. To determine the equilibrium model the results were fitted with linear equations of Langmuir, Freundlich, Temkin and Sips isotherm models presented with equations 2-5 as follows. The Langmuir Isotherm[41,45]

$$\frac{1}{q_e} = \frac{1}{q_e K_L} . \frac{1}{C_e} + \frac{1}{q_m} \qquad (2)$$

where Ce is the concentration of As (V) solution at equilibrium (mg/L), qe is the amount of As(V) adsorbed by the adsorbent (mgg-1), KL is the Langmuir constant related to the free energy of adsorption(L/mg), qm is the maximum adsorption capacity in (mgg-1). 1/qe was plotted against 1/Ce to obtain the linear correlation isotherm (Figure S3).

The Freundlich isotherm[41]

$$\log\frac{1}{q_e} = \frac{1}{n}\log C_e + \log K_f \qquad (3)$$

where qe is the amount of As (V) adsorbed by the adsorbent (mgg-1)

Ce is the equilibrium concentration of As (V) (mg/L), KF is the Freundlich constant indicates the relative uptake capacity of the adsorbent material and 1/nF is the heterogeneity factor. The log of 1/qe was plotted against Ce to obtain a linear co-relation (Figure S4).

The Temkin isotherm[24]

$$q_e = B\ln K_T + B\ln C_e \qquad (4)$$

where qe is the amount of As(V) adsorbed by the adsorbent, Ce is the equilibrium concentration of As(V) solution, KT is the equilibrium binding energy and corresponds to the maximum binding energy and B corresponds to the binding energy. The value of B is calculated Equation 5:

$$B = R\frac{T}{b_T} \qquad (5)$$

R is the gas constant, T is the temperature (K) and bT is the Temkin isotherm constant. The constants B and KT were calculated from the slope and intercept respectively (Figure S5).

The Sips model [46,47] represented by Equation 6:

$$\frac{1}{Q_e} = \frac{1}{Q_{max}K_s}\left(\frac{1}{C_e}\right)^{\frac{1}{n}} + \frac{1}{Q_{max}} \quad (6)$$

where q_e is the experimental amount of As(V) adsorbed by the adsorbent (mgg^{-1}), K_s and n are the equilibrium and heterogeneity factors respectively, Q_{max} is the theoretical amount adsorbed by adsorbent (mgg^{-1}), C_e is the equilibrium concentration of the As (V) solution (Figure S6). Surface heterogeneity is based on the value of n. At low concentrations (when n=0) the equation approaches the Freundlich model while at high concentrations when (n=1) the data approach the Langmuir model. **Table 3.1** represents all the data from the equations and the actual graphs are found in the supplementary data. All the correlation coefficients (R^2) show a good correlation (>0.9) but the model that best describes the adsorption of As (V) is the Sips model (R^2- 0.99). The Sips model also known as the Langmuir-Freundlich model accounts for the limiting behavior of the Freundlich and Langmuir isotherms. This model also assumes localized adsorption without adsorbate-adsorbate interactions. This model predicts the surface heterogeneity and homogeneity in heterogeneous systems.[46,47]

The calculated value of n is 0.97 which means that more surface homogeneity exists than heterogeneity. The n value relates the model more to Langmuir which also indicates that As(V) adsorption is monolayer.[24] These data agree well with BET data for PDVB-VT that show that the pore sizes were mainly monomodal (93Å) indicating homogenous sites. The theoretical adsorption n maximum (Q_{max}) is 49.3 mgg^{-1} also agrees well with the experimental value (Q_e) of 46 mgg^{-1}.

Adsorption kinetics. To determine the adsorption kinetics, time dependent experiments were performed for 3 hours and the results were fitted into the pseudo-first order and pseudo-second order models represented by Equations 7 and 8. **Table 3.2** presents these data.

$$\log(Q_e - Q_t) = \log Q_e - \left(\frac{k1t}{2.303}\right) \qquad (7)$$

$$\frac{t}{Qt} = \frac{1}{k_2\ Q_t} + \frac{1}{Q_e}t \qquad (8)$$

where Qe and Qt are the amounts adsorbed at equilibrium and time t, respectively, K1 and K2 are the rate constant for pseudo first-order and pseudo second order (g/mg.min). The linear plots are obtained by plotting Log(Qe-Qt) against t and t/Qt against t respectively.

Table 3.2 Adsorption isotherm models.

Langmuir			**Freundlich**			**Temkin**			**Sips**		
$\frac{1}{Q_e} = \frac{1}{Q_e K_L}.\frac{1}{C_e} + \frac{1}{Q_m}$			$\log\frac{1}{Q_e} = \frac{1}{n}\log C_e + \log K_f$			$Q_e = B\ln K_T + B\ln C_e$			$\frac{1}{Q_e} = \frac{1}{QmaxK_s}(\frac{1}{C_e})^{\frac{1}{n}} + \frac{1}{Q_{max}}$		
Q_{max}(mg/g)	**K_L (L/mg)**	**R^2**	**K_F (mg/g)**	***N***	**R^2**	**B**	**K_T**	**R^2**	**Q_{max}**	**n**	**R^2**
0.41	104.7	0.964	2.38	1.96	0.983	12.0	2.86	0.97	49.3	0.97	0.991

Both PDVB and PDVB-VT0.2 show fast adsorption kinetics with the greatest adsorption occurring within the first 30 minutes. Sorption Kinetics fit well with the pseudo first order model with a correlation coefficient R^2 value of 0.99 for PDVB and second order for PDVB-VT0.2 (R2-0.99). However, the correlation coefficient R^2 value for the pseudo first order model value for PDVB-VT0.2 is 0.98 which indicates that the adsorption could also be occurring through both models. **Table 3.3** presents the obtained kinetic parameters for both pseudo first order and second order. As(V) adsorption in PDVB is mainly described by physisorption which follows first-order kinetics. In PDVB-VT0.2 adsorption is an interplay of both physisorption and chemisorption[48,49].

Table 3.3 Pseudo first and second order results.

	Pseudo-first –order		Pseudo-second-order	
Adsorbent	R^2	K (1/min)	R^2(g/mg) min)	K_2
PDVB	0.996	0.056	0.42	0.024
PDVB-VT0.2	0.98	0.062	0.99	0.11

Incorporation of amine groups increases the nucleophilicity of adsorption sites which facilitates chemisorption since electrostatic forces increase. PDVB-VT0.2 shows superior adsorption compared to PDVB. The corresponding first order rate constants (K1) for PDVB and PDVB-VT0.2 are 0.056 and 0.062. The rate constants for the 2nd order model (K2) of both PDVB and PDVB-VT0.2 are 0.024 and 0.11 respectively. Adsorption is 4.6 times higher through chemisorption and 1.12 times higher through physisorption and is induced by amine incorporation.

Adsorbent comparison. PDVB-VT0.2 was also compared to activated carbon (Char-carbon from fly-ash), and Zeolite Y (NaY) which are common adsorbents used in water purification (**Figure 3.7**). The capacity of the material is quite good compared to this adsorbent. The capacity coupled with the easy single-step synthesis make this material a great candidate for water purification.

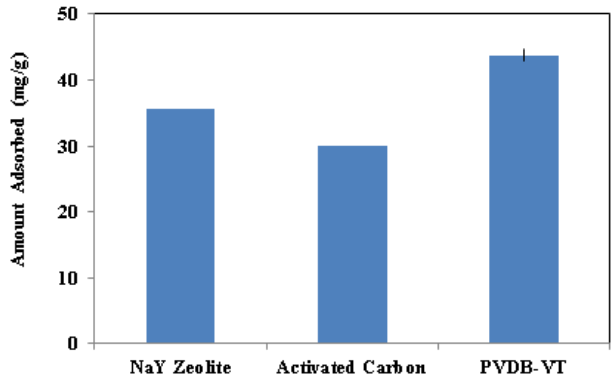

Figure 3.7 PDVB-VT0.2 comparisons with other state of the art adsorbents.

Regeneration of adsorbent. For practical industrial use adsorbent recycling and reuse is quite critical and an economic necessity. Both adsorbents showed poor adsorption at high pH, therefore, 0.1M NaOH was used to regenerate the adsorbents. The main species of As (V) recovered from the adsorbents is AsO_4^{3-} which is quite soluble at high pH (>10). The adsorption-desorption cycles were repeated five times using the same batch of PDVB-VT0.2. After the fifth cycle, only 10% of the adsorption capacity was lost (**Figure 3.7**). The material maintained a 90% desorption efficiency after the fifth cycle indicating that the material could easily be regenerated and reused. The slight decrease in capacity could be attributed to the incomplete desorption of As

(V) ions from the adsorbent surface. Overall, the material could be easily recycled and used for long term water purification.

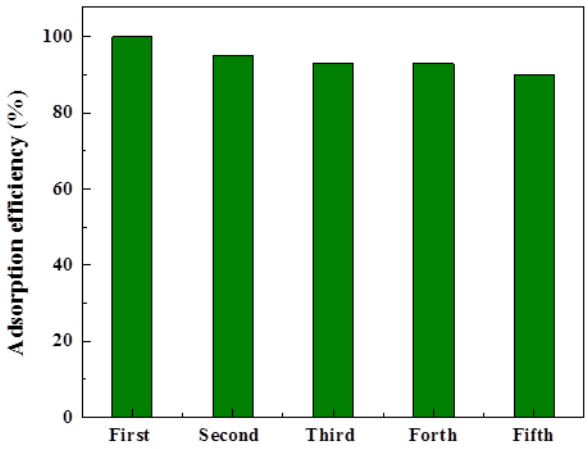

Figure 3.8 . Regeneration of PDVB-VT0.2 for the removal of As (V).

3.3.3 Computational Study

Finding the active adsorbent site is one of the objectives of the computational study. The anion was placed at various positions with respect to monomers (benzene ring and triazole ring) and the corresponding lowest minimized energy configuration was determined. The selected configurations were scaled up to three attached monomers of divinylbenzene for PDVB model and two divinylbenzene molecules with triazole co-monomers in between for PDVB-VT model.

The adsorption energy of $H_2AsO_4^-$ on PDVB was found to be 0.65 eV calculated from Equation 2 with arsenate ion interacting with two benzene rings from the side **Figure 3.9a**. The distance of O ($H_2AsO_4^-$) from the closest hydrogen on the benzene ring is calculated to be 2.22 Å. For the copolymer model of triazole (PDVB-VT) $H_2AsO_4^-$ coordinates most stably to the nitrogen on the triazole ring with a binding energy of 0.86 eV and distance of 2.07 Å for O ($H_2AsO_4^-$) to H-site

Figure 3.9c. The greater adsorption energy on the triazole N-sites of the copolymer is consistent with the experimental results in providing greater number of adsorption sites. Similarly, for $HAsO_4^{2-}$ anion, the adsorption energy is greater for VT (2.31 eV **Figure 3.9d**) compared to benzene (1.95 eV **Figure 3.9b**). The distance of O ($HAsO_4^{2-}$) with the closest hydrogen on the benzene ring in PDVB model is 2.03 Å. With the PDVB-VT model the corresponding distance between $HAsO_4^{2-}$ and the H-site on triazole ring is 1.99 Å.

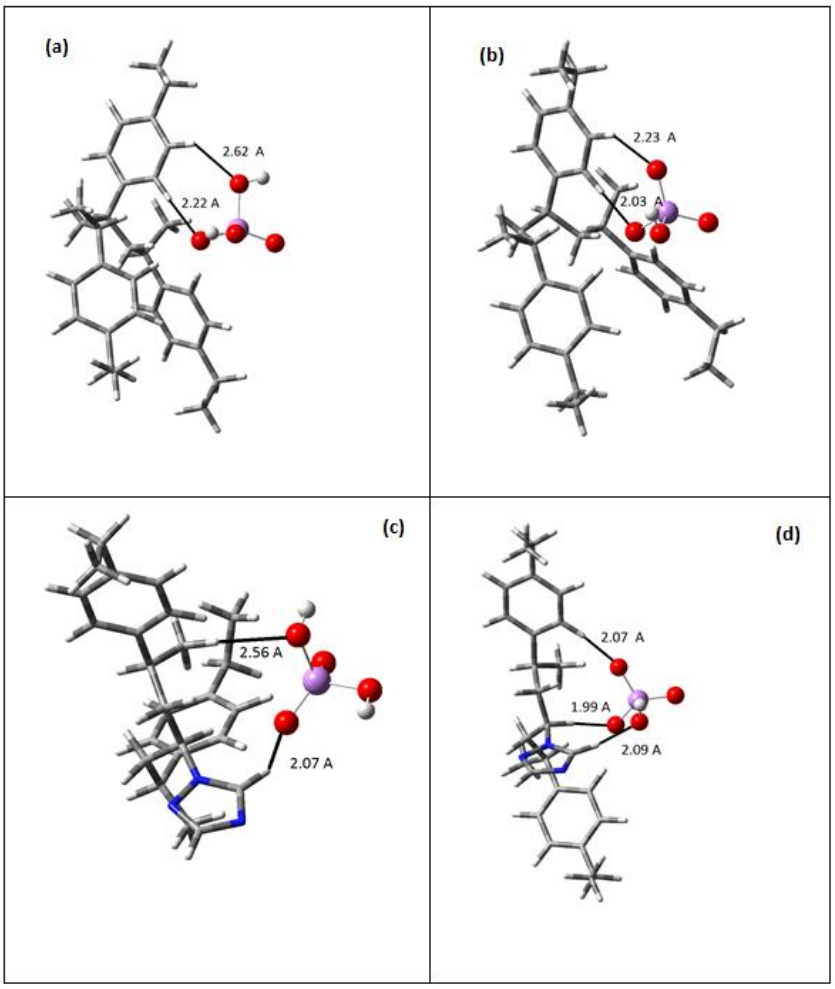

Figure 3.9 Models of PDVB and PDVB-VT0.2 with anionic species ($H_2AsO_4^-$ and $H_2AsO_4^{2-}$) a) PDVB model with $H_2AsO_4^-$ b) PDVB with $H_2AsO_4^{2-}$, c) PDVB-VT0.2 with $H_2AsO_4^-$ d) PDVB-VT0.2 with $H_2AsO_4^{2-}$.

3.4 Discussion

The incorporation of the co-monomer vinyl-triazole into the structure of PDVB was successful as confirmed by FTIR and X-ray spectroscopy. This led to improved adsorbent properties such stability by 20°C as confirmed by thermogravimetric analysis (TGA). Nitrogen sorption (BET) reveal an increase in the pore size and volume which improved accessibility to adsorption sites leading to a higher adsorption capacity in comparison with non-functionalized PDVB. Both benzene and triazole are sufficiently nucleophilic.[50] Introducing amine moieties in triazole increase nucleophilic sites on the backbone of PDVB which led to improved adsorption despite the decrease in surface area. From pH data the species that were adsorbed the most were $H_2AsO_4^-$ and $HAsO_4^{2-}$ for PDVB-VT0.2 (pH 5) and PDVB (pH 8) respectively. DFT calculations reveal that the mechanism of adsorption is through the interaction of π groups in both PDVB and PDVB-VT, and anionic species ($H_2AsO_4^-$ and $HAsO_4^{2-}$). Anion-π interactions are favorable non-covalent contacts between an electron deficient (π-acidic) aromatic system and an anion.[51] These interactions are dominated by electrostatic energy, anion-induced polarization, and dispersion energies. The electrostatic component is related to the permanent quadrupole moment, Q_{zz}. Higher positive values result in stronger electrostatic interactions. The anion-induced polarization is proportional to the molecular polarizability α of the aromatic compound.[31] These interactions involve the HOMO of the anions and the LUMO of π systems which promote charge transfer from anions to π systems. The magnitude of the charge transfer is proportional to the total induction energy.[52] Dispersion energies are markedly higher with interactions involving organic anions.[52] Our system involved inorganic anions therefore only electrostatic and anion induced polarizations were relevant. Benzene has a negative quadrupole

moment, $Q_{zz}(C_6H_6)$= -8.48B. Triazole is analogous to s-triazine which has a positive quadrupole moment Q_{zz}= +0.90 B.[53] This indicates that introducing the amine groups induces positive charges on these sites which interact strongly with the $H_2AsO_4^-$ and $HAsO_4^{2-}$ ions. PDVB-VT adsorption of As (V) (46 mgg^{-1}) was found to be higher than that of PDVB (27 mgg^{-1}) which could be as a result of these induced positive charges. Zeta potential measurements (**Figure S11**) confirm that at pH 5 where the adsorption is maximum for PDVB-VT the surface is positive (0.95 mV) and at pH 8 for PDVB the surface is negative (-1.73 mV). Theoretical studies have shown that aromatic rings with negative quadrupole moments, although weak, exhibit anion-π interactions in the gas phase, e.g. benzene has an F^- binding enthalpy of -5.51 kcal mol^{-1}.[54] This explains why in spite of the negative charge on the surface, PDVB was able to still adsorb As (V) species. The species adsorbed the most by PDVB is, however, $HAsO_4^{2-}$ which would induce more polarization than $H_2AsO_4^-$ because of the stronger negative charge. From experimental data pH also played a big role in affecting the anionic interactions. Electrostatic interactions for PDVB-VT0.2 seem to have played a bigger role than anion induced interactions since adsorption of $H_2AsO_4^-$ was preferred over $HAsO_4^{2-}$. From **Figure 3.5b** at pH 5 the main species in the solution is $H_2AsO_4^-$. As the pH reduces the presence of H_3AsO_4 seems to reduce these interactions since the adsorption decreases significantly. As the pH increases the second highest adsorbed value is at pH 9 (35 mgg^{-1}). The dominant species is $HAsO_4^{2-}$. Zeta potential measurements at this pH are 1.16 mV. Electrostatic interactions are quite high but competition between OH^- and $HAsO_4^{2-}$ anions seems to reduce the amount of As (V) adsorbed. DFT calculations reveal that $HAsO_4^{2-}$ - H distances are 1.99 A° indicating that strong anionic induced polarizations are present. PDVB shows that anion induced polarization dominates over electrostatic interactions. The maximum adsorbed amount occurs at pH 8 (27 mg/g) where the

dominant species is $HAsO_4^{2-}$. The zeta potential measurement at this point is -1.73 mV. Amine incorporation thus enables electrostatic interactions to dominate over anion induced polarization. Therefore, both DFT and experimental data agree that the mechanism of adsorption is conducted through both electrostatics and anion induced polarization in PDVB-VT0.2.

3.5 Conclusions

Amine-functionalized mesoporous polymer was successfully synthesized by hydrothermal synthesis and applied for As (V) removal from water for the first time. Amine-incorporation into the polymer was confirmed by surface characterization techniques (FTIR and XPS). The optimal adsorption capacity for PDVB-VT0.2 was found to be 46 mgg^{-1} while that of PDVB was 27 mg/g. Amine incorporation was found to increase both the rate and capacity of adsorption by introducing positive charges on these sites which interact strongly with the ions of arsenic. The Sip's model describes the best adsorption isotherm PDVB-VT0.2 which indicated the presence of homogenous sites and monolayer adsorption. Also, our adsorbent showed 90% recyclability after 5 cycles. Anion induced interactions were found to describe the mechanism of interaction for PDVB whereas electrostatic interactions dominated in PDVB-VT0.2. DFT calculations complemented experimental data confirming that amine incorporation increases electrostatic forces between the As (V) species and the adsorption sites greatly reducing the interatomic distance.

3.6 References

(1) Fu, F.; Wang, Q. Removal of heavy metal ions from wastewaters: A review. *J. Environ. Manage.* **2011**, *92* (3), 407–418.

(2) Shawabkeh, R.; Al-Harahsheh, A.; Al-Otoom, A. Copper and zinc sorption by treated oil

shale ash. *Sep. Purif. Technol.* **2004**, *40* (3), 251–257.

(3) Järup, L. Hazards of heavy metal contamination. *Br. Med. Bull.* **2003**, *68*, 167–182.

(4) Roy, P.; Mondal, N. K.; Bhattacharya, S.; Das, B.; Das, K. Removal of arsenic(III) and arsenic(V) on chemically modified low-cost adsorbent: batch and column operations. *Appl. Water Sci.* **2013**, *3* (1), 293–309.

(5) Ungureanu, G.; Santos, S.; Boaventura, R.; Botelho, C. Arsenic and antimony in water and wastewater: Overview of removal techniques with special reference to latest advances in adsorption. *J. Environ. Manage.* **2015**, *151*, 326–342.

(6) Litter, M. I.; Morgada, M. E.; Bundschuh, J. Possible treatments for arsenic removal in Latin American waters for human consumption. *Environ. Pollut.* **2010**, *158* (5), 1105–1118.

(7) Kobya, M.; Gebologlu, U.; Ulu, F.; Oncel, S.; Demirbas, E. Removal of arsenic from drinking water by the electrocoagulation using Fe and Al electrodes. *Electrochim. Acta* **2011**, *56* (14), 5060–5070.

(8) Zhu, W. P.; Gao, J.; Sun, S. P.; Zhang, S.; Chung, T. S. Poly(amidoamine) dendrimer (PAMAM) grafted on thin film composite (TFC) nanofiltration (NF) hollow fiber membranes for heavy metal removal. *J. Memb. Sci.* **2015**, *487*, 117–126.

(9) Santhosh, P.; Sridevi, A. a Lab-Scale Study on Reduction of Heavy Met- Als From Electroplating Effluent Using Conventional Chemical Precipitation. **2013**, *8* (1), 102–108.

(10) Sudilovskiy, P. S.; Kagramanov, G. G.; Kolesnikov, V. A. Use of RO and NF for treatment of copper containing wastewaters in combination with flotation. *Desalination* **2008**, *221* (1-3), 192–201.

(11) Lin, L. C.; Li, J. K.; Juang, R. S. Removal of Cu(II) and Ni(II) from aqueous solutions using batch and fixed-bed ion exchange processes. *Desalination* **2008**, *225* (1-3), 249–259.

(12) Dabrowski, A.; Hubicki, Z.; Podkocielny, P.; Robens, E. Selective removal of the heavy metal ions from waters and industrial wastewaters by ion-exchange method. *Chemosphere* **2004**, *56* (2), 91–106.

(13) Hunsom, M.; Pruksathorn, K.; Damronglerd, S.; Vergnes, H.; Duverneuil, P. Electrochemical treatment of heavy metals (Cu2+, Cr 6+, Ni2+) from industrial effluent and modeling of copper reduction. *Water Res.* **2005**, *39* (4), 610–616.

(14) Gumpu, M. B.; Sethuraman, S.; Krishnan, U. M.; Rayappan, J. B. B. A review on detection of heavy metal ions in water - An electrochemical approach. *Sensors Actuators, B Chem.* **2015**, *213*, 515–533.

(15) Hlihor, R. M.; Figueiredo, H.; Tavares, T.; Gavrilescu, M. Biosorption potential of dead and living Arthrobacter viscosus biomass in the removal of Cr(VI): Batch and column studies. *Process Saf. Environ. Prot.* **2016**, No. Vi, 1–13.

(16) Ihsanullah; Abbas, A.; Al-Amer, A. M.; Laoui, T.; Al-Marri, M. J.; Nasser, M. S.; Khraisheh, M.; Atieh, M. A. Heavy metal removal from aqueous solution by advanced carbon nanotubes: Critical review of adsorption applications. *Sep. Purif. Technol.* **2016**, *157*, 141–161.

(17) Wanna, Y.; Chindaduang, A.; Tumcharern, G.; Phromyothin, D.; Porntheerapat, S.; Nukeaw, J.; Hofmann, H.; Pratontep, S. Efficiency of SPIONs functionalized with polyethylene glycol bis(amine) for heavy metal removal. *J. Magn. Magn. Mater.* **2016**, *414*, 32–37.

(18) Barakat, M. A. New trends in removing heavy metals from industrial wastewater. *Arab. J. Chem.* **2011**, *4* (4), 361–377.

(19) Baccar, R.; Bouzid, J.; Feki, M.; Montiel, A. Preparation of activated carbon from Tunisian olive-waste cakes and its application for adsorption of heavy metal ions. *J. Hazard. Mater.* **2009**, *162* (2-3), 1522–1529.

(20) Hua, M.; Zhang, S.; Pan, B.; Zhang, W.; Lv, L.; Zhang, Q. Heavy metal removal from water/wastewater by nanosized metal oxides: A review. *J. Hazard. Mater.* **2012**, *211-212*, 317–331.

(21) Lata, S.; Samadder, S. R. Removal of arsenic from water using nano adsorbents and challenges: A review. *J. Environ. Manage.* **2016**, *166*, 387–406.

(22) Mohan, D.; Pittman, C. U. Arsenic removal from water/wastewater using adsorbents-A

critical review. *J. Hazard. Mater.* **2007**, *142* (1-2), 1–53.

(23) Montero-campos, V.; Puente-urbina, A.; Rica, T. D. C.; Rica, C. Continuous-Flow Removal of Arsenic in Drinking Water by Filtering down through Fe 3 O 4 @ SiO 2 Magnetic Composite. **2016**, No. May, 619–630.

(24) Ajmal, M.; Demirci, S.; Uzun, Y.; Siddiq, M.; Aktas, N.; Sahiner, N. Introduction of double amidoxime group by double post surface modification on poly(vinylbenzyl chloride) beads for higher amounts of organic dyes, As (V) and Cr (VI) removal. *J. Colloid Interface Sci.* **2016**, *470* (February), 39–46.

(25) Hong, G.; Li, X.; Shen, L.; Wang, M.; Wang, C.; Yu, X.; Wang, X. High recovery of lead ions from aminated polyacrylonitrile nanofibrous affinity membranes with micro/nano structure. *J. Hazard. Mater.* **2015**, *295*, 161–169.

(26) Kampalanonwat, P.; Supaphol, P. Preparation and adsorption behavior of aminated electrospun polyacrylonitrile nanofiber mats for heavy metal ion removal. *ACS Appl. Mater. Interfaces* **2010**, *2* (12), 3619–3627.

(27) Xing, H. T.; Chen, J. H.; Sun, X.; Huang, Y. H.; Su, Z. B.; Hu, S. R.; Weng, W.; Li, S. X.; Guo, H. X.; Wu, W. B.; et al. NH2-rich polymer/graphene oxide use as a novel adsorbent for removal of Cu(II) from aqueous solution. *Chem. Eng. J.* **2015**, *263*, 280–289.

(28) Akhavan, B.; Jarvis, K.; Majewski, P. Plasma polymer-functionalized silica particles for heavy metals removal. *ACS Appl. Mater. Interfaces* **2015**, *7* (7), 4265–4274.

(29) Hans-Jörg Schneider, F. W. and T. B. Attractive interactions between negative charges and polarizable aryl parts of host–guest systems. *J. Phys. Org. Chem.* **1993**, *6* (10), 590–594.

(30) Quionero, D.; Garau, C.; Rotger, C.; Frontera, A.; Ballester, P.; Costa, A.; Dey??, P. M. Anion-pi interactions: Do they exist? *Angew. Chemie - Int. Ed.* **2002**, *41* (18), 3389–3392.

(31) Schottel, B. L.; Chifotides, H. T.; Dunbar, K. R. Anion-p interactions.

(32) Zhu, W.; Kong, W.; Noshadi, I.; Zhao, L.; Liu, F. Solvothermal synthesis of nanoporous, polymeric solid bases with controlled wettability and good catalytic activity. *Colloids Surfaces A Physicochem. Eng. Asp.* **2014**, *444*, 314–320.

(33) Jafari, T.; Noshadi, I.; Khakpash, N.; Suib, S. L. Superhydrophobic and stable mesoporous polymeric adsorbent for siloxane removal: D4 super-adsorbent. *J. Mater. Chem. A* **2015**, *3* (9), 5023–5030.

(34) Noshadi, I.; Kanjilal, B.; Jafari, T.; Moharreri, E.; Khakpash, N.; Jiang, T.; Suib, S. L. Hydrophobic mesoporous adsorbent based on cyclic amine–divinylbenzene copolymer for highly efficient siloxane removal. *RSC Adv.* **2016**, *6* (81), 77310–77320.

(35) Mou, F.; Guan, J.; Xu, L.; Shi, W. Magnetic Iron Oxide Chestnutlike Hierarchical Nanostructures: Preparation and Their Excellent Arsenic Removal Capabilities. *ACS Appl. Mater. Interfaces* **2012**, *4*, 3987−399.

(36) Kohn, W.; Sham, L. J. Self-Consisten Equations IncludingExchange and Correlation Effects. *Phys. Rev.* **1965**, *140* (4A), A1133–A1138.

(37) Rajagopal, A. K.; Callaway, J. Inhomogeneous electron gas. *Phys. Rev. B* **1973**, *7* (5), 1912–1919.

(38) MJ, F.; GW, T.; HB, S.; GE, S.; MA, R.; JR, C.; G, S.; V, B.; B, M.; GA, P.; et al. Gaussian 09, Revision A. 02; Gaussian: Wallingford, CT, 2009. **2009**.

(39) Uzun, L.; Kara, A.; Tüzmen, N.; Karabakan, A.; Beşirli, N.; Denizli, A. Synthesis and characterization of poly(ethylene glycol dimethacrylate-1- vinyl-1,2,4-triazole) copolymer beads for heavy-metal removal. *J. Appl. Polym. Sci.* **2006**, *102* (5), 4276–4283.

(40) Uzun, L.; Kara, A.; Osman, B.; Yılmaz, E.; Beşirli, N.; Denizli, A. Removal of heavy-metal ions by magnetic beads containing triazole chelating groups. *J. Appl. Polym. Sci.* **2009**, *114* (4), 2246–2253.

(41) Belhachemi, M.; Addoun, F. Comparative adsorption isotherms and modeling of methylene blue onto activated carbons. *Appl. Water Sci.* **2011**, *1* (3-4), 111–117.

(42) Xie, K.; Wang, X.; Liu, Z.; Alsaedi, A.; Hayat, T.; Wang, X. Synthesis of flower-like α-Fe2O3 and its application in wastewater treatment. *J. Zhejiang Univ. Sci. A* **2014**, *15* (8), 671–680.

(43) Zhu, H.; Jia, Y.; Wu, X.; Wang, H. Removal of arsenic from water by supported nano zero-valent iron on activated carbon. *J. Hazard. Mater.* **2009**, *172* (2-3), 1591–1596.

(44) Chang, Q.; Lin, W.; Ying, W. Preparation of iron-impregnated granular activated carbon for arsenic removal from drinking water. *J. Hazard. Mater.* **2010**, *184* (1-3), 515–522.

(45) Kumara, N. T. R. N.; Hamdan, N.; Petra, M. I.; Tennakoon, K. U.; Ekanayake, P.; Kumara, N. T. R. N.; Hamdan, N.; Petra, M. I.; Tennakoon, K. U.; Ekanayake, P. Equilibrium Isotherm Studies of Adsorption of Pigments Extracted from Kuduk-kuduk (*Melastoma malabathricum* L.) Pulp onto TiO_2 Nanoparticles. *J. Chem.* **2014**, *2014*, 1–6.

(46) R. Sips. Combined form of Langmuir and Freundlich equations. *J. Chem. Phys.* **1948**, *16* (5), 490–495.

(47) Jeppu, G. P.; Clement, T. P. A modified Langmuir-Freundlich isotherm model for simulating pH-dependent adsorption effects. *J. Contam. Hydrol.* **2012**, *129-130*, 46–53.

(48) Ho, Y. S. Review of second-order models for adsorption systems. *J. Hazard. Mater.* **2006**, *136* (3), 681–689.

(49) Qiu, H.; Lv, L.; Pan, B.; Zhang, Q. Q.; Zhang, W.; Zhang, Q. Q. Critical review in adsorption kinetic models. *J. Zhejiang Univ. Sci. A* **2009**, *10* (5), 716–724.

(50) Stranks, D. R.; Withers, G. R. A. *Chemistry; a structural view*; Melbourne University Press, 1965.

(51) Alberto, M. E.; Mazzone, G.; Russo, N.; Sicilia, E. The mutual influence of non-covalent interactions in p-electron deficient cavities: the case of anion recognition by tetraoxacalix[2]arene[2]triazinew.

(52) Kim, D.; Tarakeshwar, P.; Kim, K. S. Theoretical Investigations of Anion-π Interactions: The Role of Anions and the Nature of π Systems.

(53) Garau, C.; Frontera, A.; Quiñonero, D.; Ballester, P.; Costa, A.; Deyà, P. M. A Topological Analysis of the Electron Density in Anion - π Interactions. *ChemPhysChem* **2003**, *4* (12), 1344–1348.

(54) Clements, A.; Lewis, M. Arene-Cation Interactions of Positive Quadrupole Moment Aromatics and Arene-Anion Interactions of Negative Quadrupole Moment Aromatics.

Chapter 4. Functionalized PDVB for CO_2 Capture

4.1 Introduction

Adversely contributing to climate changes, greenhouse gas (GHG) emission has been a serious environmental concern. Carbon dioxide (CO_2) being the predominant part of GHG, primarily comes from fossil fuel consumption in the transportation, energy generation, and industrial sectors[1,2]. GHG emission results in increasing the earth surface temperature which is predicted to be as high as 3ºC by the year 2100 (according to IPCC report)[3,4]. Mitigation of CO_2 emission by an alternative source of energy[5] needs significant changes to the current infrastructure of carbon based power plants. Therefore, CO_2 capture and storage techniques (CCS) could be applied to the current fossil-fueled power plants to tackle the problem in the short term[6]. Among various approaches in CCS techniques[7] the post-combustion methodology shows advantages over the others[8].

While absorption by amine-solution has drawbacks of corrosion, considerable energy loss, and inefficient regeneration, this has been the most widely adopted strategy[9]. Adsorption by solids provides some advantages such as (i) high CO_2 capture capacity, (ii) low energy requirement of adsorbent regeneration, (iii) adsorbent stability, (iv) fast kinetics, (v) easy handling, and (vi) efficiency under flue gas moisture[10,11]. On the atomic scale, polarizability or the quadrupole moment of the adsorbent functional site plays a significant role in the selective capture of CO_2 during physisorption[12,13]. However, for chemisorptive adsorption, selectivity is obtained based on chemical interactions between individual components of the gas mixture and surface functionalities of the adsorbent[14]. A regeneration step should follow the adsorption to recover the

solid adsorbent. To regenerate the adsorbents a pressure/vacuum swing adsorption (PSA/VSA) and temperature swing adsorption (TSA) procedure could be employed[15,16].

An efficient solid CO_2 adsorbent needs high adsorption capacity and selectivity, high stability, scalability, low moisture sensitivity, and low energy of regeneration[17]. Several porous adsorbents have been evaluated for CO_2 capture including alkaline earth metal oxides[18], porous carbons[19], silica[20,21], zeolites[22], metal organic frameworks (MOFs)[23], porous organic frameworks (POFs),[24] and nanoporous organic polymers (NOPs)[25]. Chemical adsorption of CO_2 by alkaline earth metal oxides and metal salts at high temperatures requires high energy for regeneration[26–28]. Physical adsorbents like activated carbons (ACs) with advantages of prevalent precursor materials, hydrophobicity, and low heat of adsorption, still have the challenges of low selectivity and capacity[1]. Moreover, silicas and zeolites have been widely used as adsorbents to capture many impurities[29,30] especially CO_2[22,31]. Zeolites capture the CO_2 molecules very rapidly with high chemical and thermal stability[32]. However, the moisture sensitivity, the low selectivity and high energy of regeneration has limited their application[33–35]. MOFs of M_2(dobdc) have shown the highest CO_2 capacities of 5-8 $mmolg^{-1}$ (M= Mg/Co/Ni/Zn)[36], though M_2(dobdc) is highly sensitive toward moisture resulting in much lower capacity (16-85% drop in capacity) in the presence of moisture[37]. Recently, a perfluorinated covalent triazine-based framework (FCTF-1) has been designed for selective CO_2 capture which is a moisture resistant adsorbent[38]. However, synthesis of fluorinated compounds is expensive and dangerous. To address low selectivity of widely used adsorbents of ACs and zeolites, different functionalities such as carboxylic, sulfonic, and amine groups have been applied to enhance CO_2 adsorption[39,40]. Based on loading methods of functional groups which mainly involve amines, there are two categories of adsorbents; amine-impregnated[41,42] and amine-grafted[43,44] materials. Impregnated adsorbents are easy to

synthesize and provide high capacity. However, such materials have several drawbacks like blockage of support surface area and pores by increasing amine-loading, decomposition of loaded amines upon heating during CO_2 capture, and high diffusion resistivity[45]. Amine grafting by chemical reaction provides higher thermal stability for the adsorbent[43,46]. Recently, functional groups like N-donor Lewis base sites such as in organic amines have more tendency to adsorb CO_2 molecules[47]. Amine functionality provides Lewis base sites with lone pair electrons which coordinate favourably with CO_2 molecules[48] with several triazine-based polymeric adsorbents being developed for CO_2 adsorption[49–51]. Amine functionalized silicas have been shown to experimentally and theoretically influence the CO_2 adsorption mechanism[52] by the formation of intermolecular ammonium carbamates with primary amines, while being stabilized with secondary amines by forming carbamic acid.

Porous polymers provide several advantages of (i) clear design of the high surface area and well-defined porosity, (ii) easy processing, (iii)and light elemental composition which provide weight advantages[53]. Recently, several porous polymers (mesoporous or microporous) have been developed for CO_2 capture[54,55]. Amine modified porous polymers have also been drawn up to adsorb CO_2 more efficiently[56,57]. The new class of triazine-based microporous frameworks with high thermal and chemical stability have been developed through the Sonogashira-Hagihara reaction using Pd-based catalysts to improve CO_2 adsorption of polymeric materials[51]. In 2013, Liebl and Senker synthesized a series of triazine-based porous polyimide polymers via condensation reactions which resulted in microporous polymeric networks with the highest CO_2 uptake of 2.45 $mmolg^{-1}$ at 273 K and 1 bar[49]. Later on, Wang et al. developed ultramicropores and nitrogen-rich covalent triazine-based frameworks for CO_2 capture with the capacity of 2.61 $mmolg^{-1}$ at 298K for the adsorbent with 27.64% amine loading[24].

Previously, PDVB based polymers have been synthesized with various morphologies and textural properties including monodispersed microspheres[58], macroporous[59], nanoporous sheets[60] and as mesoporous materials[61]. Biogas purification from siloxane impurities has been conducted by highly hydrophobic mesoporous PDVB based materials[61,62]. The effect of synthesis parameters such as various solvent effects (type and ratio of solvent mixture),[63] synthesis temperature,[64] and initiator amount[65] have also been studied on textural properties of PDVB-based materials. Feng et al. have synthesized mesoporous poly-ionic liquids of divinylbenzene copolymerized with alkylvinylimidazolium (P(DVB-IL))[65], for which decreasing the amount of initiator enhanced the textural properties (higher surface area). Recently, PDVB-based materials which were modified by ionic liquids (ILs)[65] or amine rich monomers[66,67] for CO_2 adsorption. PDVB functionalized with ionic liquids of alkylvinylimidazolium salt showed CO_2 uptake of 0.5 $mmolg^{-1}$ at 298K/1 bar[65]. PDVB was also functionalized with co-monomer of tartardiamide under long hydrothermal reaction which resulted in porous polymers with CO_2 adsorption capacity of 8.76 $mmolg^{-1}$ at 273K under high pressure of 3 bar[66]. Copolymerization of divinylbenzene and triallylamine under solvothermal conditions, also resulted in amine modified porous polymers with CO_2 uptake of 19.5 $mmolg^{-1}$ at 273K and high pressure of 3 bar[67]. However, there are no reported works on CO_2 adsorption by non-functionalized PDVB. Therefore, the roles of functional groups were not clearly understood.

All previously reported synthesis procedures of PDVB-based materials have been obtained by long hydrothermal reactions. However, microwave assisted synthesis of polymeric materials provides several advantages such as a uniform and fast heating process, non-contact, and highly specific heating[68,69]. Very recently a comparative study on thermal- and microwave assisted synthesis has been reported by Raj et al. in which higher molecular weight polymers were

obtained in shorter reaction time by a microwave approach [70]. Hoogenboom et al. [71] have reported batch mode microwave-assisted polymerization with up to 250 fold scale up. Recent advances in flow mode microwave-assisted polymerization[72,73] have proved that the process will become less challenging from a commercial production perspective. Herein we study CO_2 uptake performance both experimentally and theoretically for non-functionalized and amine functionalized hydrophobic mesoporous poly divinylbenzene (PDVB) which were synthesized for the first time by microwave heating. The effect of amine type and amount of incorporation into the porous structure of the polymer and the effect of initiator amount were studied on the textural and adsorptive properties of the developed adsorbents. Theoretical calculations were conducted to enhance the understanding of the nature of the interactions between substrate and the adsorbates.

4.2 Experimental Section

4.2.1 Chemicals

Divinylbenzene (technical grade, 80%) 1-vinylimidazole (VI), 1-Vinyl-1,2,4-triazole (VT), 2,2´-azobis(2-methylpropionitrile) (AIBN), and dimethylformamide (DMF) were purchased from Sigma-Aldrich. Solvents and materials were used as received.

4.2.2 Synthesis of Mesoporous PDVB

Highly In a typical run, non-functionalized PDVB was obtained through a microwave assisted procedure as follows. A Biotage initiator microwave synthesizer was used in this study which has been recently employed for inorganic nanoparticle synthesis[74]. The microwave reactor has a built-in computer and touch screen with the ability to reach a maximum temperature of 250^{o}C

with a heating rate of 2-5^{o}C min-1 providing a maximum pressure of 20 bars with power of 400 W. Divinylbenzene (DVB) (2 g) in 20 ml of organic solvent of dimethylformamide (DMF) were mixed. After the addition of initiator, 2,2′-Azobis(2-methylpropionitrile) (AIBN) (0.07 g), the solution was stirred for 3 h at room temperature followed by transferring to a capped microwave vial and treated at 165^{o}C for 2 h. The amine functionalized PDVB materials were synthesized similarly except with addition of amine containing co-monomers such as vinyl imidazole (VI) or vinyl triazole (VT). The type of co-monomer, amount of co-monomer, and initiator (AIBN) were varied to obtain an efficient CO_2 adsorbent. The obtained polymers with co-monomer of VI or VT are called PDVB-VI or PDVB-VT, respectively. The various amounts of VT incorporated into PDVB resulted in PDVB-VTx where x is the weight of co-monomer of VT (x= 0.2-0.9 g). Furthermore, the samples with varied amounts of initiator are labelled as PDVB-VT-INy where y represents the weight of AIBN (y= 0.0065-0.09 g).

4.2.3 Characterization of Functionalized PDVB

The Brunauer, Emmett, and Teller (BET) specific surface area was determined using a N2 sorption method. Fourier transform infrared spectroscopy (FTIR) spectra were obtained with a Bruker 66V FTIR spectrometer. X-ray photoelectron spectroscopy (XPS) was carried out to prove further the presence of amine functionalities for both PDVB-VT and PDVB-VI using a PHI 595 multiprobe system using a monochromatic Al Kα source (20 mA, 14 kV). The morphology of amine rich polymers was determined by scanning electron microscopy (SEM) using an FEI Nova NanoSEM 450. Samples were coated to decrease charging with an Au-Pt alloy with a Polaron model E5100 instrument.

4.2.4 CO_2 Adsorption

The main evaluations of CO_2 adsorption of PDVB and amine-functionalized PDVB were conducted with a Quanta Chrome (autosorb iQ2) under atmospheric pressure. To calculate the isosteric heat of adsorption (Q_{st})[75,76] based on the Clausius-Clapeyron relation (Equation 1), the adsorption was performed at two different temperatures :

$$Q_{st} = R\left[\frac{T_2 \times T_1}{T_2 - T_1}\right] \times Ln\left[\frac{P_1}{P_2}\right] \quad (1)$$

The where R is the universal gas constant; T_2 and T_1 are two different temperatures which are considered to be 298 and 273 K; P_2 and P_1 are the partial pressures at the same amounts of adsorbed CO_2 for T_2 and T_1. Moreover, the hysteresis loop in the adsorption-desorption of CO_2 (Figure S3) provides information on the adsorption pathway if the physisorption is more dominant or chemisorption which is obtained by calculating the isothermal adsorbate retention (IAR)[77,78] based on the difference between CO_2 adsorbed and desorbed at a certain pressure:

$$IAR\ (mmol.g^{-1}) = C_{des} - C_{ads} \quad (2)$$

C_{ads} is the equilibrium amount of adsorbed CO_2 at a certain pressure, and C_{des} is the equilibrium amount of adsorbed CO_2 at the same pressure on the desorption isotherm. The recyclability of the adsorbents was evaluated by heating at low temperatures of less than 100°C. Then, at least seven cycles of adsorption and regeneration will be carried out by the most efficient adsorbent.

4.2.5 Computational Study

Ab initio calculations using density functional theory are performed for CO_2 adsorption on PDVB, PDVB-VI, and PDVB-VT employing the plane wave pseudo-potential method. The Generalized Gradient Approximation (GGA) parameterized by Perdew-Burke-Ernzhof (PBE)[79]

is used for the exchange-correlation functional. Vienna ab initio Simulation Package (VASP)[80] is employed with the projector-augmented wave (PAW)[81] method for the electron-core interactions. Finite systems with large enough simulation box of sizes (17×34×34) $Å^3$: PDVB, (22×40×22) $Å^3$: PDVB-VI and (20×40×26) $Å^3$ **:** PDVB-VT are considered to minimize the interaction with its periodic images. All calculations are performed with plane wave cut-off energy of 800 eV. The integration over the Brillouin zone is done at one k-point, i.e., the Γ- point only. The geometry optimization is done using the conjugate gradient method and the total energy convergence criteria are taken as 10-6 eV. The binding energy (E_{ads}) of CO_2 on the polymer is defined as:

$$E_{ads}\,(CO_2) = E(CO_2) + E(PDVB) - E(CO_2 - PDVB) \qquad (3)$$

where *E(CO_2), E(PDVB),* and *E(CO_2-PDVB)* are total energies of free CO_2, the polymer, and the CO_2-PDVB complex, respectively. The binding energy of the second CO_2 molecule is calculated using:

$$E_{ads}(^{second}CO_2) = E(CO_2) + E\left(^{first}CO_2 - PDVB - X\right) - E(2 \times CO_2 - PDVB - X) \quad (4)$$

where *E(CO_2), E(first CO_2-PDVB-X), E(2×CO_2-PDVB-X),* are total energies of the free CO_2, adsorbed CO_2-copolymer complex, and two CO_2-PDVB-X complexes. X refers to the co-monomer of VT or VI.

4.3 Results

4.3.1 Characterization of Fresh Adsorbent

N_2 Adsorption-Desorption (BET). Textural properties of MW-assisted PDVB-based materials were investigated based on BET methods. **Figure 4.1** displays the N_2 adsorption-desorption

isotherms of various porous PDVB materials synthesized under different conditions of co-monomer with different nitrogen densities (**Figure 4.1a**), amount of co-monomer (**Figure 4.1b**) and amount of initiator (**Figure 4.1c**).

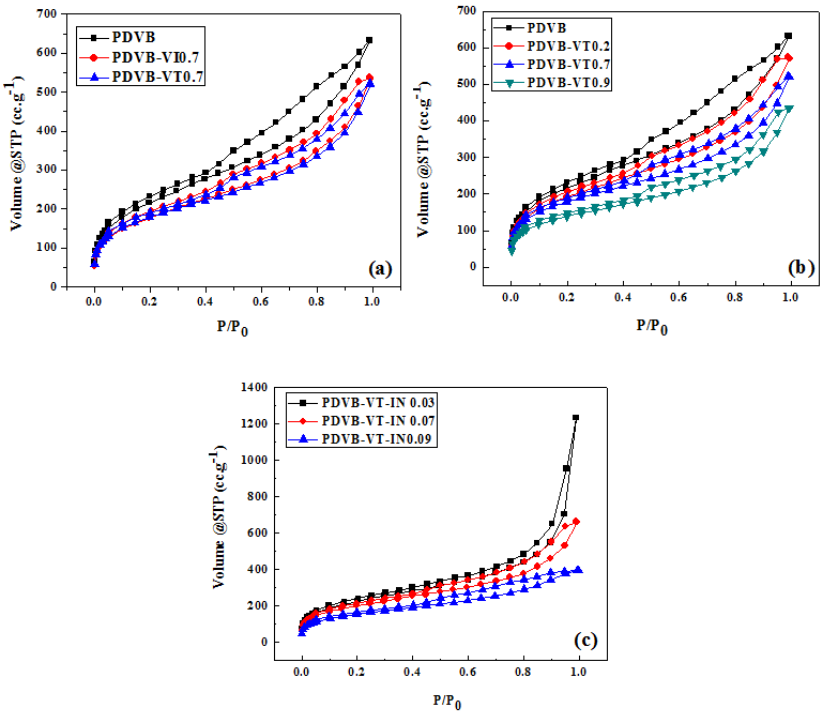

Figure 4.1 N_2 adsorption-desorption isotherms of PDVB a) different co-monomers, b) various amount of co-monomer incorporation, and c) different amount of initiator (AIBN).

Co-monomer decreased the surface area from 789 m^2g^{-1} for PDVB to 649 and 646 m^2g^{-1} for PDVB-VI and PDVB-VT, respectively (Figure 1a). Similarly, the pore volume reduced from 0.97 to 0.82 and 0.81 ccg^{-1} after introducing VI and VT to the PVDB. Figure 1b displays BET isotherms of PDVBs with different amounts of triazole based-co-monomer. The higher level of co-monomer incorporation into the PDVB led to the lower surface area and pore volume. The surface area of non-functionalized PDVB (no co-monomer) was dropped from 789 to 500 m^2g^{-1} for the maximum amount of VT (PDVB-VT0.9). Besides, the amount of initiator was optimized by varying the AIBN from 0.0065 to 0.09 g which resulted in PDVB-VT-IN0.0065 to PDVB-

VT-IN0.09 (Figure 1c). Increasing the amount of initiator led to more incorporation of VT into PDVB structure which resulted in less surface area. Since polymerization did not occur for the lowest amount of AIBN (PDVB-VT-IN0.0065), there is no isotherm for this sample in Figure 1c.

Fourier Transform Infrared Spectroscopy (FTIR). Figure 4.2 displays the IR bands of PDVB in comparison with the amine functionalized ones. The existence of C-N bands in the porous amine-functionalized PDVB was observed which confirmed the successful integration of VI and VT into PDVB.

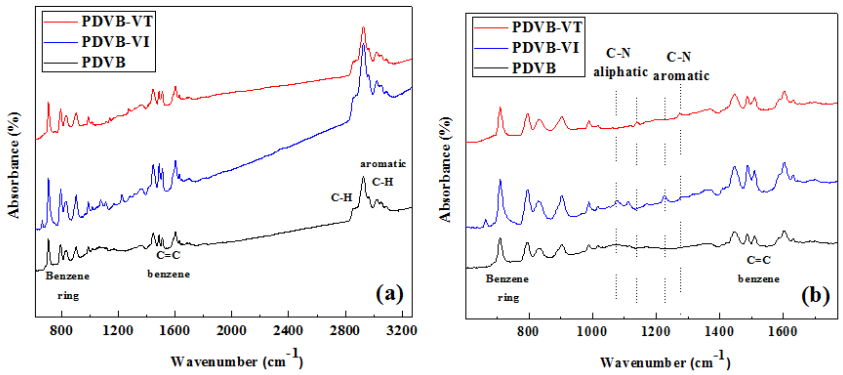

Figure 4.2 FTIR spectra a) PDVB with and without VI and VT co-monomers, b) same spectra zoomed in 600 – 1800 cm-1 indicating amine incorporation to the polymer.

IR bands of PDVB in **Figure 4.2a**, indicates the characteristic bands of benzene rings at 700-750 cm^{-1} And the benzene C=C stretching vibration bands at 1500 and 1600 cm^{-1}[167]. The IR bands at 2920 cm^{-1} and 3030 cm^{-1} are related to aliphatic C-H stretching vibrations and aromatic C-H stretching vibrations, respectively. For PDVB-VI and PDVB-VT, both aliphatic and aromatic C-N bands were detected in the range of 1020-1240 cm^{-1} and 1250-1360 cm^{-1}[160] (**Figure 4.2b**).

X-ray photoelectron Spectroscopy (XPS). The incorporation of VI and VT co-monomers into PDVB was evaluated by XPS. **Figure 4.3(a-b)** indicates the high-resolution peaks on carbon and nitrogen. High-resolution spectra of C 1s and N 1s for both PDVB-VI and PDVB-VT were taken using a 50 eV passing energy. The instrument was calibrated to give an Au 4f7/2 metallic gold binding energy of 83.96 eV[82]. To insure the cleanliness of the standard calibration sample, a gold foil was argon ion bombarded and spectral data were subsequently recorded over the full energy range, C 1s and N 1s spectra were deconvoluted using CasaXPS software (version 2.3.12).

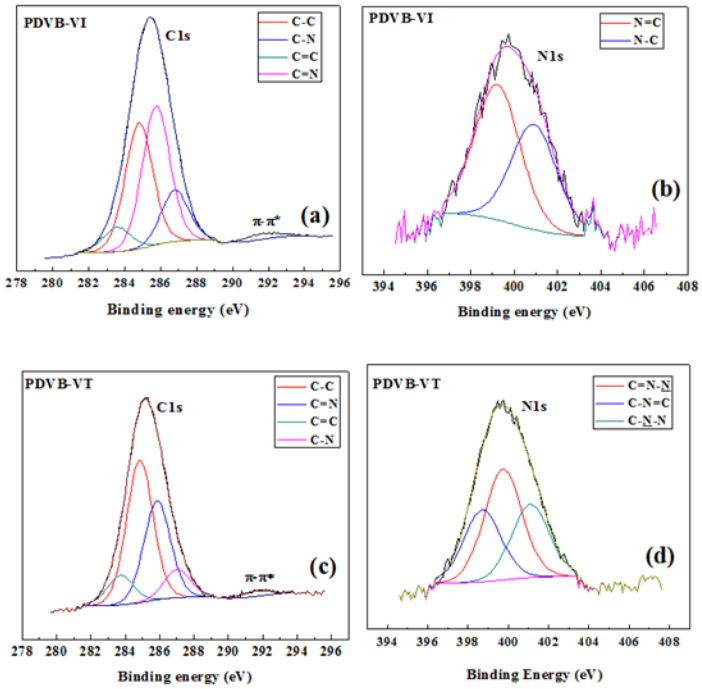

Figure 4.3 C 1s and N 1s XPS spectra a, b) PDVB-VI; c,d) PDVB-VT.

High-resolution spectra of C 1s and N 1s for PDVB-VI were collected to reveal its atomic components. Deconvoluted C 1s for PDVB-VI showed C=N and C-N peaks at 286.8 eV and 285.7 eV, respectively. Although the deconvolution pattern and binding energies of synthetic

peaks of C 1s in PDVB-VI resembled the corresponding one in PDVB-VT, the high-resolution spectrum of N 1s in PDVB-VI showed a lower number of synthetic peaks. In the C 1s spectrum of PDVB-VT, five different areas were resolved which indicated different types of carbon atoms in PDVB-VT. The peak at 284.8 eV was assigned to adventitious carbon and all other peaks were referenced to that one[83]. The peaks at 285.8 and 287.0 eV correspond to C=N and C-N, respectively[84]. The π-π* transition (291.6 eV) which is a characteristic shake-up line in aromatic compounds emphasized the presence of aromatic rings in the final product[85]. The N 1s spectrum in PDVB-VI was deconvoluted into only two peaks. The synthetic peak appeared at 399.23 eV and showed the contribution of imine nitrogen in PDVB-VI. The sp^3 nitrogen was also assigned to the peak appeared at 400.91 eV[86]. However, the high-resolution spectrum of N 1s of PDVB-VT was deconvoluted using three peaks. Binding energies of 398.72, 399.75, and 401.10 eV belonged to C=N-N, C=N-N, and C-N-N, respectively.

Scanning Electron Microscopy (SEM). Figure 4.4 shows SEM images of PDVB and the amine functionalized materials. This indicates porosity in the polymeric structures of PDVB materials which are ideal for fast diffusion of gas molecules.

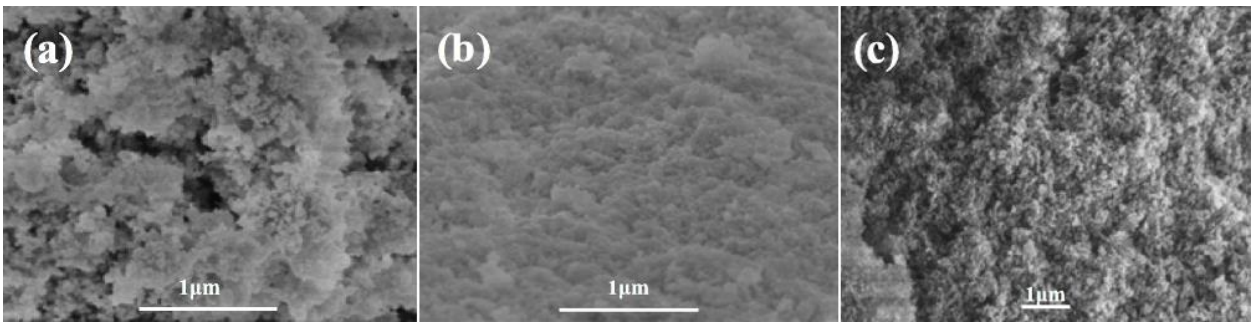

Figure 4.4 SEM images of a) PDVB, b) PDVB-VI0.7 and c) PDVB-VT0.7.

4.3.2 CO_2 Adsorption Study

All synthesized PDVB adsorbents (various co-monomers, different amounts of co-monomer, and changing initiator amounts) were evaluated under similar conditions to obtain CO_2 adsorptive capacities at a pressure of 1 bar. **Table 4.1** and **Figure 4.5** represent the CO_2 adsorptive properties of all PDVB adsorbents at 273K and atmospheric pressure.

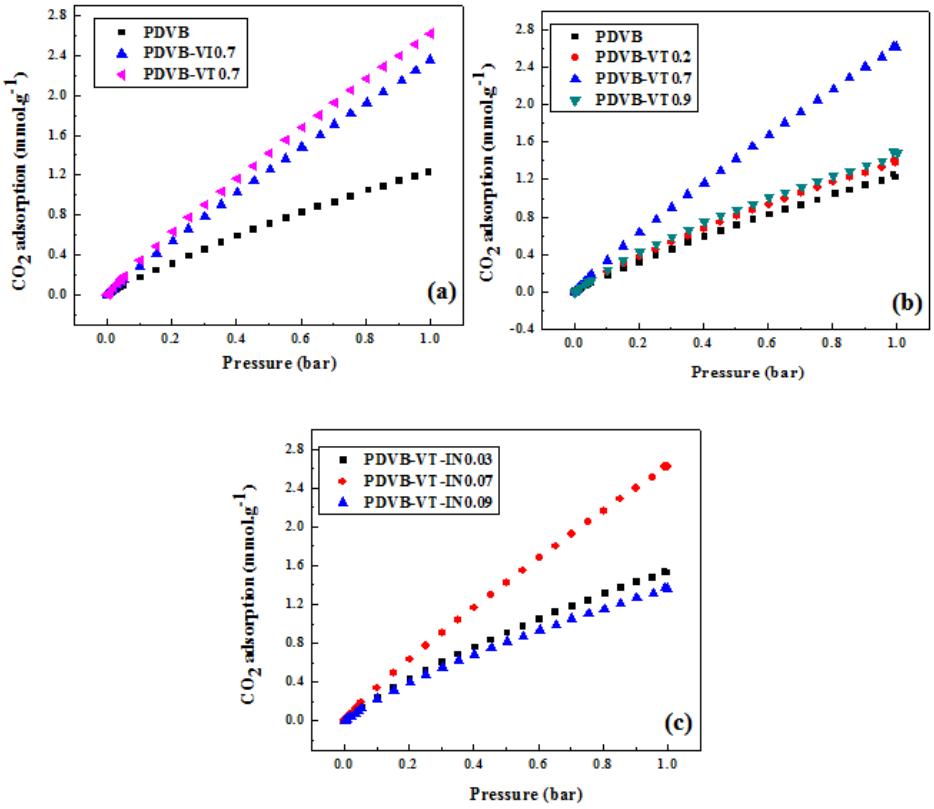

Figure 4.5 CO_2 uptake by a) PDVB with co-monomers of VI and VT, b) PDVB-VT with varied VT amount, c) PDVB-VT with varied initiator (AIBN) amount.

Table 4.1a and **Figure 4.5a** indicate the effect of amine functionalization of PDVB through VI and VT incorporation (where the amount of initiator (AIBN) is constant 0.07 g). Although surface area and pore volume were reduced by co-monomer insertion, the CO_2 adsorption

capacity of PDVB was increased by the factors of 1.9 and 2.2 for VI and VT, respectively. **Table 4.1b** shows that the optimum level of VT was obtained at 0.7 g.

Table 4.1 Effect of co-monomers types, co-monomer, and initiator amount on the textural and adsorptive properties of porous PDVB.

	Materials	Co-monomer/ Initiator	Surface area (m^2g^{-1})	Pore volume (cc g^{-1})	CO_2 Adsorption (mmol g^{-1})
a	PDVB	--	789	0.97	1.23
AIBN constant	PDVB-VI0.7	VI	649	0.82	2.35
	PDVB-VT0.7	VT	646	0.81	2.65
b	PDVB-VT0.2	VT=0.2	697	0.88	1.39
AIBN constant	PDVB-VT0.7	VT=0.7	646	0.81	2.65
	PDVB-VT0.9	VT=0.9	500	0.67	1.49
c	PDVB-VT-IN0.0065*	IN=0.0065	N/A	N/A	N/A
VT constant	PDVB-VT-IN0.03	IN=0.030	815	1.9	1.48
	PDVB-VT-IN0.07	IN=0.070	646	0.81	2.65
	PDVB-VT-IN0.09	IN=0.090	559	0.61	1.39

The lower amount of VT (0.2 g) led to very few CO_2 enhancements that could be in the range of error which is demonstrated in **Figure 4.5b** (the amount of initiator (AIBN) is constant and equal to 0.07 g). Therefore, a small amount of VT has a negligible effect on the CO_2 adsorption capacity of PDVB adsorbent. **Table 4.1c** and **Figure 4.5c** show the effect of initiator (AIBN) on the textural properties and CO_2 adsorptive characteristics. At a very low amount of AIBN (0.0065 g), polymerization did not occur. By increasing the initiator amount to 0.03 g, the highest surface area (815 m^2g^{-1}) and pore volume (1.9 ccg^{-1}) was obtained. More addition of

initiator deteriorates the textural properties. Regarding CO_2 uptake, by increasing the initiator amount, the adsorption efficiency improved then declined (IN= 0.09 g). Initiator helps the incorporation of VT into the polymer during polymerization due to an increase of CO_2 uptake while the surface area was reduced. Therefore, the addition of more AIBN led to involving more VT monomers onto the surface of the porous polymer. Consequently, there is an optimum point for initiator amount (0.07 g) in which high surface area and high amount of VT were maintained at the same time to obtain the highest CO_2 uptake. **Figure 4.6** illustrates the selectivity of CO_2 capture over N_2 at 273K for PDVB and amine functionalized materials. All PDVB based adsorbents have negligible N_2 uptake at 273K.

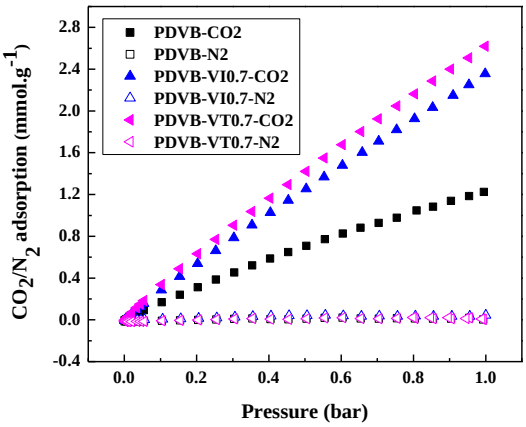

Figure 4.6 Comparison of CO_2 versus N_2 adsorption by PDVB adsorbents with different co-monomers at T=273K.

Based on the CO_2 adsorptive isotherms of PDVB materials under two temperatures of 273 and 298K, the isosteric heat of adsorption (Q_{st}) was calculated using the Clausius-Clapeyron relation (Equation 1). **Figure 4.7a** shows the range of heat of adsorption for PDVB (20-35 $KJmol^{-1}$)

decreased by integration of VI to the structure (25-35 $KJmol^{-1}$) and increased by VT incorporation (17-35 $KJmol^{-1}$).

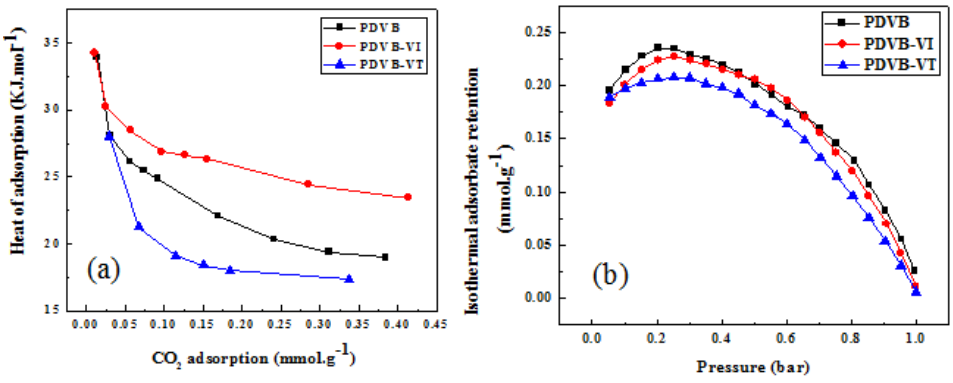

Figure 4.7 a) Isosteric heat of CO_2 adsorption (Qst) on PDVB with co-monomers; b) Isothermal adsorbate retention (IAR) of PDVB adsorbents with different co-monomers.

The energy of adsorption sites could be estimated based on the hysteresis in the adsorption-desorption isotherms of CO_2 which is calculated based on isothermal adsorbate retention (IAR) (Equation 2) which is shown in **Figure 4.7b**. Retained CO_2 during desorption (IAR) occurred more at low pressures, and the CO_2 amount is minuscule which confirms easy regeneration of PDVB adsorbents. The onset pressures of IAR were obtained through extrapolation of two rising and falling regions of IAR for PDVB, PDVB-VI, and PDVB-VT which were 0.27, 0.32, and 0.35 bar respectively. The larger onset pressure implies a higher energy of active sites[78]. This indicates that amine incorporation led to the formation of more adsorption sites.

4.3.3 Computational Study

Computational Findings. To determine the active site of the adsorbents, a CO_2 molecule is placed at several inequivalent sites of the PDVB polymer, where CO_2 attaches itself to one of the benzene rings and the C-C chain. Among these two configurations, CO_2 shows relative stability on the benzene ring of PDVB as shown in **Figure 4.8a** with a binding energy of 0.11 eV calculated using Equation 3. The distance of O(CO_2) from the benzene ring of the polymer is calculated to be 3.87 Å. While the adsorbed CO_2 is slightly bent with bond angle 0.70° as compared to the linear free CO_2, the average C-O bond length (dC-O) remains almost the same relative to the free standing CO2. For the copolymers of vinylimidazol (PDVB-VI) and vinyl triazole (PDVB-VT) CO_2 molecule is adsorbed on several sites of these copolymers.

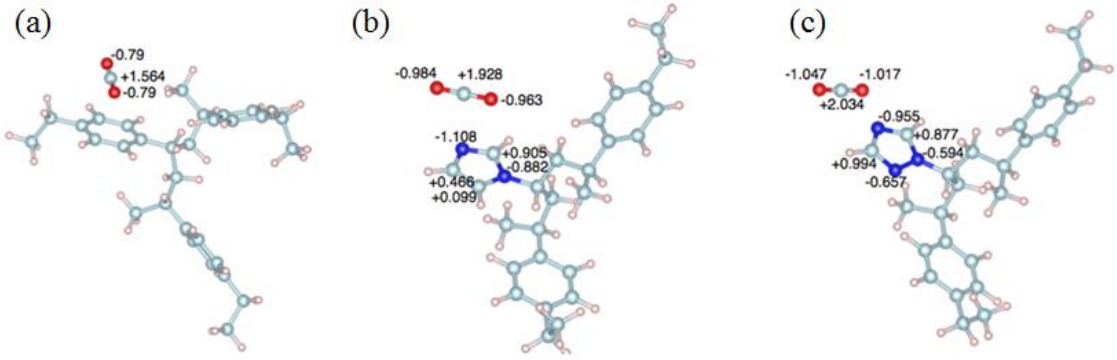

Figure 4.8 The optimized structures of CO_2-polymer complexes. Red, cyan, blue and white balls denote the O, C, N and H atoms, respectively. The partial charge is calculated using Bader charge analysis.[78]

Figure 4.8 (b-c) shows the optimized structures of CO_2-(PDVB-VI, PDVB-VT) complexes. For both polymers, CO_2 prefers to adsorb near the N-site of the copolymer with binding energies of 0.15 eV and 0.19 eV for PDVB-VI and PDVB-VT, respectively. The difference in the binding energy can be due to the different adsorption orientation of CO_2 on the imidazole/triazole ring. For the PDVB-VI case, CO_2 adsorbs almost parallel to the imidazole ring with an average vertical distance of 3.65 Å from C(CO_2) to the imidazole ring. For the PDVB-VT case, CO_2 remains almost along the plane of the triazole rings with a horizontal distance of 2.89 Å from C(CO_2) to one of the nitrogen atoms. The adsorption energies on the copolymers are larger compared to the PDVB polymer and stronger on PDVB-VT. This finding is in agreement with the experimental results. Due to enhanced binding strengths on the copolymers relative to PDVB, the CO_2 molecule shows increased bending (1.74°:PDVB-VI, 3.28°: PDVB-VT) as compared to free CO_2 with no significant change in dC(C-O). However, the adsorption sites of the polymers exhibit some local charges as shown in **Figure 4.9(a-c)** in which Bader charge analysis was used[87]. To probe the adsorption capacity, we added a second CO_2 molecule on different sites of PDVB-VI and PDVB-VT with CO_2 co-adsorbed. Various configurations are possible with the added CO_2 molecules such as dimerization[88] or odd clusters[89] as pointed out in previous literature. However here we only considered CO_2-adsorbent interactions. For the adsorption of the second CO_2, we have chosen only PDVB-VI and PDVB-VT since they show high binding for CO_2 as compared to pure PDVB. The low energy optimized complexes are shown in **Figure 4.9 (a, b)**. As already observed for the first molecule, the second CO_2 also shows a high stability near the N-site of the copolymers with binding energies (calculated using Equation 4) 0.01 eV, 0.08 eV for PDVB-VI and PDVB-VT, respectively.

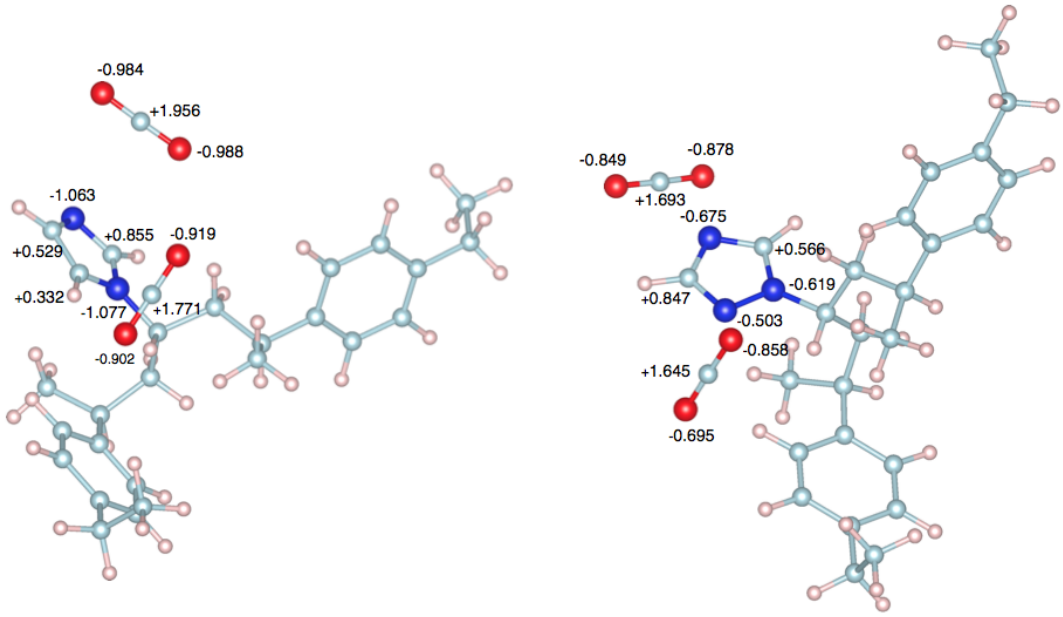

Figure 4.9 The optimized structures of two CO_2 molecules with the copolymer. Red, cyan, blue and white balls denote the O, C, N and H atoms, respectively. The partial charge is calculated using Bader charge analysis.

4.4 Adsorbent Recycling

Up to seven cycles of CO_2 adsorption and desorption were performed on PDVB-VT0.7 which indicates high chemical and physical stability (**Figure 4.10**). The CO_2 adsorption efficiency was maintained at 100% after the 7th cycle. In the porous adsorbents, inter-particle spaces should be considered under high pressure gas adsorption and storage (pre-combustion process) [90]. However, our work focused on CO_2 adsorption under atmospheric pressure (post-combustion process).

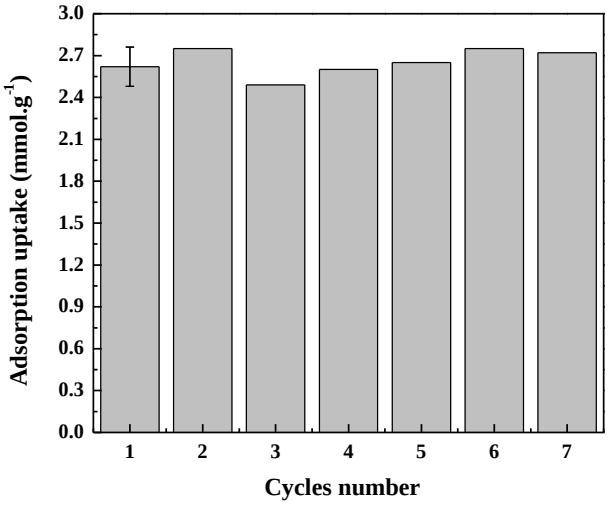

Figure 4.10 Regeneration of PDVB-VT0.7 for seven cycles (The error bar represents standard deviation of ±0.14 $mmolg^{-1}$).

4.5 Discussion

Previously reported amine functionalized PDVB by tartardiamide co-monomer[66] with more hydrophilic functionalities of –OH and =O might have less moisture resistivity which is detrimental for CO_2 adsorption from flue gas. Furthermore, in the earlier works on CO_2 adsorption by amine-functionalized PDVB, active adsorption sites, type of adsorption, and the trade-off between functionality and surface area have not been established[65–67]. Finally,

adsorptive properties of non-functionalized PDVB have not been studied in comparison with the modified ones which are important to clarify the role of various functionalities.

Here, we systematically studied the surface area and CO_2 adsorptive properties of highly hydrophobic PDVB-based materials to illuminate the role of amine rich co-monomers and to identify active sites for CO_2 molecules. The CO_2 uptake and heat of adsorption of non-functionalized PDVB were compared with the amine-modified ones to investigate the role of different co-monomers with various densities of nitrogen species and the loading amount of nitrogen-rich co-monomers. Water contact angle measurements of PDVB-VT (150^o)[60] have shown high hydrophobicity and moisture resistivity which makes this material a good candidate for CO_2 removal from flue gas. Utilizing microwave assisted synthesis is helpful in screening various types of polymer modifications since this is much quicker than hydrothermal methods. For microwave assisted synthesis of functionalized PDVB we used 2 h of heating, while the hydrothermal approach takes about 20 h.

The surface area and pore volume dropped about 20% when co-monomer functionalities (VI or VT) were incorporated into the PDVB structure. In fact, there was a trade-off between textural properties and amine functionality loading. An optimum condition could be obtained where enough amounts of amine functionalities were loaded while surface area and pore volumes were maintained at relatively high levels. Decreasing the amount of initiator led to more elevated surface area[65] partly due to controlling the rate of polymerization and formation of pores while limiting co-monomer incorporation. IR spectroscopy confirmed incorporation of amine species for PDVB-VI and PDVB-VT. According to deconvoluted patterns of N1s for PDVB-VT in XPS analysis, different types of nitrogen atoms corresponding to the triazole ring were observed. The XPS results simultaneously confirmed the incorporation of nitrogen resulting from

copolymerization of PDVB with VI and VT and distinguished PDVB-VI from PDVB-VT. Morphological studies of PDVB, PDVB-VI, and PDVB-VT also revealed the porous structure of these materials. However, the SEM image of bare PDVB showed a less dense three-dimensional structure with higher accessible surfaces. SEM images of PDVB-VI and PDVB-VT at high magnification illustrated relative packed structures, and fewer available surfaces than the non-functionalized PDVB. Microstructural analyses of these samples were in good agreement with surface area analysis, which showed that nitrogen incorporation led to declining of the surface area of the polymer.

Extensive theoretical studies have shown that different types of interaction takes place between CO_2 on the triazole and imidazole subunits. Dalbouha et al. have shown that there is significant orientation dependence for intermolecular interactions between CO_2 and imidazole [91]. The orientation we figured was closer to a C1 structure comparing to their study which could be due to the side units added in the polymeric environment. Another study which extensively examined configurational analysis between CO_2 and triazole showed strong anisotropic interactions [92]. Here we have shown that comparing CO_2 – adsorbent interactions with the same level of theory we get stronger interactions with triazole. Nitrogen-rich co-monomer of VT resulted in enhancements in the CO_2 adsorptive properties due to providing abundant active sites toward CO_2 molecules[24]. However, further increase in the amount of VT (PDVB-VT0.9) led to reduction in the surface area and pore volume which showed less activity in comparison with PDVB-VT0.7. Although amine functionalities improve the adsorption efficiency, low surface area adversely impacts CO_2 adsorption capacity. High selectivity of CO_2 over N_2 was obtained by the hydrophobic structure of all PDVB materials which was enhanced by amine functionalities (**Figure 4.6**). Calculated heats of adsorption (Q_{st}) for all PDVB materials revealed

similar changes of Q_{st} for CO_2 uptake. Higher Q_{st} at the beginning of CO_2 adsorption is due to stronger interaction between CO_2 molecules and adsorbents which resulted from more available active sites[93]**.** However, as adsorption progressed, the heat of adsorption decreases due to fewer accessible pores and active sites. Electrostatic fields within pores are attributed to CO_2 uptake by adsorbent at low coverage of CO_2 (low pressure). However, at high coverage of CO_2, the interaction between electrostatic field gradients in the adsorbent and the CO_2 quadrupole moment is the main factor affecting the adsorption efficiency. Physisorption could be considered for Q_{st} less than 80 $kJmol^{-1}$, while for Q_{st} of 80-200 $kJmol^{-1}$, chemisorption of CO_2 is dominant[94]. Onset pressure calculations based on IAR diagrams, indicated that more nitrogen-rich amine functionality of VT provided higher energy of active sites. All PDVB materials showed Q_{st} less than 80 $kJmol^{-1}$ which are attributed to a more physical adsorption pathway. Our computational studies reveal that the presence of a model with adsorbed CO_2 reduces the adsorption energy of the second CO_2 on the copolymer complex. However, PDVB-VT still maintains the trend of high adsorption capacity for CO_2 than PDVB-VI due to the more amine-rich structure.

4.6 Conclusions

We utilized microwave assisted synthesis to optimize surface area and functionality of thermally and chemically stable porous PDVB for ecological sustainability through CO_2 adsorption. The amine incorporation into PDVB was confirmed by FTIR and XPS for both imidazole and triazole based co-monomers. Different densities of amine in each co-monomer led to various textural properties and adsorption capacities. With more amine functionalities loaded into PDVB, lower surface areas and pore volumes were obtained. The optimization of the amount of amine functionalities and initiator regarding CO_2 adsorption, led to high adsorption efficiency while

achieving relatively high surface areas and pore volumes. The CO_2 adsorptive properties of PDVB were enhanced more than 116% by the optimized synthesis condition of more amine rich functionality (VT) into the mesoporous polymer (PDVB-VT0.7-IN0.07). Calculated heat of adsorption showed physical adsorption of CO_2 molecules by PDVB based adsorbents. Isothermal adsorbate retention also showed that VT incorporation provides active sites with higher energy to capture CO_2. Computational studies confirm that the triazole ring has a higher capacity of attracting CO_2 as compared to the imidazole ring.

4.7 References

(1) Rashidi, N. A.; Yusup, S. An overview of activated carbons utilization for the post-combustion carbon dioxide capture. *J. CO2 Util.* **2016**, *13*, 1–16.

(2) Sumida, K.; Rogow, D. L.; Mason, J. a; Mcdonald, T. M.; Bloch, E. D.; Herm, Z. R.; Bae, T.; Long, J. R. Carbon Dioxide Capture in Metal À Organic Frameworks. *Chem. Rev.* **2012**, *112*, 724–781.

(3) Ipcc. *Contribution of Working Group I to the Third Assessment Report of the Intergovernmental Panel on Climate Change*; 2001; Vol. 446.

(4) IPCC WGI AR5. Climate Change 2013: The Physical Science Basis. *Ipcc* **2013**, 31.

(5) Wall, T. F. Combustion processes for carbon capture. *Proc. Combust. Inst.* **2007**, *31 I*, 31–47.

(6) Espinal, L.; Poster, D. L.; Wong-Ng, W.; Allen, A. J.; Green, M. L. Measurement, standards, and data needs for CO2 capture materials: A critical review. *Environ. Sci. Technol.* **2013**, *47* (21), 11960–11975.

(7) Yang, H.; Xu, Z.; Fan, M.; Slimane, R. B.; Bland, A. E.; Wright, I. Progress in carbon dioxide seperation and capture: A review. *J. Environ. Sci.* **2008**, *20*, 14–27.

(8) Samanta, A.; Zhao, A.; Shimizu, G. K. H.; Sarkar, P.; Gupta, R. Post-combustion CO 2 capture using solid sorbents: A review. *Ind. Eng. Chem. Res.* **2012**, *51* (4), 1438–1463.

(9) Hwang, C.-C.; Tour, J. J.; Kittrell, C.; Espinal, L.; Alemany, L. B.; Tour, J. M. Capturing carbon dioxide as a polymer from natural gas. *Nat. Commun.* **2014**, *5*, 3961.

(10) Kapdi, S. S.; Vijay, V. K.; Rajesh, S. K.; Prasad, R. Biogas scrubbing, compression and storage: Perspective and prospectus in Indian context. *Renew. Energy* **2005**, *30* (8), 1195–1202.

(11) Satyapal, S.; Filburn, T.; Trela, J.; Strange, J. Performance and properties of a solid amine

sorbent for carbon dioxide removal in space life support applications. *Energy and Fuels* **2001**, *15* (2), 250–255.

(12) Builes, S.; López-Aranguren, P.; Fraile, J.; Vega, L. F.; Domingo, C. Analysis of CO 2 Adsorption in Amine-Functionalized Porous Silicas by Molecular Simulations. *Energy & Fuels* **2015**, *29* (6), 3855–3862.

(13) Chang, G.; Yang, L.; Yang, J.; Huang, Y.; Cao, K.; Ma, J.; Wang, D. A nitrogen-rich, azaindole-based microporous organic network: synergistic effect of local dipole–π and dipole–quadrupole interactions on carbon dioxide uptake. *Polym. Chem.* **2016**, *7* (37), 5768–5772.

(14) Auta, M.; Umaru, M.; Yahya, M. D.; Adeniyi, O. D.; Aris, I. M.; Suleiman, B. Diethanolamine Functionalized Waste Tea Activated Carbon for CO 2 Adsorption. **2015**.

(15) Siriwardane, R. V.; Shen, M. S.; Fisher, E. P.; Poston, J. A. Adsorption of CO2 on molecular sieves and activated carbon. *Energy and Fuels* **2001**, *15* (2), 279–284.

(16) Grande, C. a. Advances in Pressure Swing Adsorption for Gas Separation. *ISRN Chem. Eng.* **2012**, *2012*, 1–13.

(17) Choi, S.; Drese, J. H.; Jones, C. W. Adsorbent materials for carbon dioxide capture from large anthropogenic point sources. *ChemSusChem* **2009**, *2* (9), 796–854.

(18) Kim, K.; Han, J. W.; Lee, K. S.; Lee, W. B. Promoting alkali and alkaline-earth metals on MgO for enhancing CO2 capture by first-principles calculations. *Phys. Chem. Chem. Phys.* **2014**, *16* (45), 24818–24823.

(19) Mahurin, S. M.; Górka, J.; Nelson, K. M.; Mayes, R. T.; Dai, S. Enhanced CO2/N2 selectivity in amidoxime-modified porous carbon. *Carbon N. Y.* **2014**, *67*, 457–464.

(20) Li, K.; Jiang, J.; Tian, S.; Yan, F.; Chen, X. Polyethyleneimine–nano silica composites: a low-cost and promising adsorbent for CO\n 2\n capture. *J. Mater. Chem. A* **2015**, *3* (5), 2166–2175.

(21) Gargiulo, N.; Peluso, A.; Aprea, P.; Pepe, F.; Caputo, D.; Ingegneria, D.; Sannio, U.; Roma, P. CO 2 Adsorption on Polyethylenimine-Functionalized SBA-15 Mesoporous Silica : Isotherms and Modeling. *J. Chem. Eng. Data* **2014**, *59*, 896−902.

(22) Hudson, M. R.; Queen, W. L.; Mason, J. A.; Fickel, D. W.; Lobo, R. F.; Brown, C. M. Unconventional, highly selective CO 2 adsorption in zeolite SSZ-13. *J. Am. Chem. Soc.* **2012**, *134* (4), 1970–1973.

(23) Zhang, Z.; Yao, Z.-Z.; Xiang, S.; Chen, B. Perspective of microporous metal–organic frameworks for CO 2 capture and separation. *Energy Environ. Sci.* **2014**, *7* (9), 2868.

(24) Wang, K.; Huang, H.; Liu, D.; Wang, C.; Li, J.; Zhong, C. Covalent Triazine-Based Frameworks with Ultramicropores and High Nitrogen Contents for Highly Selective CO2 Capture. *Environ. Sci. Technol.* **2016**, *50* (9), 4869–4876.

(25) Xiong, S.; Fu, X.; Xiang, L.; Yu, G.; Guan, J.; Wang, Z.; Du, Y.; Xiong, X.; Pan, C. Liquid acid-catalysed fabrication of nanoporous 1,3,5-triazine frameworks with efficient

and selective CO2 uptake. *Polym. Chem.* **2014**, *5* (10), 3424.

(26) Martunus; Helwani, Z.; Wiheeb, A. D.; Kim, J.; Othman, M. R. Improved carbon dioxide capture using metal reinforced hydrotalcite under wet conditions. *Int. J. Greenh. Gas Control* **2012**, *7*, 127–136.

(27) Lee, Z. H.; Lee, K. T.; Bhatia, S.; Mohamed, A. R. Post-combustion carbon dioxide capture: Evolution towards utilization of nanomaterials. *Renew. Sustain. Energy Rev.* **2012**, *16* (5), 2599–2609.

(28) Besson, R.; Rocha Vargas, M.; Favergeon, L. CO 2 adsorption on calcium oxide: An atomic-scale simulation study. *Surf. Sci.* **2012**, *606* (3-4), 490–495.

(29) Jiang, T.; Zhong, W.; Jafari, T.; Du, S.; He, J.; Fu, Y.-J.; Singh, P.; Suib, S. L. Siloxane D4 adsorption by mesoporous aluminosilicates. *Chem. Eng. J.* **2016**.

(30) Jafari, T.; Jiang, T.; Zhong, W.; Khakpash, N.; Deljoo, B.; Aindow, M.; Singh, P.; Suib, S. L. Modified Mesoporous Silica for Efficient Siloxane Capture. *Langmuir* **2016**, *32* (10), 2369–2377.

(31) Chen, C.; Park, D. W.; Ahn, W. S. CO2 capture using zeolite 13X prepared from bentonite. *Appl. Surf. Sci.* **2014**, *292*, 63–67.

(32) Cheung, O.; Bacsik, Z.; Liu, Q.; Mace, A.; Hedin, N. Adsorption kinetics for CO2 on highly selective zeolites NaKA and nano-NaKA. *Appl. Energy* **2013**, *112*, 1326–1336.

(33) Li, G.; Xiao, P.; Webley, P. A.; Zhang, J.; Singh, R. Competition of CO2/H2O in adsorption based CO2 capture. *Energy Procedia* **2009**, *1* (1), 1123–1130.

(34) Ferreira, L. S.; Trierweiler, J. O. Modeling and simulation of the polymeric nanocapsule formation process. *IFAC Proc. Vol.* **2009**, *7* (PART 1), 405–410.

(35) Himeno, S.; Tomita, T.; Suzuki, K.; Yoshida, S. Characterization and selectivity for methane and carbon dioxide adsorption on the all-silica DD3R zeolite. *Microporous Mesoporous Mater.* **2007**, *98* (1-3), 62–69.

(36) Keskin, S.; van Heest, T. M.; Sholl, D. S. Can metal-organic framework materials play a useful role in large-scale carbon dioxide separations? *ChemSusChem* **2010**, *3* (8), 879–891.

(37) Kizzie, A. C.; Wong-Foy, A. G.; Matzger, A. J. Effect of humidity on the performance of microporous coordination polymers as adsorbents for CO2 capture. *Langmuir* **2011**, *27* (10), 6368–6373.

(38) Zhao, Y.; Yao, K. X.; Teng, B.; Zhang, T.; Han, Y. A perfluorinated covalent triazine-based framework for highly selective and water-tolerant CO2 capture. *Energy Environ. Sci.* **2013**, *6* (12), 3684–3692.

(39) Lu, W.; Yuan, D.; Sculley, J.; Zhao, D.; Krishna, R.; Zhou, H. C. Sulfonate-grafted porous polymer networks for preferential Co 2 adsorption at low pressure. *J. Am. Chem. Soc.* **2011**, *133* (45), 18126–18129.

(40) Ragon, F.; Campo, B.; Yang, Q.; Martineau, C.; Wiersum, A. D.; Lago, A.; Guillerm, V.; Hemsley, C.; Eubank, J. F.; Vishnuvarthan, M.; et al. Acid-functionalized UiO-66(Zr)

MOFs and their evolution after intra-framework cross-linking: structural features and sorption properties. *J. Mater. Chem. A* **2015**, *3* (7), 3294–3309.

(41) Lee, M. S.; Park, S. J. Silica-coated multi-walled carbon nanotubes impregnated with polyethyleneimine for carbon dioxide capture under the flue gas condition. *J. Solid State Chem.* **2015**, *226*, 17–23.

(42) Guo, L.; Hu, X.; Hu, G.; Chen, J.; Li, Z.; Dai, W.; Dacosta, H. F. M.; Fan, M. Tetraethylenepentamine modified protonated titanate nanotubes for CO2 capture. *Fuel Process. Technol.* **2015**, *138*, 663–669.

(43) Yao, M.; Dong, Y.; Feng, X.; Hu, X.; Jia, A.; Xie, G.; Hu, G.; Lu, J.; Luo, M.; Fan, M. The effect of post-processing conditions on aminosilane functionalizaiton of mesocellular silica foam for post-combustion CO2 capture. *Fuel* **2014**, *123*, 66–72.

(44) Wang, D.; Sentorun-Shalaby, C.; Ma, X.; Song, C. High-capacity and low-cost carbon-based "molecular basket" sorbent for CO2 capture from flue gas. *Energy and Fuels* **2011**, *25* (1), 456–458.

(45) Yu, C. H.; Huang, C. H.; Tan, C. S. A review of CO2 capture by absorption and adsorption. *Aerosol Air Qual. Res.* **2012**, *12* (5), 745–769.

(46) Bollini, P.; Brunelli, N. A.; Didas, S. A.; Jones, C. W. Dynamics of CO2 adsorption on amine adsorbents. 1. impact of heat effects. *Ind. Eng. Chem. Res.* **2012**, *51* (46), 15145–15152.

(47) Alkordi, M. H.; Haikal, R. R.; Hassan, Y. S.; Emwas, A.-H.; Belmabkhout, Y. Poly-functional porous-organic polymers to access functionality – CO 2 sorption energetic relationships. *J. Mater. Chem. A* **2015**, *3* (45), 22584–22590.

(48) Yang, F.-M.; Liu, Y.; Chen, L.; Au, C.-T.; Yin, S.-F. Synthesis of amine-modified solid Fe-Zr adsorbents for CO $_2$ adsorption. *J. Chem. Technol. Biotechnol.* **2015**, No. August, n/a – n/a.

(49) Liebl, M. R.; Senker, J. Microporous functionalized triazine-based polyimides with high CO 2 capture capacity. *Chem. Mater.* **2013**, *25* (6), 970–980.

(50) Sekizkardes, A. K.; Altarawneh, S.; Kahveci, Z.; Timur, I.; El-kaderi, H. M. Highly Selective CO 2 Capture by Triazine-Based Benzimidazole- Linked Polymers ˙ lamog l. *Macromolecules* **2014**, *47*, 8328–8334.

(51) Gu, C.; Liu, D.; Huang, W.; Liu, J.; Yang, R. Synthesis of covalent triazine-based frameworks with high CO 2 adsorption and selectivity. *Polym. Chem.* **2015**, *6*, 7410–7417.

(52) Hahn, M. W.; Jelic, J.; Berger, E.; Reuter, K.; Jentys, A.; Lercher, J. A. Role of Amine Functionality for CO2 Chemisorption on Silica. *J. Phys. Chem. B* **2016**, *120* (8), 1988–1995.

(53) Wu, D.; Xu, F.; Sun, B.; Fu, R.; He, H.; Matyjaszewski, K. Design and preparation of porous polymers. *Chem. Rev.* **2012**, *112* (7), 3959–4015.

(54) Neti, V. S. P. K.; Wang, J.; Deng, S.; Echegoyen, L. High and selective CO 2 adsorption

by a phthalocyanine nanoporous polymer. *J. Mater. Chem. A* **2015**, *3* (19), 10284–10288.

(55) Tan, M. X.; Zhang, Y.; Ying, J. Y. Mesoporous poly(melamine-formaldehyde) solid sorbent for carbon dioxide capture. *ChemSusChem* **2013**, *6* (7), 1186–1190.

(56) Puthiaraj, P.; Kim, S. S.; Ahn, W. S. Covalent triazine polymers using a cyanuric chloride precursor via Friedel-Crafts reaction for CO<inf>2</inf> adsorption/separation. *Chem. Eng. J.* **2016**, *283*, 184–192.

(57) Das, S. K.; Wang, X.; Ostwal, M. M.; Zhao, Y.; Han, Y.; Lai, Z. Highly stable porous covalent triazine-piperazine linked nanoflower as a feasible adsorbent for flue gas CO2 capture. *Chem. Eng. Sci.* **2016**, *145*, 21–30.

(58) Feng Bai; Xinlin Yang, and; Huang, W. Synthesis of Narrow or Monodisperse Poly(divinylbenzene) Microspheres by Distillation−Precipitation Polymerization. **2004**.

(59) Kanamori, K.; Nakanishi, K.; Hanada, T. Rigid Macroporous Poly(divinylbenzene) Monoliths with a Well-Defined Bicontinuous Morphology Prepared by Living Radical Polymerization. *Adv. Mater.* **2006**, *18* (18), 2407–2411.

(60) Zhu, W.; Kong, W.; Noshadi, I.; Zhao, L.; Liu, F. Solvothermal synthesis of nanoporous, polymeric solid bases with controlled wettability and good catalytic activity. *Colloids Surfaces A Physicochem. Eng. Asp.* **2014**, *444*, 314–320.

(61) Jafari, T.; Noshadi, I.; Khakpash, N.; Suib, S. L. Superhydrophobic and stable mesoporous polymeric adsorbent for siloxane removal: D4 super-adsorbent. *J. Mater. Chem. A* **2015**, *3* (9), 5023–5030.

(62) Noshadi, I.; Kanjilal, B.; Jafari, T.; Moharreri, E.; Khakpash, N.; Jiang, T.; Suib, S. L. Hydrophobic mesoporous adsorbent based on cyclic amine–divinylbenzene copolymer for highly efficient siloxane removal. *RSC Adv.* **2016**, *6* (81), 77310–77320.

(63) Zhang, Y.; Wei, S.; He, Y.; Nawaz, F.; Liu, S.; Zhang, H.; Xiao, F.-S. Solvothermal synthesis of carboxyl and amido functionalized mesoporous resins for water treatments. *J. Mater. Chem.* **2010**, *20* (22), 4609.

(64) Kuzmicz, D.; Coupillaud, P.; Men, Y.; Vignolle, J.; Vendraminetto, G.; Ambrogi, M.; Taton, D.; Yuan, J. Functional mesoporous poly(ionic liquid)-based copolymer monoliths: From synthesis to catalysis and microporous carbon production. *Polym. (United Kingdom)* **2014**, *55* (16), 3423–3430.

(65) Feng, X.; Gao, C.; Guo, Z.; Zhou, Y.; Wang, J. Pore structure controllable synthesis of mesoporous poly(ionic liquid)s by copolymerization of alkylvinylimidazolium salts and divinylbenzene. *RSC Adv.* **2014**, *4* (45), 23389–23395.

(66) Bhanja, P.; Gomes, R.; Bhaumik, A. N-rich porous organic polymer with suitable donor–donor–acceptor functionality for the sensing of nucleic acid bases and CO_2 storage application. *RSC Adv.* **2015**, *5* (91), 74916–74923.

(67) Gomes, R.; Bhaumik, A. Highly porous organic polymers bearing tertiary amine group and their exceptionally high CO2 uptake capacities. *J. Solid State Chem.* **2015**, *222*, 7–11.

(68) Wiesbrock, F.; Hoogenboom, R.; Schubert, U. S. Microwave-assisted polymer synthesis: State-of-the-art and future perspectives. *Macromol. Rapid Commun.* **2004**, *25* (20), 1739–1764.

(69) Bensebaa, F.; Farah, A. A.; Wang, D.; Bock, C.; Du, X.; Kung, J.; Le Page, Y. Microwave synthesis of polymer-embedded Pt-Ru catalyst for direct methanol fuel cell. *J. Phys. Chem. B* **2005**, *109* (32), 15339–15344.

(70) Raj, M. R.; Kim, M.; Kim, H. Il; Lee, G.-Y.; Park, C. W.; Park, T. A comparative study on the thermal- and microwave-assisted Stille coupling polymerization of a benzodithiophene-based donor–acceptor polymer (PTB7). *J. Mater. Chem. A* **2017**, *5* (Scheme 1), 3330–3335.

(71) Hoogenboom, R.; Paulus, R. M.; Pilotti, Åke; Schubert, U. S. Scale-up of Microwave-Assisted Polymerizations in Batch Mode: The Cationic Ring-Opening Polymerization of 2-Ethyl-2-oxazoline. *Macromol. Rapid Commun.* **2006**, *27* (18), 1556–1560.

(72) Sauks, J. M.; Mallik, D.; Lawryshyn, Y.; Bender, T.; Organ, M. A continuous-flow microwave reactor for conducting high-temperature and high-pressure chemical reactions. *Org. Process Res. Dev.* **2014**, *18* (11), 1310–1314.

(73) Paulus, R. M.; Erdmenger, T.; Becer, C. R.; Hoogenboom, R.; Schubert, U. S. Scale-up of microwave-assisted polymerizations in continuous-flow mode: Cationic ring-opening polymerization of 2-ethyl-2-oxazoline. *Macromol. Rapid Commun.* **2007**, *28* (4), 484–491.

(74) He, J.; Liu, Y.; Meng, Y.; Sun, X.; Biswas, S.; Shen, M.; Luo, Z.; Miao, R.; Zhang, L.; Mustain, W. E.; et al. High-rate and long-life of Li-ion batteries using reduced graphene oxide/Co 3 O 4 as anode materials. *RSC Adv.* **2016**, *6* (29), 24320–24330.

(75) Mason, J. A.; Sumida, K.; Herm, Z. R.; Krishna, R.; Long, J. R. Evaluating metal–organic frameworks for post-combustion carbon dioxide capture via temperature swing adsorption. *Energy Environ. Sci.* **2011**, *4* (8), 3030.

(76) Patil, R. S.; Banerjee, D.; Zhang, C.; Thallapally, P. K.; Atwood, J. L. Selective CO2 Adsorption in a Supramolecular Organic Framework. *Angew. Chemie - Int. Ed.* **2016**, 4599–4602.

(77) Tamilarasan, P.; Ramaprabhu, S. Amine-rich ionic liquid grafted graphene for sub-ambient carbon dioxide adsorption. *RSC Adv.* **2016**, *6* (4), 3032–3040.

(78) Tamilarasan, P.; Ramaprabhu, S. Integration of polymerized ionic liquid with graphene for enhanced CO 2 adsorption. *J. Mater. Chem. A* **2015**, *3* (1), 101–108.

(79) Perdew, J. P.; Yue, W. Accurate and simple density functional for the electronic exchange energy: Generalized gradient approximation. *Phys. Rev. B* **1986**, *33* (12), 8800–8802.

(80) Kresse, G.; Furthmuller, J. Efficiency of ab-initio total energy calculations for metals and semiconductors using a plane-wave basis set. *Comput. Mater. Sci.* **1996**, *6* (1), 15–50.

(81) Blöchl, P. E. Projector augmented-wave method. *Phys. Rev. B* **1994**, *50*, 17953–17979.

(82) Seah, M. P.; Gilmore, I. S.; Beamson, G. XPS: binding energy calibration of electron

spectrometers re-evaluation of the reference energies. *Surf. Interface Anal.* **1998**, *26* (9), 642–649.

(83) Miller, D. J.; Biesinger, M. C.; McIntyre, N. S. Interactions of CO2 and CO at fractional atmosphere pressures with iron and iron oxide surfaces: One possible mechanism for surface contamination? *Surf. Interface Anal.* **2002**, *33* (4), 299–305.

(84) Dementjev, A. P.; De Graaf, A.; Van de Sanden, M. C. M.; Maslakov, K. I.; Naumkin, A. V.; Serov, A. A. X-ray photoelectron spectroscopy reference data for identification of the C3N4 phase in carbon-nitrogen films. *Diam. Relat. Mater.* **2000**, *9* (11), 1904–1907.

(85) Guo, Z.; Cheng, J. K.; Hu, Z.; Zhang, M.; Xu, Q.; Kang, Z.; Zhao, D.; Asahi, R.; Morikawa, T.; Ohwaki, T.; et al. Metal-organic frameworks (MOFs) as precursors towards TiO x /C composites for photodegradation of organic dye. *RSC Adv.* **2014**, *4* (65), 34221–34225.

(86) Vinu, A.; Ariga, K.; Mori, T.; Nakanishi, T.; Hishita, S.; Golberg, D.; Bando, Y. Preparation and characterization of well-ordered hexagonal mesoporous carbon nitride. *Adv. Mater.* **2005**, *17* (13), 1648–1652.

(87) Bader, R. F. W. *Atoms in Molecules - A Quantum Theory (International Series of Monographs on Chemistry)*; Press, O. U., Ed.; New York, 1990.

(88) Chen, L.; Johnson, J. K. Formation of odd-numbered clusters of CO2 adsorbed, on nanotube bundles. *Phys. Rev. Lett.* **2005**, *94* (12), 1–4.

(89) Chang, C. M.; De Leon, A.; Alvaro, P. A.; Jalbout, A. F. Theoretical insights on the storage of carbon dioxide using single-walled carbon nanotubes. *Comput. Mater. Sci.* **2012**, *63*, 191–196.

(90) Marco-Lozar, J. P.; Juan-Juan, J.; Suárez-García, F.; Cazorla-Amorós, D.; Linares-Solano, A. MOF-5 and activated carbons as adsorbents for gas storage. *Int. J. Hydrogen Energy* **2012**, *37* (3), 2370–2381.

(91) Dalbouha, S.; Prakash, M.; Timón, V.; Komiha, N.; Hochlaf, M.; Senent, M. L. Explicitly correlated interaction potential energy profile of imidazole + CO2 complex. *Theor. Chem. Acc.* **2015**, *134* (5), 63.

(92) Boulmène, R.; Prakash, M.; Hochlaf, M. Microscopic investigations of site and functional selectivity of triazole for CO2 capture and catalytic applications. *Phys. Chem. Chem. Phys.* **2016**, *18* (43), 29709–29720.

(93) Singh, V. K.; Anil Kumar, E. Measurement and analysis of adsorption isotherms of CO2 on activated carbon. *Appl. Therm. Eng.* **2016**, *97*, 77–86.

(94) Zhou, X.; Yi, H.; Tang, X.; Deng, H.; Liu, H. Thermodynamics for the adsorption of SO2, NO and CO2 from flue gas on activated carbon fiber. *Chem. Eng. J.* **2012**, *200-202* (2), 399–404.

Chapter 5. Future Work- Metal incorporation in the adsorbent for CO_2 adsorption

5.1 Background

Another polar functionality could be metal ions which enhance the CO_2 selectivity over other gas molecules such as N_2. In zeolites, the presence of charge balancing cations (mostly alkali cation) inside pores enhances CO_2 selectivity[1]. Some transition metals such as cobalt, copper and manganese coordinate with amine groups which are obtained by bond formation or steric interactions between amine species and transition metals. Further incorporation of active metal ions in porous polymers can make them more active toward CO_2 adsorption. Copper complexes the polymers such as polyvinylamine[1] and polyvinylpyridine (P4VP)[2,3] have been reported. Thereby, the treatment of amine containing co-monomers with copper during copolymerization is expected to result in copper loaded amine-rich mesoporous PDVB. It is expected to capture more CO_2 by copper coordinated polymers than the ones without copper ions due to locally induced polarizability. A high degree of copper grafting by *in situ* methods in the mesoporous polymer is also expected. Metals (Co, Cr, Au, Cu) with poly vinylpyridine (P4VP) by simple mixing at room temperature have been investigated[2,3]. Reflux[4] or supercritical carbon dioxide[5] approaches also were employed to coordinate copper with P4VP. The variation of band intensity, wavenumber and bandwidth are the characteristics of the bonds between Cu^{2+} and the pyridine ring[2]. Pyrazine (Pyz) also coordinated with metals (Fe, Co, Ni) are acquired by hydrothermal reaction of pyrazine and metal salts[6]. Elsewhere, formation of copper salt complexes with pyrazine have been studied by Graham and Pike[7] which showed that copper halide forms a

complex with pyrazine which can have an advantages in preparing polymeric adsorbents with high CO_2 capacity and selectivity. As $CuCl_2$ coordination to the nitrogen atoms of the pyridine rings in P4VP matrices was demonstrated by IR spectroscopy[8], the copper precursor is $CuCl_2$.

5.2 Specific aims

The most significant long-term goal in CO_2 storage and sequestration technology (CCS) is to uptake CO_2 effectively from flue gas. Development of efficient adsorbents has been continued in order to overcome current CCS drawbacks such as low capacity and selectivity of CO_2 over other flue gas components, low stability and moisture sensitivity. A series of copper incorporated amine-rich mesoporous polydivinylbenzene will be obtained through a one-step polymerization of divinylbenzene (DVB) with an amine containing co-monomer (X) (PDVB-X/Cu-*in situ*). To assess the effectiveness of copper grafting into the polymer by one-step synthesis method, a two-step copper grafting (impregnation) in the polymer should be carried out on (PDVB-X/Cu-*ex situ*). Comprehensive characterization will be applied to the obtained polymers. So, the specific aims are summarized as:

- Study the effect of methods of metal ion incorporation (*in situ* or *ex situ*) on its loading efficiency and CO_2 adsorptive properties.
- Investigating the effect of moisture on gas adsorption properties.

5.3 Adsorbent Synthesis

5.3.1 *In-Situ* incorporation of copper into polymeric network

Co-monomer (X) and copper (II) salts at a molar ratio of (X/Cu: 1/3) will be mixed in DMF solution overnight at 30^{o}C in order to incorporate copper ions with the amine species of the

co-monomer. Then DVB and initiator will be added and the solution will be stirred for 3 h followed by hydrothermal treatments at 100^{o}C for 48 h and 150^{o}C for 12 h. The obtained monolith will be washed with water and ethanol to remove un-reacted monomers and copper ions. The powder will be dried at 60^{o}C to remove the solvent.

5.3.2 *Ex-Situ* incorporation of copper into polymeric network

The obtained PDVB-X will be impregnated by copper (II) salt at a molar ratio of (X/Cu: 1/3) in DMF solution overnight at 30^{o}C in order to incorporate copper ions with amine species of the polymer. The impregnated polymer will be washed with water and ethanol to remove un-reacted copper ions. The powder will be dried at 60^{o}C.

5.4 Adsorbent Characterization

Similar characterization will be applied for both PDVB-X/Cu-*in situ* and PDVB-X/Cu-*ex situ*. To confirm the incorporation of copper ions into the polymer, electron paramagnetic resonance (EPR) will be applied. To determine the ratio and oxidation states of coordinated copper, X-ray photoelectron spectroscopy (XPS) will be conducted. Fourier transforms infrared (FT-IR) and Raman spectroscopy will be carried out to display the incorporated copper in the polymer. The morphology of coordinated metal polymers will be determined by scanning electron microscopy (SEM). Textural properties of polymers will be assessed by N_2 sorption methods (BET for surface area and BJH methods for pore size distributions). Thermogravimetric analysis (TGA) will be carried out to determine thermal stability of copper incorporated polymeric adsorbents.

5.5 CO_2 capture evaluation and breakthrough

CO_2 adsorption under atmospheric pressure (up to 1 bar) should be conducted at two different temperatures in order to calculate the isosteric heat of adsorption (Q_{st}). The CO_2 adsorption breakthrough of adsorbents should be obtained under a dry and humid gas stream of CO_2/N_2. Recyclability of the adsorbents should be evaluated for at least 10 cycles of CO_2 adsorption-desorption process. To obtain CO_2 breakthrough curves a mixture of CO_2/N_2 (15/85) should be purged through a mass flow controller (MFC) and passing a gas stream through the adsorbent bed followed by analysis it with gas chromatography (GC) with a thermal conductivity detector (TCD) (**Figure 5.1**).

The breakthrough curves for CO_2 adsorption should be obtained under dry and humid conditions. A relative humidity of 5-10% should be fixed by setting the gas flow of a water bubbler to CO_2/N_2 at a specific ratio. After passing the gas mixture through the adsorbent bed, the CO_2 and N_2 can be detected by GC-TCD. For humid conditions, before the injection of the outlet gas into the GC, it is necessary to eliminate moisture by placing a moisture removal column in line after passing gas through the adsorbent bed.

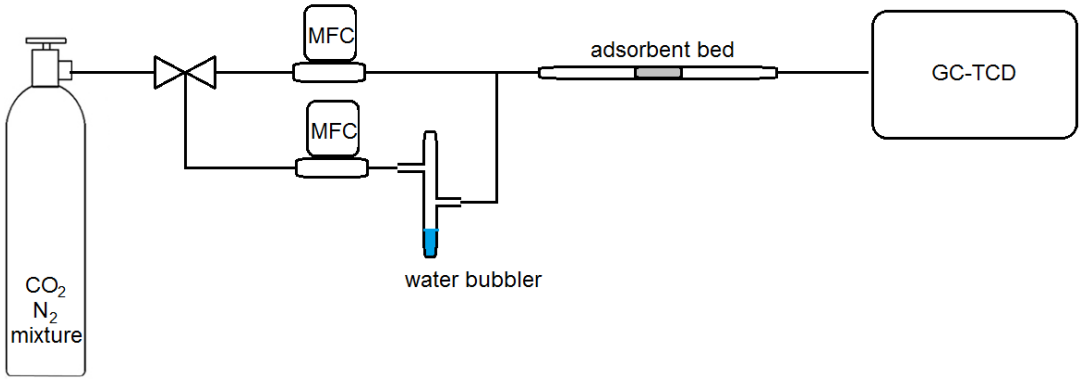

Figure 5.1 Schematic diagram of CO_2 breakthrough set-up under ambient pressure.

The adsorbent performance then should be evaluated by calculating[9] the total CO_2 uptake capacity (q, $mg.g^{-1}$) according to Equation 1:

$$q = \frac{1}{m}\sum_0^t Q \times (C_{in} - C_{out})\Delta t \quad (1)$$

Where m is adsorbent mass in the adsorbent bed (g), t is the contact time (min), Q is the gas flow rate ($L.min^{-1}$), Cin and Cout are the inlet and outlet concentrations of CO_2 ($mg.L^{-1}$), respectively.

Formation of metal incorporated polymers will be conducted for two co-monomers which have shown the ability to coordinate with copper or other metals such as vinyl pyridine (VPyd)[4,10] and pyrazine[6]. **Table 5.1** shows the selected co-monomers (X) to prepare different metal incorporated polymeric adsorbents. Another co-monomer of vinyl diamino- triazine (VDT) will also be used to prepare copper grafted mesoporous PDVB.

Table 5.1 selected co-monomers (X) to prepare different metal incorporated polymeric adsorbents.

Co-monomer (X)	Molecular configuration
vinyl pyridine (VPyd)	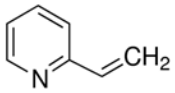
vinyl pyrazine (VPyz)	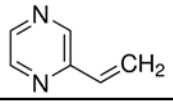
vinyl diamino- triazine (VDT)	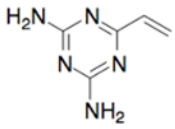

5.6 References

(1) Zhang, J.; Singh, R.; Webley, P. A. *Microporous Mesoporous Mater.* **2008**, *111* (1-3), 478–487.

(2) Wu, K. H.; Wang, Y. R.; Hwu, W. H. *Polym. Degrad. Stab.* **2003**, *79* (2), 195–200.

(3) Orhan Lekesiz, T.; Kaleli, K.; Uyar, T.; Kayran, C.; Hacaloglu, J. *J. Anal. Appl. Pyrolysis* **2014**, *106*, 81–85.

(4) Gao, B.; Kong, D.; Zhang, Y. *J. Mol. Catal. A Chem.* **2008**, *286* (1-2), 143–148.

(5) Cao, L.; Ma, C.; Wang, J.; Chen, P. *J. Supercrit. Fluids* **2013**, *75*, 152–158.

(6) Nather, C.; Greve, J.; Jeb, I. *Zeitschrift fur Naturforsch. - Sect. B J. Chem. Sci.* **2003**, *58* (1), 52–58.

(7) Graham, P. M.; Pike, R. D.; William, C.; Bailey, R. D.; Pennington, W. T. **2000**, No. I, 5121–5132.

(8) Groppo, E.; Uddin, M. J.; Bordiga, S.; Zecchina, A.; Lamberti, C. *Angew. Chemie - Int. Ed.* **2008**, *47* (48), 9269–9273.

(9) Gui, M. M.; Yap, Y. X.; Chai, S. P.; Mohamed, A. R. *Int. J. Greenh. Gas Control* **2013**, *14*, 65–73.

(10) Jiang, K.; Zhao, D.; Guo, L. B.; Zhang, C. J.; Yang, R. N. *Chinese J. Chem.* **2004**, *22* (20271017), 1297–1302.